Estimation of maximum transient voltages

A study on the Stedin 50 kV powergrid

Master Thesis

R.G. van Krieken

Delft University of Technology and Stedin

TU Delft

Estimation of maximum transient voltages

A study on the Stedin 50 kV powergrid

by

R.G. van Krieken

Student Name	Student Number
Roy van Krieken	5013321

Supervisors:	Prof. dr. ir. M. Popov & Prof. ir. P.T.M. Vaessen
Co-supervisors:	Ir. A.G.A. Lathouwers & Dr. ir. D. van der Born
Company Co-supervisors:	Dr. ir. E.J. Coster & Ing. F. van Bavel
Project Duration:	Sep 2024 - Jun 2025
Faculty:	Faculty of Electrical Engineering, Mathematics and Computer Science (EEMCS), Delft

Style:	TU Delft Report Style, with modifications by Daan Zwaneveld
Cover:	Stedin Goes Evertsenstraat, L-SEP GIS installatie, *Courtesy of Stedin*

TU Delft

STEDIN.NET

Abstract

This master's thesis investigates the feasibility of retrofilling existing L-SEP Gas Insulated Switchgear (GIS). This is motivated by the European F-Gas regulations phasing out the usage of Sulphur Hexafluoride (SF_6) due to its large Global Warming Potential (GWP). Retrofilling the L-SEP GIS with a dielectrically weaker insulation gas is a two-pronged problem. One side is on a component level, where the physical required alterations are investigated to obtain a new withstand voltage based upon alternative insulation gas. The other side is a system based study, where the grid of Stedin is examined on what transient overvoltages can occur. The latter part is the focus of this thesis and is important as some locations might stress the L-SEP to its rated maximum withstand voltage, not allow for retrofill.

The research methodology involves devolvement and investigation of the key transient origin applicable to the Stedin grid by usage of the ATP-EMTP software. An analysis of transient origins identified fault clearing as the highest priority for investigation. Key components (such as cables and transformers) were identified and represented using frequency dependent models such as the ULM and BCTRAN Grey box model. Both of which were tuned and validated using theory, measurement data and datasheets. A sensitivity analysis was then performed for differing fault locations and component parameters to identify the primary drivers of the maximum transient overvoltages.

The results show that the magnitude of the overvoltages are governed by grid earthing configuration and total shunt capacitance on the source side of the breaker. Non effectively earthed systems consistently produce higher overvoltages due to a large pole clearing factor. Furthermore, larger parallel capacitance reduces circuit damping which increases the contribution of the oscillatory part to the overvoltage. The highest simulated transient overvoltage was simulated to be a phase to phase overvoltage. In the case of a non effectively earthed systems with very low damping, where the oscillations of different phases align in opposition.

This study concludes that the worst case transient overvoltages remain well below the L-SEPs (rated at 72.5kV) rated lightning withstand voltage of 325kVp for SF_6. This implies that the possibility of retrofilling the GIS with weaker insulation gas (which lowers the withstand voltage) might be possible. In order for this to be confirmed, tests must be done on the altered GIS to find the new withstand voltage for the alternative gas. To improve the grid overvoltages remedial actions can be taken such as improving grid earthing and strategic installation of surge arresters.

Keywords: ATP-EMTP, ATPDraw, Transient analysis, Transient overvoltage, Circuit Breakers, Power Transformers, Power Cables, Grid Earthing/Grounding, First Pole to Clear Factor, Gas insulated Switchgear (GIS), L-SEP GIS

Preface

Het werk wat nu voor je ligt, is het resultaat van 10 maanden intensief onderzoek! Naast het afronden van mijn masterthesis, markeert het ook het einde van een fantastische periode van zes jaar studeren aan de TUDelft. Ik ben in deze tijd enorm gegroeid, zowel academisch door de complexe materie als persoonlijk door te leren omgaan met de uitdagingen.

Het schrijven van deze thesis was zonder twijfel een van de lastigste dingen die ik ooit heb gedaan in mijn leven. Het zelf definieren van een onderzoek, beslissen zonder alle informatie en het doorbijten wanneer het tegenzit zijn enkele van de obstakels die ik heb overbrugd. Gelukkig stond ik er niet alleen voor!

Ten eerste wil ik iedereen bedanken die heeft bijgedragen aan de begeleiding gedurende deze thesis. Met name André, Freek en Edward, met wie ik wekelijks kon sparren en waardevolle feedback van heb ontvangen. De steun die ik van hen heb ontvangen was niet alleen academisch maar ook op persoonlijk vlak, wat mij enorm heeft geholpen met deze monumentale taak. Het heeft mij altijd gerustgesteld om te weten dat het niet alleen draaide om het werk, maar ook de persoon erachter.

Zonder mijn vrienden, oude en nieuwe, had ik het ook niet kunnen doen. Het heeft me ontzettend geholpen om te kunnen spiegelen, klagen en relateren aan jullie ervaringen. Jullie waren essentieel. Tot slot wil ik ook mijn familie te bedanken voor het feit dat ik altijd bij hun terecht kon en voor hen onvoorwaardelijke steun.

R.G. van Krieken
Delft, June 2025

Contents

Nomenclature

Abbreviations

AIS	Air Insulated Switchgear
AOS	Assumed Overvoltage Severity
ARMA	Auto-Regressive Moving Average
ATP	Alternative Transients Program
BCTRAN	A transformer model routine in ATPDraw
BIL	Basic Insulation Level
C2OT	Cable to Outgoing Transformer
DSO	Distribution System Operator
E.M.C.	Electromagnetic Compatibility
EMT	Electromagnetic Transient
FAT	Factory Acceptance Test
FPTC	First Pole to Clear
GIS	Gas Insulated Switchgear
GWP	Global Warming Potential
L	Long cable length (10km)
L-SEP	Specific type of GIS switchgear used by Stedin
M	Medium cable length (5km)
MCOV	Maximum Continuous Operating Voltage
Min	Minimal cable length (100m)
NLRES92	A nonlinear resistance element in ATPDraw
OE	Open End (for a cable)
OV	Origin Validity
RRRV	Rate of Rise of Recovery Voltage
S	Short cable length (1km)
SA	Surge Arrester
SAT	Site Acceptance Test
SF_6	Sulphur Hexafluoride
SLF	Short Line Fault
TRV	Transient Recovery Voltage
TSO	Transmission System Operator
ULM	Universal Line Model
VS	Very Short cable length (500m)
XMFR	A transformer model in ATPDraw based on geometry
Yd	Star-Delta transformer connection
YnY	Transformer grounding: Primary star earthed, secondary unearthed
Ynd	Transformer grounding: Primary star earthed
YYn	Transformer grounding: Primary unearthed and secondary star earthed

1

Introduction

The electrical powergrid is arguably one of the largest man made invention on earth. It consists of countless nodes, branches and components, connecting millions of people across countries and continents. As civilization advanced, its demands for electrical power did too. To facilitate this, more generation was required, and by extension more transmission and distribution infrastructure. More people came to rely on this safe, stable and cheap electrical power. To ensure that the power met these criteria, electricity had to be controlled in terms of voltages or electrical fields and currents. Voltages are raised using transformers to increase efficiency in transporting power. Power which then flows to its required location via cables or lines. However, should anything be out of the ordinary, a means of control is needed. A pivotal component is the circuit breaker, which allows connections to be opened up stopping current and therefore power from flowing. This is not a trivial task. Analogous to *Isaac Newton*'s principles of mechanical motion, a current in motion tends to stay in motion due to system inductance. In other words, it will resist the interruption.

An electrical substation facilitates many of the requirements mentioned before. One key point is that it should operate reliably and safely at regular power frequency (50/60Hz) and during transient events. The insulation should be set up to avoid flashovers and power system protection should be tuned to break the current in case of faults. This thesis studies the transient effects or phenomena on substation switchgear installed on the 50 kV Stedin powergrid.

1.1. Motivation

A large share of the power demand is near or in large population centers where land is scarce. SF_6 GIS has been a pivotal tool for Transmission Service Operators (TSOs), Distribution Service Operators (DSOs) all over the world. One of these DSOs is Stedin, which operates on the Dutch distribution grid, as shown in Figure 1.1.

Figure 1.1: Stedin's service area for solely gas and gas and electricity combined [1]

Stedin operates in densely populated areas, servicing a large number of customers. As of 2023 [2] the customers consist of:

- 21 HV (50kV) customer connections
- 6073 MV (20kV-10kV) customer connections
- 2,384,599 LV customer connections

Many challenges arise with the current Dutch energy transition. In the most conservative scenario, Stedin (for base year 2019: 119TWh) needs to facilitate delivery of 129TWh in 2025 and 170TWh in 2030. Increased electrification demand strains the current infrastructure leading to congestion. This must be resolved by upgrading or creating additional new connections while optimally utilizing existing infrastructure. Due to physical space constraints compact GIS is preferred over AIS installations.

Before the introduction of sulfur hexafluoride (SF_6) Gas Insulated Switchgear (GIS) in the sixties, most electrical installations utilized Air Insulated Switchgear (AIS)[3]. The main disadvantage was its large physical size of the AIS to avoid flashovers. SF_6 has superior insulation and arc quenching properties to alternative gases [4] due to their atomic mass and electron affinity (at equal pressure and temperature). Additional advantages [5] are:

- Low boiling point of $-64°C$
- Non-Toxic (except for its decomposits due to arcing: S_2F_{10}, SF_4 and HF)
- Non-Flammable
- Non-Corrosive (except for its decomposits: SF_4, HF, F_2)
- Good thermal conductivity compared to air to allow for higher currents

The application of SF_6 based GIS led to smaller, more compact installations compared to AIS.

1.1.1. The L-SEP GIS

In the past Stedin installed the L-SEP GIS in its 50kV transport grid. The Dutch manufactured L-SEP is a metal-enclosed 3 phase, enclosed switchgear. It uses SF_6 as an insulation and switching medium and is rated for 72.5kV. It is used in locations where physical space is limited and/or local area is polluted by dust, humidity or salinity.

Originally designed by ELIN Holec High Voltage (now owned by Siemens Energy), the focus of the design can be summarized in the following points **L-SEP2024**:

- Safety
  - Safety is optimized due to double gap disconnector design
- Reliability
  - Minimum amount of components
- Compactness
  - Insulation gas is low pressure SF_6
- Modularity
  - Standardised busbar, circuitbreaker and termination compartments
- E.M.C. Compatibility
  - Control, protection and monitoring compliant to IEC694 (nowadays IEC 60694)
- Flexibility
  - Single or Double busbar design, connection facilities for all cable types
- Minimum maintenance
  - Maintenance restricted to routine checks

A schematic overview and more detailed specs given by the manufacturer can be seen in Figure 1.2

Stedin uses 61 of these 72.5 kV L-SEP GIS bays in their 50kV grid divided over 5 substations.

This GIS contains multiple compartments. A redundant busbar compartment (2), the circuit breaker compartment (9) and the termination compartment (5) for earthing. The final compartment is the circuit breaker itself, which operates in a separate enclosure on a higher pressure than the others. The breaker operates on a puffer design, which extinguishes the breaking arc by simultaneously pushing gas flow into the channel while opening the contacts. The L-SEP is rated for 72.5 kV, which means that all withstand voltages (power frequency and transient) fulfill the values based on IEC 62271-1, covering the values of Stedin. However in depth transient simulations or measurements have never taken place.

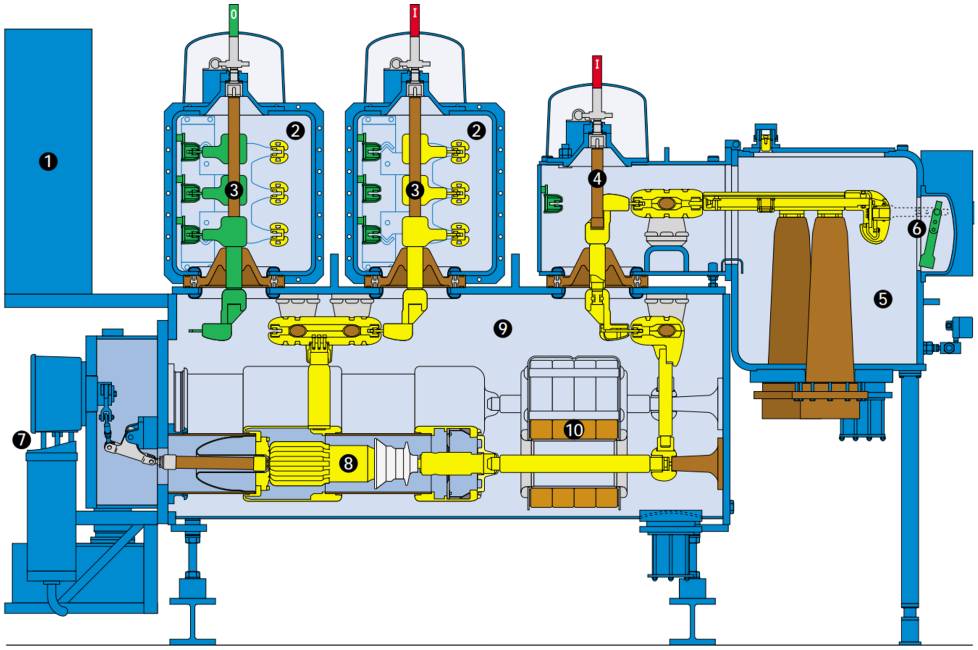

Fig 1 Type L-SEP bay arrangement (double busbar system). 1. local control cubicle; 2. busbar compartment; 3. busbar disconnector; 4. termination disconnector; 5. termination compartment; 6. termination earthing switch; 7. circuit-breaker driving mechanism; 8. single puffer interrupter; 9. circuit-breaker compartment; 10. current transformers.

B.I.L.:	72.5kV	123/145kV
- phase - earth	325 kV	650 kV
- phase - phase	410 kV	825 kV
power frequency withstand voltage	140 kV	275 kV
rated short-time current	31,5/40 kA-3 s	
peak withstand current	80/100 kA	
rated current busbars	2500/3150 A	
ambient temperature	-5 to +40 (55) °C	
	23 to 104 (131) °F	

Circuit-breaker	
rated breaking current	31,5/40 kA
breaking current in phase opposition	8/10 kA
peak making current	80/100 kA
rated current	1250/2000/ 2500/3150 A
switching cycle	O - 0,3 s - CO - 3 min. - CO
make time	60 ms
break time (arcing time)	<54 (< 24) ms

Figure 1.2: Schematic overview and relevant specifications of the L-SEP GIS **L-SEP2024**

1.1.2. European F-Gas regulations

However, in view of the climate ambitions of the European Union, the European commission is deciding to phase out fluorinated greenhouse gases [6]. While SF_6 has desirable electrical properties, the global warming potential of SF_6 is 23500 times that of CO_2 [7]. The most important new regulations state the following:

- *Article 13.7*
  From 1 January 2035, the use of SF_6 for the maintenance or servicing of electrical switchgear equipment shall be prohibited unless it is reclaimed or recycled, except if it is proven that it is reclaimed or recycled SF_6.
- *Article 13.9*
  The putting into operation of the following electrical switchgear using, or whose functioning relies upon, fluorinated greenhouse gases in insulating or breaking medium shall be prohibited as follows:

  a) from 1 January 2026, medium voltage electrical switchgear for primary and secondary distribution up to and including 24 kV;

  b) from 1 January 2030, medium voltage electrical switchgear for primary and secondary distribution from more than 24 kV up to and including 52 kV;

  c) from 1 January 2028, high voltage electrical switchgear from 52 kV up to and including 145 kV and up to and including 50 kA short circuit current, with a global warming potential of 1 or more;

  d) from 1 January 2032, high voltage electrical switchgear of more than 145 kV or more than 50 kA short circuit current, with a global warming potential of 1 or more.

In addition the regulation demands for measures that monitor and document leaks on all machines or devices using fluorized gases. [1]

[1] Given that they have a tested leakage rate > 0.1% per year and have more than 6kg of SF_6

The Dutch Government, as an EU member state, is bound by this new European regulation, impacting TSOs, DSOs and industry among others. All must comply to the new regulations.

The Stedin strategic asset management department is responsible for maintaining existing assets. The focus is to be compliant to the new regulations and not use any new SF_6 GIS after 2028. New installations shall be SF_6 free and future GIS will either use a mixture including C_4-FN or technical air combined with vacuum circuit breakers, as these are the main alternatives now being developed by the manufacturers. Old installations will be maintained whilst alternatives are explored. All depending on cost, performance and risk.

1.2. Research problem

If a retrofilling would be considered, it would imply changing the **insulation** medium to another gas with a lower Global Warming Potential (GWP). As the installation is rated for 72.5kV but used at 50kV, it might be possible to change the insulation and isolation medium to pressurized clean air in the non breaker (low pressure) compartments given some physical retrofillings. This reduces the amount of banked SF_6 and therefore the potentially leaked SF_6. **It must be emphasized that the extinguishing medium is not altered! This is because the circuit breaker puffer design is based on SF_6.** The compartments in question can be seen in Figure 1.2 and are numbered as 2,5 and 9. Compartment 8 shall remain unchanged due to the puffer design being based on SF_6.

In order to assess feasibility of retrofilling, it is important to know what the real local grid conditions are at the L-SEP locations. This gives more insight in local grid behavior and can determine where derating the installation would be allowed. The maximum allowed transient voltages of the air filled L-SEP are not known yet. The manufacturer did state that the compartments could be filled at a higher pressure compared to the current medium. When a higher pressure alternative gas (like air, which has a comparatively lower dielectric strength) is used, the maximum withstanding (transient) voltages will be reduced.

Once the grid conditions are established, some locations might not allow for a retrofilling due to the large transients occurring due to local grid topology. With this information an informed decision can be made on whether retrofilling is possible at what location under what restrictions. In general DSOs use equipment rated for higher voltages and power than at which the grid is operated, using standards and safety margins. Studies in the literature are usually only done at these higher voltage levels (for transmission) and focus on the transient recovery voltage (TRV), which is defined as the voltage across the breaker. In other words, transient phenomena are mainly investigated on transmission grids instead of distribution grids and focus on the breaker instead of the compartment insulation. Therefore, these studies have not been attempted yet on the Stedin 50kV grid. The methods and the models can however be applied to lower voltage levels to obtain the required information. This still brings challenges.

First it needs to be determined what bandwidth the transients operate at to ensure usage of the correct models. For this, the origins of these transient origins must be investigated. Once these bandwidths are determined, models should be selected to represent physical effects that lead to the worst case (transient) overvoltage that take place within the relevant frequency range(s). Afterwards, necessary parameters need to be obtained (from measurements or datasheets), approximated (whenever direct data is unavailable), or assumed (based on literature), and verified where possible. Once all models and parameters have been implemented and verified the foundation has been set and a simulation can be set up to model the behavior of the substation in the grid.

This thesis uses the terms overvoltage and transient overvoltage. A transient overvoltage is an overvoltage that lasts for a short instance, usually when transitioning from one steady state to another. An overvoltage includes transient overvoltages, but also steady state overvoltages. Overvoltages are system voltages which are larger than its nominal steady state voltage.

This leads to the following main research question:

What is the **worst case** transient overvoltage, contact to enclosure or phase-to-phase, that the GIS is exposed to at their respective locations in the Stedin grid?

As transient overvoltages have many sources, defining the worst case must be done with consideration of the chance of occurrence and impact. It is also important to consider the local grid topology; some locations might allow for a retrofilling, while others do not.

To answer this question, the main research question is separated into multiple parts:

1. What events will cause transient overvoltages given the current Stedin grid?
2. What does the Stedin grid topology and configuration look like?
3. What are the main contributors in terms of grid topology or configuration to the terminal overvoltage?
4. How can these contributors be altered to lower the maximum transient overvoltage?

1.3. Thesis Outline

Chapter 1: Introduction
The introduction describes the main motivation behind the thesis. It briefly touches on why SF_6 is used by stating the main advantages. Then the thesis partner Stedin is introduced. The chapter then elaborates on how the new (tentative) European F-Gases regulation impact Stedin, after which the research problem is formulated.

Chapter 2: Transient origins
In this chapter the first sub-question of the research problem is explored. The chapter addresses what origins are of transient overvoltages, where they come from and in what manner they occur in the Stedin grid.. The results of this will be a list on which transients will be evaluated.

Chapter 3: Component Modeling
To model the previously mentioned overvoltage origins, the grid of Stedin must be investigated first. This chapter will describe the commonalities and differences of the substations where L-SEP GIS are installed, relating to the second sub-question. In addition the most occurring components are denoted of which models need to be selected. After model selection and implementation they are then validated.

Chapter 4: Simulation Setup
This chapter describes the implementation of the transient origin studies in ATPDraw. An overview is given on how the answer sub-question 3 can be obtained by sharing a simulation plan. The practical simulation implementation in ATPDraw is then shared.

Chapter 5: Results
This chapter shares the results gained from running the simulations from chapter 4. It selects the most extreme/interesting cases and interprets the results. From these results the answer to sub-questions 3 and 4 can be answered.

Chapter 6: Discussion
This chapter elaborates on the findings in the results and what influences changes in configuration have on the overvoltages. It links the results to the real life substations and goes in depth on what the limitations of the study are in terms of assumptions and approximations.

Chapter 7: Remedial Actions
This chapter will describe remedial actions on how to manage high overvoltages stemming from their respective origins. This will be in line with the respective real life substations and makes clear what Stedin needs to consider if they are to go through with the L-SEP retrofilling.

Chapter 8: Conclusions and Recommendations
Chapter 8 summarizes the work done in this thesis. The main results and conclusions are discussed and recommendations on further improvements are given.

2

Transient Origins

Overvoltages occur due to switching actions and power system disturbances. A transient occurs in the time period in which a system transfers from one steady state to another. These disturbances act like the origin of these transients. There are many origins that lead to transients in power systems. Simulating them often requires different models due to the frequency bandwidth belonging to the respective physical phenomena. Some lead to higher overvoltages while others can not occur due to grid topology. To estimate the maximum transient overvoltage these transient origins need to be investigated and prioritized. Please note that the study focuses on the overvoltages from phase-to-enclosure and phase-to-phase. The transients across switching contacts, which are usually defined as the Transient Recovery Voltage [TRV], are not of interest for this study.

2.1. Transient origins

As mentioned before, transient overvoltages occur when a power system is disturbed. These disturbances are from now on referred to as transient origins. A list of origins for transient overvoltages sorted by frequency range[8], can be seen in Table 2.1.

Table 2.1: Transient origins and Their Frequency Ranges [8]

Transient origin	**Frequency Ranges**	**Designation**
Transformer energization	0.1Hz – 1kHz	Low frequency transients
Load Switching	0.1Hz – 3kHz	Low frequency transients
Fault clearing	50Hz – 3kHz	Low frequency transients
Fault initiation	50Hz – 20kHz	Slow/Fast front transients
Line/Cable energization	50Hz – 20kHz	Slow/Fast front transients
Line reclosing	50Hz – 20kHz	Slow/Fast front transients
Terminal short circuit fault	50Hz – 20kHz	Slow/Fast front transients
TRV due to SLF	50Hz – 100kHz	Fast front transients
Inductive switching with restrikes	10kHz – 3MHz	Fast front transients
Capacitative switching with restrikes	10kHz – 3MHz	Fast front transients
Lightning surge	10kHz – 3MHz	Fast front transients
Bus charging / faults in GIS	100kHz – 50MHz	Very fast front transients

However, this table only contains a generalized collection of transient origins. The network topology can alter the transient overvoltages such that scenarios with the same transient origin have differing overvoltages. For example: fault clearing can be a (bolted) fault current which is limited by a cable or transformer. It can be a three phase fault (grounded or ungrounded) or a single phase fault, which in turn is dependent on earthing configuration.

2.2. Scenario Selection

As there are many origins of transients it is important to assess which ones lead to the most extreme behavior in the grid. As the research question assumes the worst case, a prioritization is required on what transient origins will be considered.

The following terminology will be used in this thesis:

- **Transient Origin**: This is the root cause of the disturbance and the most general term of an occurring transient. It describes the fundamental physical events behind the transient overvoltage. It is the broadest term to use
- **Scenario**: A scenario is a collection of circumstances, in event and grid topology. A single transient origin can lead to multiple scenarios that lead to overvoltages.
- **Case**: A case is a specific instance within a scenario. This is the most detailed level and describes the exact simulation.

An example can be seen here. Transient Origin: Fault current switching. Scenario: three phase fault to earth. Case: Switching a three phase to earth fault at the L-SEP terminal of a network with floating earth.

As mentioned before, transient overvoltages are a combination of both system disturbance and topology. This can lead to different types of overvoltages. These different configurations for the same transient origin are considered to be **scenarios** in this thesis. Before scenarios are considered a pre-selection of transient origins is created. this is done by a decision matrix with the following criteria:

- Assumed Overvoltage Severity (AOS)
  - AOS is a metric describing the expected relative severity in terms of overvoltage stemming from the transient origin.
- Origin Validity (OV)
  - The origin validity is a measure on whether or not it can occur in the Stedin grid topology or the breaking characteristics of the L-SEP.

Note, when either AOS or OV are LOW, the case is immediately not considered

2.2.1. Transformer energization

Whenever a part of the circuit is de-energized, upon energization inrush currents to the transformer will occur, leading to overvoltages. There are two distinct cases: No load inrush current and loaded inrush currents. Interactions with cables and transformer can however lead to resonant voltages, as the inrush current is high and contains many harmonics. These harmonics can occur at the resonant frequencies of the system leading to high overvoltages. The inrush currents stem from the magnetizing inductance of the transformer and are highly dependent on the magnetic remanence of the core (i.e. the remaining flux from when the transformer was de-energized making the core act like a permanent magnet).

Whenever the transformer is reconnected in such that the resulting flux from the input voltage is in phase with the remanent flux, the transformer enters saturation. This instance is at voltage zero of the input sinusoidal (as the flux is 90 degrees out of phase of the voltage)[9].

Whenever the transformer enters saturation the core material decreasing its permeability and thus inductance. Take the following relations below [10]

$$v = N\frac{d\phi}{dt} \text{ where } \phi = \frac{N i_m}{\mathfrak{R}(i)} \text{ and } \mathfrak{R}(i) = \frac{l}{\mu(i)A} \tag{2.1}$$

When the reluctance drops due to saturation (decreasing mu) the magnetizing current (i_m) needs to increase to uphold the applied voltage $v \propto \frac{di_m}{dt}$. This leads to sharp nonlinear waveforms or, in other words, odd harmonics in the primary current.

In principle, this resulting transient is in the form of a current. But due to its non 50Hz contents it can induce overvoltages due to resonances. This is very dependent on system inductance and capacitance.

When parallel RLC circuits are in resonance due to the harmonics, impedance increases drastically. This in turn leads to an overvoltage. In short, the main transient stemming from transformer is in terms of current. The overvoltage stems from harmonics meeting the resonant condition of the connected components.

A case of a resonance condition is when a transformer on stilts (transformer with direct cable connection) is energized. This occurs in the Stedin grid and can be seen in Figure 2.1

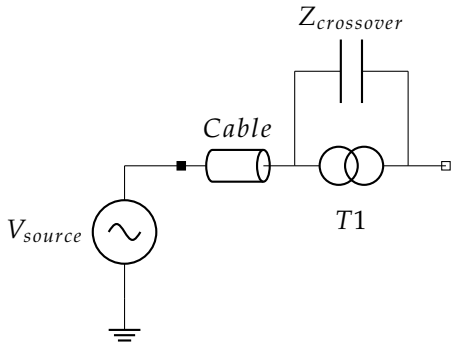

Figure 2.1: Cable transformer resonance condition. Note that there is no breaker between cable and transformer. Therefore they can not be energized separately

Initially the cable is energized by a source operating at 50Hz, and the following interaction is observed. Whenever the transformer resonant frequencies match those of the cable a resonance occurs. This resonance can then transfer to the secondary side via the transformer inter-winding or crossover capacitance, leading to potentially severe overvoltages in the L-SEP compartment. Resonances like this only occur for very specific cable lengths in combination with transformer inductances and capacitances [11].

A larger problem, but outside of the scope of this thesis, is the following phenomena. Whenever this resonance occurs a high frequency voltage is seen at the interface of the cable and primary winding of the transformer. As this is a high frequency signal, the voltage distribution on the primary winding is non uniform. A large part of the voltage will be across the first few windings which leads to breakdown. This is a separate problem as it is not seen on the L-SEP terminals.

In the Stedin grid it is most likely that the HV-MV transformers (50-20/10 kV) are the ones that are energized, leading to these phenomena. The worst case would be a large 150-50kV feeding transformer, which is why it is policy for Stedin to install surge arresters at these cable transformer connections. Every time a fault occurs in the grid there is a large chance that the transformer needs to be re-energized. However, it should be noted that it is the resonant condition that leads to the over**voltage**. Therefore the following scores are given:

AOS: High, **OV: Medium**.

2.2.2. Load Switching

For load switching a regular switching operation is considered where the power factor > 0.8 leading or lagging. In other words, mainly a resistive load. As the voltage and currents are almost in phase, the breaker interrupts at current zero, the voltage is also near zero. The transient overvoltage is in this case largely determined by the mainly inductive feeding impedance at the source side of the breaker and the network impedance connected to the load side of the circuit breaker. In other words, the voltage at the terminal of the feeding side will recover to its normal level, with a relatively small oscillation. The voltage on the side where the fault is located will decay to zero volt once disconnected. Note that a transient overshoot will occur on this new baseline voltage.

Switching resistive loads is a relatively uncommon occurrence in the Stedin grid. Only in the case of power quality/stability issues loads may be shed to ensure proper operation. Therefore the following scores are given:

AOS: Medium, **OV: Medium**.

2.2.3. Fault clearing

Fault clearance is a form of de-energization during the occurrence of a short circuit. It is the the process where a circuit breaker interrupts fault currents at a natural current zero. This fault current is determined by network topology and creates a voltage transient when the breaker interrupts the current. The transient overvoltage is also influenced by the system earthing, as different earthing configurations can lead to higher transient voltages on the second and third poles to clear.

Usually the fault current is inductive (fed from inductive, line dominated network through one or more transformer) and interrupted at the current zero crossing (voltage maximum). For three phase interruptions, the current zeros in each phase are naturally displaced (e.g. by 60 degrees in a symmetrical three phase systems) depending on earthing configuration. Clearing faults are relatively common occurrences for a circuit breaker and can be characterized by Figure 2.2.

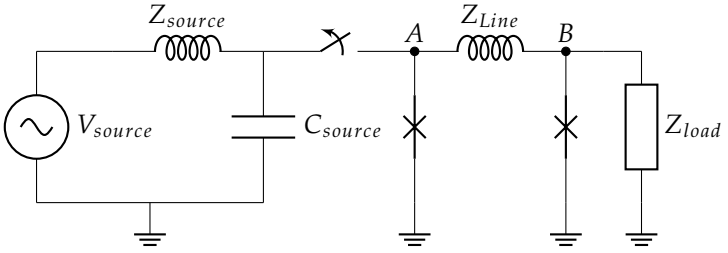

Figure 2.2: Fault current switching schematic

When a short circuit occurs (at point A or B) a new steady state will come from the faulted topology. This is a higher current due to the lowered outgoing impedance. When the faulted system reaches a new steady state, the energy stored in the magnetic and electric fields (of system capacitances and inductances respectively) is also stable at new levels. When a breaker interrupts a fault current at the current zero, the voltage is at its maximum. The feeding contact is then subjected to a voltage transient determined by the source network. This is influenced by the instantaneous system voltage at the moment of current interruption. But as the system is inductive there is an additional transient voltage component superimposed, proportional to $\frac{di}{dt}\Big|_{i=0}$.

The transient voltage is also dependent on location and therefore source reactance. source reactance, or short circuit power, determines the transient overvoltage on the feeding side of the transformer. The distance to (which is proportional to impedance) the fault location determines the voltage at the outgoing side of the breaker. In the case of a bolted fault (also known as terminal fault) the fault is at the terminal of the outgoing breaker and the voltage there is equal to zero.

It can also be stated that clearing fault currents is a relatively common and essential function for a circuit breakers helping to stabilize the grid. Therefore the following scores are given:

AOS: High, **OV: High**.

2.2.4. Fault initiation

A fault initiation is the process of a sound system converting to a faulted state. Usually this faulted state is a short circuit, where the new steady state is a drastically lowered voltage. Even though may be an over/undershoot of the voltage, the steady state is significantly lower than that of other transient origins. This event occurs as often as a fault clearing occurs, giving it the same likelihood to happen.

AOS: Low, **OV: High**.

2.2.5. Line/Cable energization

The Stedin grid is dominated by cables. In fact, there are no L-SEP GIS directly connected to overhead lines. Therefore only cable energization will be considered. Overvoltages stemming from cable

energization are related to those of transformers. It is mainly due to the interactions of system inductance and cable capacitances leading to resonance and potentially high inrush currents. This is also referred to as inrush current. In this case the currents are dependent on cable length, where longer cables (having higher capacitance) lead to higher inrush currents. This inrush current contains harmonics in its charging current due to the wave like behavior of the voltage and current. For open ended or loaded cables these waves reflect. This can be seen in by the following relationship:

$$I = C\frac{dV}{dt} \text{ where } C \propto \text{cable length} \tag{2.2}$$

Whenever the cable, which is potentially floating, is energized a sudden jump to the input voltage is made at the instance of connection. This step contains a wide bandwidth in the spectral domain, which in turn generates the current harmonics. In steady state these harmonics do not exist. Just like with transformer energization, the largest overvoltages come from interaction of current harmonics with the resonant frequency of the connected grid. The magnitude of the charging current is directly proportional to the connected capacitance and thus cable length. However, Stedin operates in densely populated areas. This makes finding long cables (>10km) very uncommon. Therefore the following scores are given:

AOS: Medium, **OV: Medium**

2.2.6. Line reclosing

In the case of line reclosing a circuit breaker opens and recloses multiple times to clear a disturbance. This origin can be seen as multiple system disturbances (i.e. switching events) where a fault is switched off and a line is re-energized.

The Stedin grid however, employs few lines of which none are directly connected to a L-SEP switchgear. The main reason to install an auto-reclosing scheme on the line is to take advantage of the self restoring insulating properties of air insulated lines in case of flashovers due to lightning. It does this with an open close open operation (O-C-O). However, this effect does not occur in cables as when breakdown occurs the insulation is damaged permanently (in the case of solid insulation). Therefore the following scores are given:

AOS: Medium, **OV: Low**

2.2.7. Terminal Short Circuit

This scenario is comparable to fault clearing. The main difference is that this fault occurs closer to the feeding network (i.e. close to the feeding transformer or GIS terminals). In essence this just leads to higher fault current magnitudes and potentially higher frequency components in the resulting overvoltage. This, because as the fault occurs closer to the source, less impedance is seen from the breaker terminal. For example, a case of a terminal short circuit could be that the earthing switch is unintentionally left closed or due to a flashover on the transformer connectors. As this case is similar to clearing other fault types, but typically with a higher fault current magnitude, it can be included in the study of the overvoltages coming from fault clearing.

AOS: High, **OV: Medium**

2.2.8. TRV due to SLF

The short line fault is a traveling wave phenomenon that occurs when, at a short (few hundred meters to several kilometers) distance from the feeding origin, a line becomes faulted [9][12]. When a line becomes short circuited the voltage distribution drops linearly from source to short circuit. When the breaker opens, this becomes the wavefront of a wave propagating from open circuit termination (open breaker) to short circuit termination (bolted fault). After two lengths of propagation the resulting signal is in the shape of a triangular wave. This wave has a very high frequency content and in context of a TRV (differential voltage between breaker contacts) this leads to a very large RRRV, but with relatively

small amplitude. This can be seen from to the relation :

$$\frac{du}{dt} = Z_c \frac{di}{dt} \text{ where } Z_c = \sqrt{\frac{L'}{C'}} \tag{2.3}$$

When the system consists of lines (where per unit length inductance L' dominates over the capacitance C') surge impedance Z_c leads to large changes in voltage. This can in turn lead to thermal restrikes and failure to interrupt.

However, as earlier said, the Stedin grid is predominantly made up of cables. These cables add a lot of capacitance to the transmission line, drastically reducing the effects of the SLF overvoltage. Moreover, there are no direct connections by overhead line to L-SEP switchgears in the Stedin grid.

AOS: Low, OV: Low

2.2.9. Switching with Restrikes

In this case the switching of (small) inductive or capacitive currents can lead to restrikes[9]. When interrupting current to a capacitive load one should keep in mind the charge on the load. This remaining charge and its resulting voltage can be high enough that the arc can reignite in the breaking compartment. This is especially the case at short arcing times when the contact gap distance is too small to withstand the recovery voltage [12]. This happens due to the following mechanism:

1. The current is capacitive, it leads the voltage. The breaker aims to interrupt at current zero.
2. At current zero the voltage on the capacity (load side) is maximum: E
3. After a half period the voltage at the supply side is at its minimum, the voltage across the breaker is now $E - -E = 2E$
4. If a restrike occurs, charge is transferred to the capacitive load leading to a new voltage of $-3E$
5. This repeats again when the polarity changes of the supply voltage where the new voltage after restrike and charge transfer will be $5E$

This voltage escalation can lead to extremely high overvoltages across the contacts.

In the case of inductive currents, large overvoltages come from a differing behavior. Assume a network consisting out of feeding inductance L_s and load inductance L_L where $L >> L_s$ with (relatively) small capacitance C_s. This implies that the current lags the voltage due to the dominant L of the load. A schematic can be seen in Figure 2.3

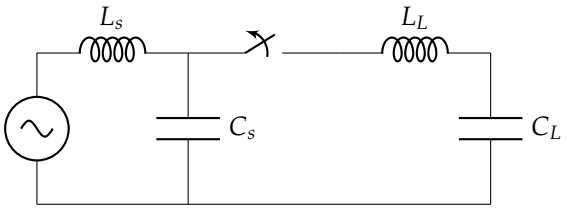

Figure 2.3: Diagram describing capacitive current switching

When the current is interrupted the C_L contains charge such that the voltage is close to the supply voltage (as the load is larger than the supply impedance). This voltage V_c can be described using the following relation:

$$V_c = L \frac{di}{dt} \tag{2.4}$$

This capacitor will then discharge at a frequency coming from interaction with the inductance L at the frequency:

$$f = \frac{1}{2\pi\sqrt{L_L C_L}} \tag{2.5}$$

This frequency is significantly higher than the supply frequency and can create large $\frac{dv}{dt}$ at the load side. In turn, reignition of the arc in the channel could occur due to the fast RRRV. Then, the capacitance C_L is connected to the supply again, which will charge it with a current at a frequency of:

$$f = \frac{1}{2\pi\sqrt{L_s C}} \text{ given } L_s >> L_L \tag{2.6}$$

When the breaker contacts move further apart the current might again get interrupted. However, due to this high frequency charging current the voltage on the load capacitance increases by Equation 2.4. This is also a form of voltage escalation which could lead to severe overvoltages after a few restrikes. Additionally the resulting large $\frac{dv}{dt}$ can then destroy capacitative grading of joints or connected transformer windings.

In the case of switching inductive currents the restrike principle is quite similar. Take the following equivalent circuit shown in Figure 2.4

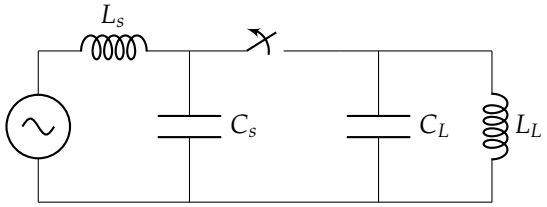

Figure 2.4: Inductive current switching circuit

In this case $L_L >> L_s$ and after breaking C_L discharges itself through L_L with the same relation as Equation 2.5, leading to an overvoltage on the load equal to Equation 2.4. This in turn creates high $\frac{dv}{dt}$ at the load side which leads to dielectric breakdown and re-ignition. Then the inductive load is connected to the supply again, which charges the capacitance at the same frequency $f = \frac{1}{2\pi L_s C_L}$.

In other words, a high frequency currents flows through the arc channel. This then leads to higher load voltages and thus voltage escalation.

The L-SEP manufacturer Siemens Energy allowed for inspection of measurement reports. For inductive switching the reports [13] [14] showed that the breaker was restrike free for 160A & 10A inductive currents. However, this is for the 170kV Trisep . This breaker uses the same circuit breaker puffer design, but at a higher pressure. This higher pressure leads to a faster quenching process and therefore a higher $\frac{di}{dt}$. The fact that the Trisep (with its faster quenching process due to higher pressure) did not restrike under these test conditions implies that restrikes are also unlikely for the L-SEP (which has lower pressure and thus a "slower" quenching process) when switching similar inductive or capacitive currents. As for switching small capacitive currents, the reports [15][16] showed no traces of restrikes occurring. In this case the BISEP 170kV was tested, where the same extinguishing mechanism at higher pressure is used as the L-SEP. In view of these test reports, restrikes are presumed to be very unlikely to occur in the L-SEP GIS. This then makes this transient origin a low priority.

AOS: High, OV: Low

2.2.10. Lightning strikes

A lightning strike on or near a powerline can induce very fast traveling waves. These transients are very high amplitude and have a very steep wavefront. They are determined by the length of the lightning strike, the magnitude of its current, the pylon surge impedance and line characteristic impedance [5].

Stedin's grid is mainly cable based and no L-SEP switchgear are directly connected with lines. However, there might be a possibility of lightning surges propagating through lines and cables to the GIS.

Imagine a high voltage transport overhead line. For simplicity the lightning strikes at the pylon or its shield wire. The pylon is grounded, and the resulting voltage wave would propagate along the earthing wire. However, when the voltage is high enough back flashover might occur and an additional wave will propagate over the phase wire. This is also the case for direct lightning impact on the overhead line.

Of all negative first stroke lightning strokes the median has the current corresponding to 35kA with wavecrest of ($t_{10/90} = 5.63\mu s$, where t is the time between 10 and 90% of the peak value)[17] [18]. Consider Figure 2.5 The circuit can be modeled as a inductance L representing the metallic pylon, a resistance R which is based on the earthing configuration and line impedance $Z_c = \sqrt{\frac{L'}{C'}}$ which is based on the distributed line inductance and capacitance.

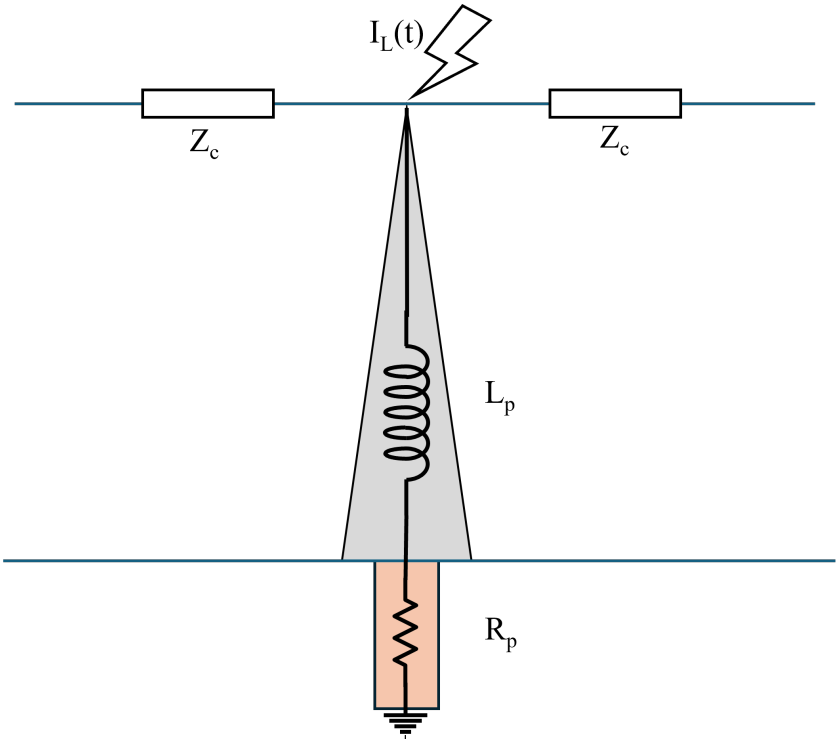

Figure 2.5: Example of lightning striking earthing wire or transmission pylon

The pylon voltage at the time of impact will then be:

$$V_p = V_{Lp} + V_{Rp} = L\frac{di}{dt} + Ri = \tag{2.7}$$

Pylon inductance consists of a surge inductance based on propagation speed and a material part based on pole length. For this example, values were taken from the lectures on lightning coordination in [5]. The characteristic impedances vary from 100-200 Ω for a pole of 30m, while propagation speeds are at the speed of light $v_p = c$. Then solving for L_p assuming $Z = 150\Omega$ gives:

$$v_p = c = \sqrt{\frac{L_p}{C_p}} \text{ where } Z_p = \frac{1}{\sqrt{L_p C_p}} \tag{2.8}$$

$$L_p = \frac{Z_p}{v_p} + L(\text{length}) \ = 0.5 + 15 = 15.5\mu H \tag{2.9}$$

As the wavefront has a time of $2\mu s$ and assuming the earthing resistance is $R_p = 25\Omega$ the voltage at the top of the pole is:

$$V_p \approx 0.98MV \tag{2.10}$$

This voltage could be high enough that a backflashover could occur from earthing wire to phase wire

Consider a line with $Z_c \approx 350\Omega$ transitions into a cable of $Z_{cable} \approx 50\Omega$), the reflection coefficient at that point would be found as follows.

$$\Gamma = \frac{Z_{cable} - Z_c}{Z_{cable} + Z_c} = -0.78 \tag{2.11}$$

The voltage at that point would be equal to:

$$V = V(1 + \Gamma) = 0.22V = 215kV \tag{2.12}$$

This disregards the fact that corona losses of the propagating voltage wave would lower the magnitude and steepness. In fact, it assumes the joint was struck directly. It should also be noted that in the cable more losses would lower the wave voltage even more before it arrives at GIS terminal [19]. In the case that surge arresters are installed before the transformer or at the line cable interface the wave surge would no longer be a problem.

The Stedin grid is mainly made up of cables and no direct line is connected to transformer or GIS terminal. For this reason the probability is quite low for the L-SEP GIS to have to deal with lightning surges.

AOS: High, OV: Low

2.2.11. Bus charging or GIS faults

Bus charging considers the event that, for any reason, there is a charge accumulation on the disconnector rail. Whenever the disconnector closes there will be a very fast transient with overvoltages. However, Siemens Energy stated that bus charging on this model does not lead to substantially high voltages to facilitate flashovers as it is also not occurring in higher voltage models [20].

AOS: Medium, OV: Low

2.2.12. Conclusion

To summarize the decisions made before, a decision matrix as shown in Table 2.2 was made. One can see that the highest priority should be an investigation of transients from the origins of transformer energization and fault clearing. **NOTE:** Terminal short circuit will be included in the fault clearing study due to it being a fault with higher fault current.

Table 2.2: Transient origins sorted by criticality (number of High values in AOS and OV).

Transient Origin	AOS	OV	Notes
Fault Clearing	High	High	Is very common and leads to recovery voltage
Transformer Energization	High	Medium	Resonance transfer
Terminal Short Circuit	High	Medium	Included in fault clearing
Lightning surges	High	Low	No direct line impact possible
Switching of capacitive currents	High	Low	Reignitions do not occur in testing
Switching of inductive currents	High	Low	Reignitions do not occur in testing
Cable Energization	Medium	Medium	Stedin only has short cables
Load Switching	Medium	Medium	Low impact for resistive current
Bus charging or GIS faults	Medium	Low	Reignitions do not occur in testing
Line Reclosing	Medium	Low	Not applicable due to cable grid
Fault Initiation	Low	High	No voltage transient
TRV due to SLF	Low	Low	Cable connected

From the table it was decided to focus the study on investigating the transient overvoltages resulting from fault clearing.

3

Component Modeling

This section will describe the implementation of the models used to simulate the selected scenarios of the previous section. The modeling is done in ATP-EMTP using ATPDraw. They are implemented based on measurement reports, company standards and literature on modeling. First the physical power substations which contain L-SEP GIS are observed in more detail. As modeling entire substations takes too much computational power, key characteristics of these substations are first identified. Using these characteristics, simulations can be set up to represent the current Stedin grid topologies in terms of the extremes.

3.1. Modeling Considerations

There are many considerations when creating a model to calculate overvoltages. One overarching factor would be what scenario is chosen. This scenario contains information about TRV origin but also the network topology that facilitates it. While the origin stays constant for a certain scenario, the topology is different for every GIS location on the grid. In the end this could mean some locations have higher worst case transient overvoltages than others and will therefore not allow for retrofilling.

When one considers the research question, defining the "worst case" is important. Modeling something for the worst case can mean very detailed models are not immediately needed (e.g. skin effect creates a higher resistance, lowering the peak voltage). It is preferred however to include these effects, as it leads to a better representation of the worst case.

The design philosophy is two-fold. As mentioned before: The worst case should be considered. Secondly, modeling will start simple. When necessary additional detail will be added.

3.1.1. Grid Topology

The Stedin grid contains 5 locations in which L-SEP GIS bays are in operation. As earlier stated, the objective is to focus on the extreme overvoltage events that can occur in the substation. Preferably while reducing simulation complexity by using more general models. One can then model key characteristics of these substations using simpler models.

Some key differing factors of these substations are:

1. Low amount of connected capacitance. In other words, short and few amount of cables connected to the busbar.
2. High amount of connected capacitance. In other words, large amount of parallel cables
3. Directly fed substation from 150-50kV YYd transformer
4. Indirectly fed via cable from other 50kV substation
5. Directly connected outgoing transformers. (transformers that have an electrically short (in terms of wavelength corresponding to transient frequency content) cable connection to the busbar

6. Grounding configuration

These factors correspond to the Stedin substations as shown in Table 3.1

Table 3.1: Overview of bays and matches of each substation

Location	# Bays	Matches
GOES EVERTSENSTRAAT	9	1, 4
SGRAVENDEEL	6	1, 4
SOEST 02	14	2, 3
UTR MERWEDEKANAAL 01 REUS	21	2, 3, 4, 5
WAAIERSLUIS	11	1, 4

Common points seen in all Stedin substations are:

1. Each substation has an outgoing Yd (50-20 or 50-10kV) transformer connected via cable
2. All L-SEP, rated for 72.5kV are operated at 52kV
3. The 150 kV transformer (YYd) neutrals are not both earthed on the same substation to ensure containment for single phase fault currents.
4. Transport cable (outside of substation) sheaths are earthed at both sides and are buried in trefoil condition.

In addition, the most commonly occurring components that influence the transient overvoltages are

1. Cables
2. Transformers
3. Circuit Breakers

The Stedin grid is located in a very densely populated area. This means that there is a low availability of building space and that the main mode of power transfer is via cables. In terms of transients, cables are the main contributor of system capacitance. The distributed nature and length of a cable can lead to resonances due to wave behavior, altering the transient overvoltage resulting from disturbances.

As mentioned before, each switchgear has at least one transformer connected to it. Be it the feeding 150-50-10 kV YYd or an outgoing 50-20/10 kV Yd transformer. The transformers determine the magnitude of the fault current, relative impedances and add a large amount of inductance to the system.

The last important component is the circuit breaker. Breakers add a few things to the system. Parasitic capacitance being one of them. This is capacitance from the breaker contacts (series) but also capacitance from the contacts to the enclosure (shunt). However, these capacitances are small in comparison to that of connected cables,it can therefore be omitted. In the case of a fault at the connection point of the GIS and the cable (shorting out the cable) the capacitance of either the feeding transformer or cable is dominant. Arc behavior should also be considered. As whenever a breaking operation is engaged an arc occurs, which then generates a voltage drop over the contacts.[12] However, this lowers the transient overvoltage due to its opposite polarity and can therefore be disregarded. Other arc behavior can be modeled whenever re or pre-strikes are considered. However, as stated in 2.2.9, the breaker considered to be restrike free.

It can therefore be concluded that the system can be modeled using 2 critical components: Cables and Transformers. These models will be selected, implemented and verified, after which simulations are done on several scenarios.

3.2. Modeling philosophy

To obtain an answer to the research question, simulations were done. Chronologically, the following iterative method was used in this thesis.

1. Start with a simple model
2. Verify the results with measurements (FAT/SAT) or theory

3. Tweak or alter the existing models
4. Return to step 2

The main idea was that the results ideally converge to an adequate (verified) accuracy. During this thesis many of these iterations have occurred. This then led to model additions, parameter changes or changes in configuration.

A schematical overview on how the model has been formed can be seen in Figure 3.1

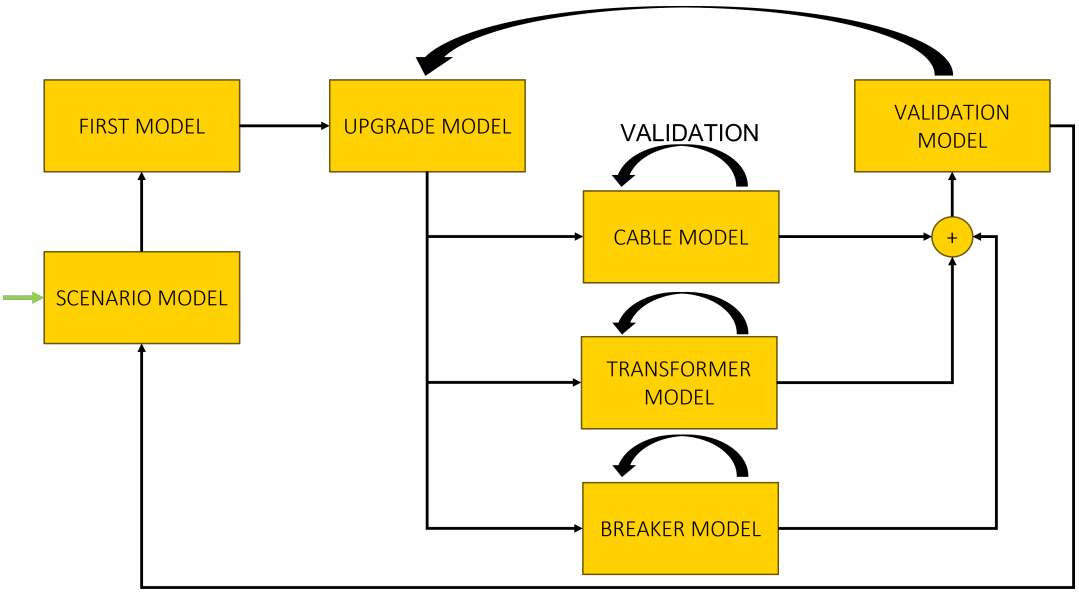

Figure 3.1: Modeling workflow

The results and chosen models discussed in this report are the final ones, chosen after 4 iterations.

To ensure that the results are representative three validation steps are implemented.

1. **Component validation.**
   To verify component behavior the models are verified on whether they behave as expected. This is done by simulation and comparison to measurement reference or theoretical validation.
2. **Sensitivity analysis.**
   This analysis is done to compare occurring changes in results when in topology and model parameters are varied. For example changes in grounding, parallel components or cable lengths.
3. **Scenario Validation**
   This validation deep dives in a few results of the simulations in more depth. It attempts reach the same results using simplified analytical or alternative simulation programs to verify the correctness.

3.3. ATPDraw

ATPDraw is a graphical preprocessor that runs the ATP executable. This program is a electromagnetic transient program that can solve power system transients such as switching and lightning but also controls and power electronics. The transient analysis is done by means of a time domain numerical technique. It solves for voltages and currents at the specified nodes by usage of nodal admittance equations and application of the trapezoid rule [21].

3.3.1. Modeling lumped elements

Modeling voltages and currents of passive components using the trapezoid rule leads to the following relations [21]:

Resistance
The behavior of a resistance is quite trivial and is represented by:

$$v_k(t) - v_m(t) = v_{km}(t) = Ri_{km}(t) \tag{3.1}$$

Where k and m are the nodes in question. The trapezoid rule is not needed in this relation.

Capacitance
The relation of current and capacitance can be modeled using a differential equation.

$$i_{km}(t) = C\frac{dv_{km}}{dt} = C\frac{d}{dt}[v_k(t) - v_m(t)] \tag{3.2}$$

$$\tag{3.3}$$

Or rearranged for voltage:

$$v_{km} = \frac{1}{C}\int_{t_0}^{t} i_{km}(\tau)d\tau + v_{km}(t_0) \tag{3.4}$$

From the trapezoidal rule the voltage can be determined to be:

$$v_{km} = v_{km}(t - \Delta t) + \frac{\Delta t}{2C}[i_{km}(t) + i_{km}(t - \Delta t)] \tag{3.5}$$

Solving for the current then gives:

$$i_{km}(t) = \frac{2C}{\Delta t}v_{km}(t) - \left[\frac{2C}{\Delta t}v_{km}(t - \Delta t) + i_{km}(t - \Delta t)\right] \tag{3.6}$$

According to [22][21], the part encapsulated by square brackets is called the history term. This term encapsulates the previous values of voltage and currents. If this is taken to be I_{km}

$$I_{km}(t) = -\left[\frac{2C}{\Delta t}v_{km}(t - \Delta t) + i_{km}(t - \Delta t)\right] \tag{3.7}$$

The current through a capacitor can be said to be

$$i_{km}(t) = \frac{2C}{\Delta t}v_{km}(t) + I_{km}(t) \tag{3.8}$$

Inductance
The relation of voltage and inductance can be shown according to the following relation:

$$v_{km}(t) = L\frac{di_{km}(t)}{dt} = v_k(t) - v_m(t) \tag{3.9}$$

Or rearranged for current:

$$i_{km}(t) = \frac{1}{L}\int_{t_0}^{t} v_{km}(\tau)d\tau + i_{km}(t_0) \tag{3.10}$$

From the trapezoidal rule the current can be determined to be:

$$i_{km}(t) = i_{km}(t - \Delta t) + \frac{\Delta t}{2L}[v_{km}(t) + v_{km}(t - \Delta t)] \tag{3.11}$$

This can be rearranged for:

$$i_{km}(t) = \frac{\Delta t}{2L}v_{km}(t) + \left[\frac{\Delta t}{2L}v_{km}(t - \Delta t) + i_{km}(t - \Delta t)\right] \tag{3.12}$$

With history term I_{km} being:

$$I_{km}(t) = \left[\frac{\Delta t}{2L} v_{km}(t - \Delta t) + i_{km}(t - \Delta t)\right] \tag{3.13}$$

The final relation of the current and inductance is then:

$$i_{km}(t) = \frac{\Delta t}{2L} v_{km}(t) + I_{km}(t) \tag{3.14}$$

Note that the equations describing capacitance and inductance Equation 3.8 and 3.14 can be modeled using an equivalent circuit as seen in Figure 3.2.

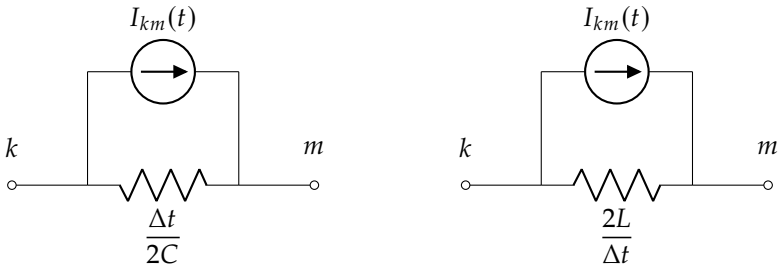

Figure 3.2: Equivalent circuits of capacitance and inductances in ATP

3.3.2. Numerical Oscillations

As the numerical representations of capacitance and inductance both have a history term, oscillatory behavior can occur. Take the case of a source with inductive impedance being switched into a separate network. At a certain point, the current will approach steady state. However, the inductor voltage (which before closing the switch was a certain value) will contribute to the current at the new timestep via the history term. In other words, a numerical oscillation occurs.

According to [22], applications of the trapezoidal rule lead to filtering of high-frequency voltages for current injections and amplifies high frequency currents for given voltages across capacitances. ATPDraw solves this by adding a damping resistance in parallel (R_p) to inductances and in series (R_s) with capacitances. If one considers an inductor the voltage (in steady state) becomes:

$$v(t) = -\alpha v(t - \Delta t) \text{ where } \alpha = \frac{R_p - \frac{2L}{\Delta t}}{R_p + \frac{2L}{\Delta t}} \tag{3.15}$$

The value for R_p from α is then found from

$$R_p = k_p \frac{2L}{\Delta t} \text{ where } k_p = \frac{1 + \alpha}{1 - \alpha} \tag{3.16}$$

In this case α is the reciprocal of the damping factor, so $\alpha = 0$ corresponds to critically dampened and $\alpha < 1$ is overdamped. In the same way the R_s can be found for capacitance modeling.

$$R_s = k_s \frac{\Delta t}{2C} \text{ where } k_p = \frac{1 - \alpha}{1 + \alpha} \tag{3.17}$$

According to [21][22] typical values for k_p =5-10 and k_s =0.1-0.2 . In ATPDraw one can fill in this damping coefficient, after which it automatically adds an equivalent resistance based on the values. Varying these values led to very small differences in simulation results. Therefore in this study $k_p = 5$ and $k_s = 0.1$ are used.

3.4. Cable Models

Most of the connections in the grid of Stedin are cables. Moreover, no overhead lines are directly connected to the L-SEP terminals making direct connections exclusively by cable. These cables are not a single continuous piece but consist of multiple cable pieces and sometimes over 20 joints. Some of these have differing (conductor) diameters, conductor materials and insulation materials and thus characteristic impedance and propagation velocity. For this study only a single continuous cable is considered of which the parameters are taken such that it represents an average cable in the Stedin grid. This generally leads to the worst case as multiple cable parts lead to reflection and transmission, increasing the amount of distance some surge components need to travel. This increases the damping and magnitude of the returning voltage surge, reducing the worst case overvoltage.

Cables can be modeled in a variety of ways, but fall within a few categories.

- Lumped
  - Lumped transmission line or cable models consist of resistances, capacitances and inductances. This is usually best for steady state studies. Wave like behavior is not modeled. An example of this is the PI model.
- Distributed
  - Modeling is done using distributed inductances, capacitances and resistances. This describes wave like behavior better. An example of this is the Bergeron model.
- Frequency dependent
  - Cables parameters are inherently non-linear. This is, among others, due to their frequency dependence. Namely the inductance is frequency dependent due to eddy currents and skin effect. Usually transient studies contain a wide range of frequencies instead of a single point, making this the most desirable solution. Examples of this are the Semylen, JMarti, NODA and ULM models

3.4.1. PI model

This model is regarded as the simplest representation as it is a lumped component model. Wavelike behavior is not supported and the model operates at a set frequency. In other words, it is used to approximate a distributed transmission line for steady state behavior. A circuit diagram of the model can be seen below in Figure 3.3.

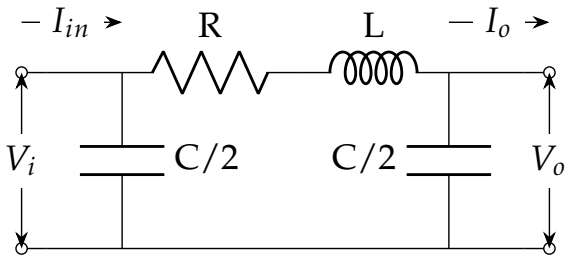

Figure 3.3: PI model equivalent circuit

From the model resistance, inductance and capacitance the series impedances (**Z**) and shunt admittances (**Y**) are calculated. Using these impedance matrices the currents and voltages are determined.

3.4.2. Bergeron model

This type models the inductance and capacitance from the geometry in a distributed configuration. This model includes losses but adds these as a lumped resistance isntead of the distributed capacitances and inductances. Note that the distributed capacitance, inductance and resistance certain operating frequency. A representative circuit diagram is included below.

To solve the voltages and the currents the telegraphers equations are used. These can be defined as follows.

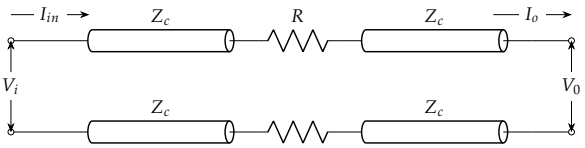

$$\frac{\partial V(x,t)}{\partial t} = -RI(x,t) - j\omega LI(x,t) \tag{3.18}$$

$$\frac{\partial I(x,t)}{\partial t} = -GI(x,t) - j\omega_0 CV(x,t) \tag{3.19}$$

When the series impedance **Z** and the shunt impedance**Y** of the line are considered, the telegraphers equations can be rewritten as follows:

$$\frac{\partial V(x,t)}{\partial t} = -\mathbf{Z}I(x,t) \tag{3.20}$$

$$\frac{\partial I(x,t)}{\partial t} = -\mathbf{Y}V(x,t) \tag{3.21}$$

The partial differential equations can be uncoupled by applying a second spacial derivative and substituting the results.

$$\frac{\partial^2 \tilde{V}(x)}{\partial t^2} = \mathbf{ZY}\tilde{V} \tag{3.22}$$

$$\frac{\partial^2 \tilde{I}(x)}{\partial t^2} = \mathbf{ZY}\tilde{I} \tag{3.23}$$

Note that, as the model is evaluated at a single frequency, voltages and currents are seen as phasors.

The propagation constant is then defined as

$$\gamma = \sqrt{\mathbf{ZY}} = \sqrt{(R + j\omega_0 L)(G + j\omega_0 C)} \tag{3.24}$$

The forms above are equivalent to the Helmholz equations in one dimension. General solutions for the current and voltages are

$$V(x,t) = V^+ e^{-\gamma x} + V^- e^{\gamma x} \tag{3.25}$$

$$I(x,t) = \frac{V^+}{Z_c} e^{-\gamma x} - \frac{V^-}{Z_c} e^{\gamma x} \tag{3.26}$$

Where the characteristic impedance is

$$Z_c = \frac{\mathbf{Z}}{\gamma} = \sqrt{\frac{R + j\omega_0 L}{G + j\omega_0 C}} \tag{3.27}$$

Where the frequency ω_0 is the operating frequency.

Cable models are inherently nonlinear. All parameters are dependent on frequency and due to the coupling to other cables and soil many separate modes of propagation occur.[21]. As earlier mentioned,

the Bergeron model evaluates the parameters at a set frequency. It then evaluates the voltages and currents by applying the trapezoid method on the telegrapher equations [22].

Between these distributed transmission lines, lumped resistances are added to model the losses.

However, transients usually do not occur at a single set frequency but a multitude. In addition, the transmission line parameters are all frequency dependent (i.e. $L(\omega), C(\omega)$ etc). Skin effect, proximity effect and eddy losses are some examples of higher frequency effects that influence the line parameters..

3.4.3. Frequency dependent models

The universal line model [23] is a model which models electromagnetic transients on transmission lines, accounting for frequency dependence. It does this by fitting calculated frequency dependent transfer functions derived from geometrical and material parameters. It is the most recent model that has been implemented in ATPDraw and builds on earlier models like JMarti and Noda. All of these models try to simulate the frequency dependence of the line parameters. JMarti does this via modal decomposition [24], Noda via Auto Regressive Moving Average (ARMA) and the ULM via a phase domain approach. In essence, this is a method to decouple multi-phase conductors in their respective propagating modes (this is, in contrast to the phase domain where all modes are coupled, regarded as the modal domain). This decoupling simplifies calculation as each mode can be calculated separately. Initially, this was done by usage of frequency independent transformation matrices and parameters. This gave good results for balanced/transposed lines only, as for unbalanced or untransposed lines the matrices are frequency dependent [25].

JMarti

For the JMarti model the modal decomposition is done first. As earlier said this decomposition decouples the equations of the voltages and currents on the conductors into modal domain equations. This is done by usage of modal transformation matrices. These matrices are frequency dependent but according to [26], quite accurate solutions could still be obtained.

The JMarti model added frequency dependence of the modal propagation constant ($\gamma(\omega)$) and characteristic impedance ($Z_c(\omega)$) to accurately model attenuation and phase distortion of the traveling waves. The model used rational function approximation and recursive convolution to implement these frequency dependent parameters in the time domain.

Noda

According to [27] there were improved models where the frequency dependence of the modal transformation matrix was taken into account. However, for an n-phase transmission line, these models took $2n(n-1)$ convolutions each time step, n for each modal propagation response and another n for the characteristic impedances. Instead of moving to the modal domain, this model stays in the phase domain. It then tries to solve the differential equations that govern the transfer using an ARMA model. This model is a discrete time model which can solve the equations in terms of a rational function in Z-domain (discrete Laplace domain) or in terms of difference equations in time domain. Speeding up calculation times drastically. The main disadvantages of this model was the fact that the fitting of the ARMA method fails, or that the time domain signal would be unstable[28][21]. Furthermore, as the z-transform is used, the resulting model is dependent on the timestep [29].

ULM

The ULM method stays away from the modal domain. It adds upon the JMarti model by accounting for the frequency dependence of the modal transformation matrix by staying in the phase domain.

The ULM method uses insights gained from modal approaches, where poles correspond to propagating waves in the medium. It stays in the phase domain where it sweeps through the bandwidth for the geometry, obtaining the frequency behavior of the cable. Using this transfer for general simulation would be too computationally intensive. It then proceeds to approximate this behavior in terms of its poles and residues by usage of rational function approximation. These rational functions can be converted to the time domain quicker than a deconvolution of the entire frequency response as the rational functions correspond to decaying exponentials. This then leads to a more efficient approximated time domain model, based on frequency domain fitting.

3.4.4. ATPDraw Implementation

ATPDraw offers a multitude of cable models which are calculated using geometrical parameters from the datasheet. The routine used to calculate this is the LCC. In this routine overhead lines, single core cables, pipe type cables and matrix import (for custom cable/line types) can be selected. In addition, operating frequency, length, ground resistivity and model type can be selected. An overview of the LCC prompt window can be seen in Figure 3.4

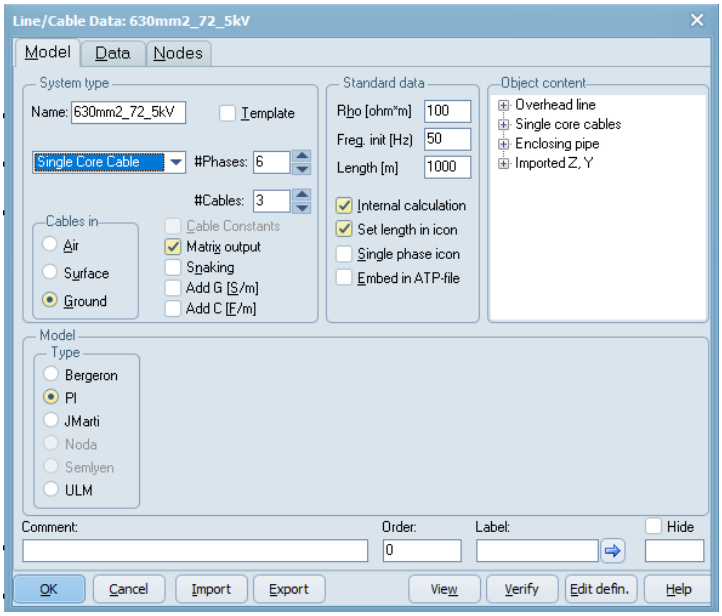

Figure 3.4: LCC prompt window

When a single phase cable is modeled the sheath connection can also be added by doubling the number of phases per cable in the program. This ensures the sheath can be connected externally to be grounded or floating. Geometrical cable parameters can be filled in the DATA tab. This includes burying depth, orientation (flatbed or trefoil), insulation strength and conductor and sheath thicknesses. Changing the soil resistivity within the ranges found in common Dutch soil of the Stedin service area did not lead to major changes in the results. Therefore a soil resistivity of 100 Ωm is used.

3.4.5. Cable parameters

The standard 50kV (rated for 72.5kV) cable used in the Stedin transport grid comes in 3 different conductor cross-sections: 630, 1200 and 1600 mm^2. For a 630 mm^2 Alcable the following parameters are given.

Table 3.2: Cable Specifications for 630mm² Cable

Dimensional characteristics	
Nominal diameter of conductor (mm)	29,1
Minimum/maximum conductor screen thickness (mm)	0,7/1,0
Minimum/maximum insulation thickness (mm)	10,2/11,2
Nominal diameter over insulation (mm)	53,6
Minimum/maximum insulation screen thickness (mm)	0,7/1,0
Nominal metallic screen cross-section (mm^2)	120
Nominal AL/PE tape thickness (mm)	0,2 (Al)
Minimum/maximum outer sheath thickness (mm)	4,0/5,0
Approximated outer diameter of cable (mm)	70
Approximated weight of cable (kg/km)	5630
Electrical characteristics	
Maximum DC conductor resistance, 20°C (Ω/km)	0,0469
AC conductor resistance, 90°C (Ω/km)	0,062
Inductance – in trefoil (mH/km)	0,365
Capacitance (μF/km)	0,273
Nominal electrical stress (kV/mm)	
Over conductor screen	4,4
Over insulation	2,6
Maximum short-circuit current, conductor, 90°C-250°C (kA)	
During 0,5 seconds	84,2
During 1 second	59,5
Maximum short-circuit current, screen, 80°C-250°C (kA)	
During 0,5 seconds	27,5
During 1 second	20,1

The cable cross section is also provided by the manufacturer and can be seen in Figure 3.5

1 – Circular stranded compacted aluminium conductor, class 2 according to IEC 60228. Waterblocked conductor by means of swellable yarns and/or tapes. A semiconducting waterblocking tape is helically applied over the outer surface of the conductor.
2 – Extruded semiconducting compound conductor screen.
3 – XLPE insulation.
4 – Extruded semiconducting compound insulation screen, fully bonded.
5 – Waterblocking semiconducting tape.
6 – Copper wires metallic screen helically applied. Over the wires, an equalizing copper tape is applied in an open counter helix.
7 – Non-conducting waterblocking tape.
8 – Aluminium/PE laminated tape adhered to the outer sheath.
9 – PE outer sheath, type ST7. Over the outer sheath, an extruded semiconducting compound is applied for testing purposes.

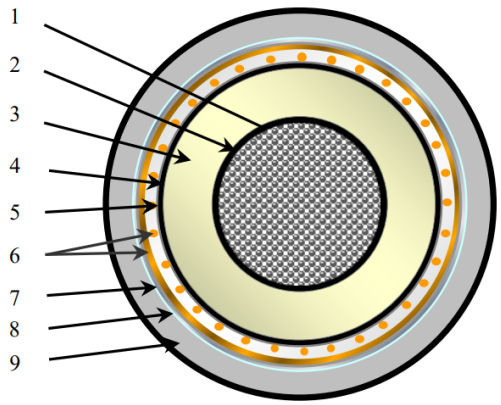

Cross-sectional drawing

Figure 3.5: Cable cross sectional diagram

Note that not all are parameters given. Namely semiconductor layer thickness, material resistivity and screen thickness.

Semiconducting layer
A semiconducting layer is added between the insulation and the core and sheath. This is done for several reasons.

One of these reasons is to control the electrical field. Semiconducting layers control and distribute the electric field within the cable. Especially at interfaces of differing materials [30]. It is implemented by attaching a semiconducting polymer based compound to the core, filled with conductive particles such as carbon black. This decreases the resistance of the compound effectively resistively grading the electrical field at the interface. Applying this semiconducting layer also improves the durability of the cable as the amount of voids between stranded conductor and insulation gets decreased. This then leads to a decrease in partial discharges, improving the lifetime of the cable. The semiconducting layer on the sheath serves the same purpose.

To see the effect of the semiconducting screens one can consider the capacitance of a simple coaxial cable. The capacitance per meter can be obtained as follows:

$$C = \frac{2\pi\epsilon_0\epsilon_r}{\ln(\frac{b}{a})} \tag{3.28}$$

Where ϵ_r is the insulation strength (of XLPE ≈ 2.3), a is the conductor radius and b is the radius from centre to the sheathe. Given the parameters in Table 3.2, this leads to a capacitance of $C = 0.232\mu F/km$. Which is substantially lower than the value given by the manufacturer of $C = 0.273\mu F/km$.

In essence, the semiconducting layer adds more capacitance to the cable due to its ϵ_r being high and it being in series with the capacitance of the insulation. This implies that the capacitance provided by the manufacturer can be used to find an equivalent ϵ_r of the insulation and semiconducting layers.

However, this disregards the resistive part of the semiconducting layer which attenuates very high frequency transients [31]. As the phenomena observed in this study are not in the very high frequency range and the worst case is assumed, the approximation of not including the attenuation is deemed valid.

The equivalent permittivity can be calculated by rearranging Equation 3.28 to solve for ϵ_r as seen below:

$$\epsilon_r = \frac{C \ln(\frac{b}{a})}{2\pi\epsilon_0} \tag{3.29}$$

This then leads to the equivalent permittivity of $\epsilon_r = 2.705$

Cable inductance
As the given inductance of the cable is measured for trefoil conditions it is not accurate to determine the propagation velocity. A coaxial geometric inductance is more appropriate as it determines the per-phase wave propagation. To still gain the inductance per meter, one can analytically determine the inductance per meter. The relation seen in Equation 3.30 is the inductance per meter of a coaxial cable.

$$L' = \frac{\mu_0\mu_r}{2\pi} \ln \frac{b}{a} \tag{3.30}$$

Using $a = 14.55$mm and $b = 25.25$mm, the lumped inductance can be determined to be $L' = 0.11\mu H/m$.

Material resistivity
Similarly the resistivity is note explicitly given. The conducting core is made of stranded aluminum with a DC resistance of 0.0469 Ω/m. To obtain a resistivity equivalent to a nominal cross sectional area (as if the conductor is a solid) the following relation is used.

$$\rho = \rho_{eq} \frac{\pi r^2}{A_c} = R_{DC} \frac{\pi r^2}{l} \tag{3.31}$$

Where r is the conductor radius, A_c is the nominal conductor cross-sectional area, l is the length of the cable and R_{DC} is the DC resistance per meter. This leads to a resistivity of $\rho = 3.12 * 10^{-8}\Omega m$ which is higher than a solid core of aluminum.

Screen thickness
The screen consists of copper wires and tape. No thickness is given by the manufacturer, instead the nominal metallic screen cross sectional area is given. To obtain a thickness the wire screen can be seen as an tubular conductor with cross sectional area equal to the wire area [31]. The radius can be calculated as follows:

$$r_3 = \sqrt{\frac{A_s}{\pi} + r_2^2} \tag{3.32}$$

Where r_3 is the distance from center to outer sheathe, r_2 the distance to the inner sheathe and A_s the sheathe cross sectional area. This leads to a outer sheathe radius of $r = 26mm$.

3.5. Cable Model Verification

To verify the correctness of the assumptions made when converting manufacturing parameters to geometrical, a preliminary simulation was done using the PI and Bergeron model. As the given inductance and capacitance were measured at 50Hz, it was decided to initially run the simulation at that set frequency.

3.5.1. Simulation setup

To simulate the behavior of the cable a step voltage was applied to the cables. This step has a large frequency content in spectral domain, which should lead to a frequency transfer that will give the resonant frequency. This resonant frequency can then be matched with the theoretical value to verify the assumptions and implementations. Additional points in the setup were:

- One side of the cable is open ended
- The sheath is earthed at both sides
- The cable is buried at a depth of 1 meter in trefoil formation.
- The timestep was equal to $\Delta t = 0.5\mu s$
- To ensure wave like behavior the cable length was set to be 1 km

The cable input current and voltage was measured. From this voltage the resonant frequency was determined by taking the FFT from the signal after the voltage step. A schematic of the simulation can be seen in Figure 3.6

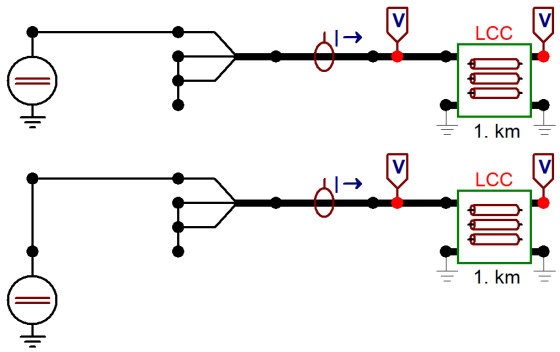

Figure 3.6: Cable simulation setup

To verify the assumptions made during the implementation of the parameters, the theoretical resonant frequency from the wave-like behavior is calculated. As the line is long enough for wave like behavior the propagation velocity should be calculated. For a cable with distributed parameters the following relation holds:

$$v_p = \frac{1}{\sqrt{L'C'}} = 1.82 * 10^8 \frac{m}{s} = 0.608c \tag{3.33}$$

Where c is the speed of light. To the find the resonant frequency the cable length and open end should be taken into account. This can be obtained using the relation:

$$f = \frac{v_p}{4L} = 45.6kHz \tag{3.34}$$

Where L is the cable length of 1 kilometer.

3.5.2. Bergeron and Pi Model

The results from the simulations were processed using a MATLAB script which would take the FFT of the measured voltage. This resulted in Figures 3.7 and 3.8. Here one can clearly see the resonant frequency of the Bergeron model being $24.2kHz$ which does not match that of the calculated theoretical value. There are some higher frequency inaccuracies, which is expected as the operating frequency of the models is set to be 50Hz. This calculates the $L(\omega)$ and $C(\omega)$ used in Equation 3.24 at a low frequency.

The time domain plots show the expected results: An oscillation that gets dampened over time. Note that the Bergeron model shows these artifacts in the time domain too, as an envelope can be observed around the start of the transient. The multiple frequency components can be attributed to its low frequency inaccuracies [32]. The PI model is off by a large amount. This can be attributed to the fact that no wave like behavior is taken into and that only one PI-section is used instead of multiple shorter ones.

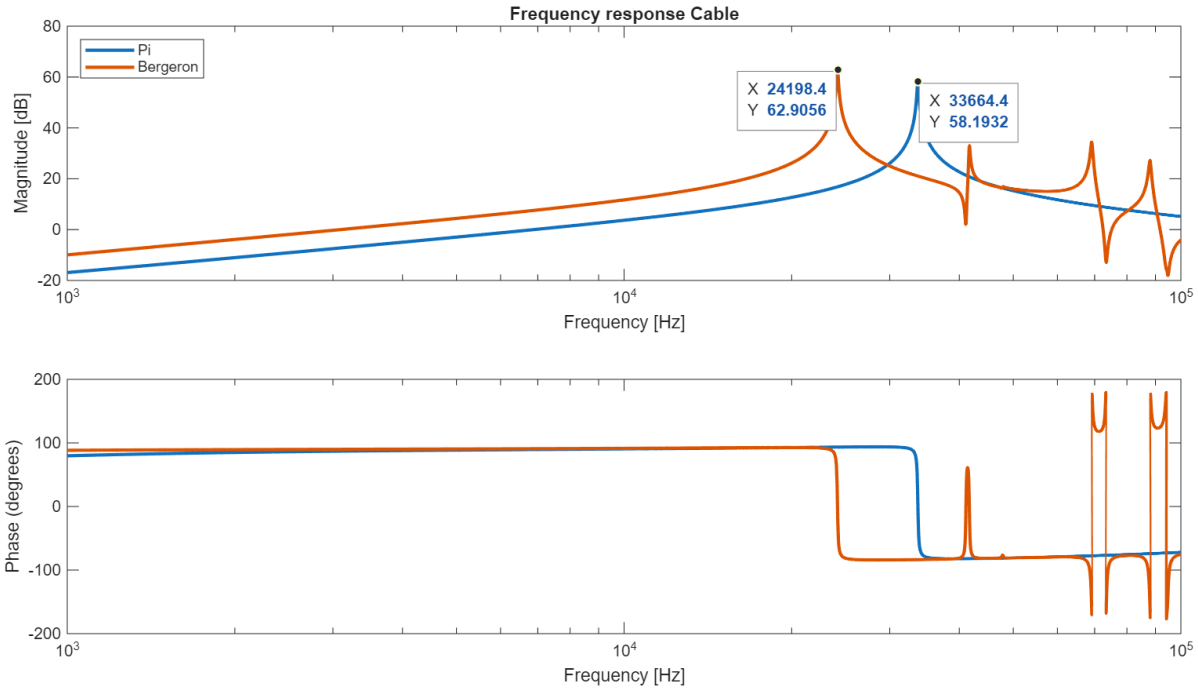

Figure 3.7: Frequency and phase spectrum of measured voltage at cable entrance

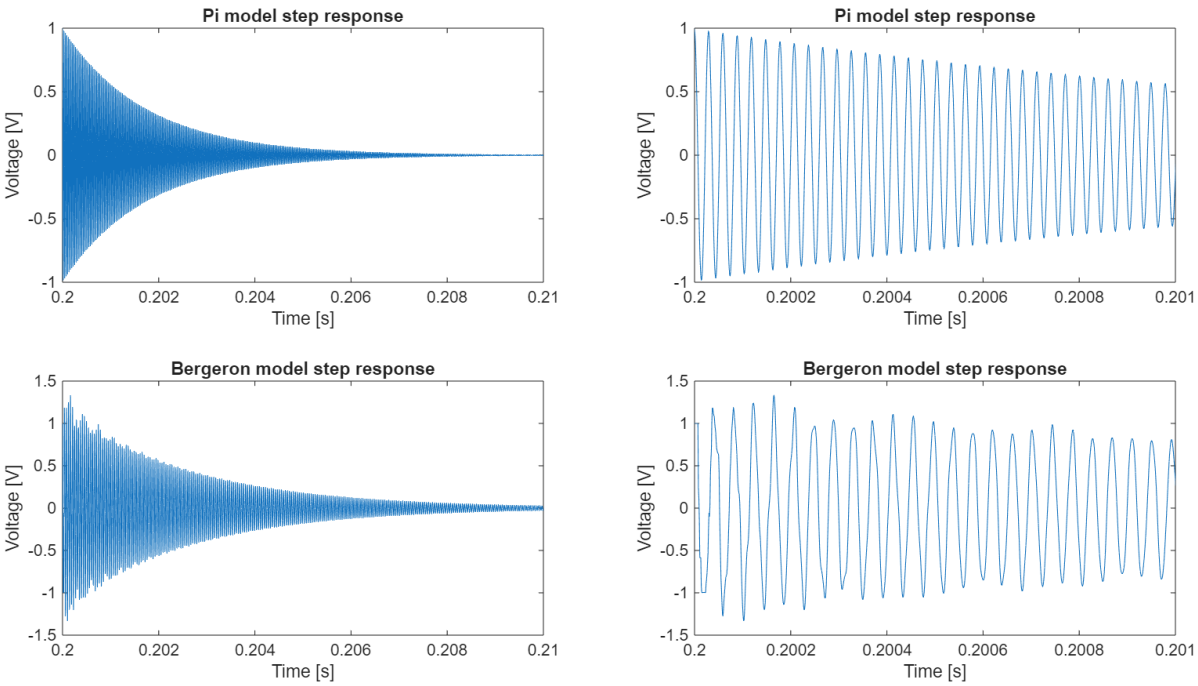

Figure 3.8: Time domain signal of measured voltage at cable entrance

3.5.3. ULM model

An initial simulation showed that the Bergeron model did not match the theoretical resonant frequency of 45.5kHz. Additionally, one could already observe inaccuracies that occur for higher frequencies due to the step excitation. As the frequencies that occur due to a transient are not a singular value or known it is preferred to use a model that takes into account multiple frequencies instead of one. This model is the ULM model. To test the behavior of the ULM model the same simulation was ran with the same parameters. The ULM model considered frequencies from 50 to 1MHz in 6 decades, with 10 fitting points per decade. The results from this simulation can be seen in figures 3.9 and 3.10

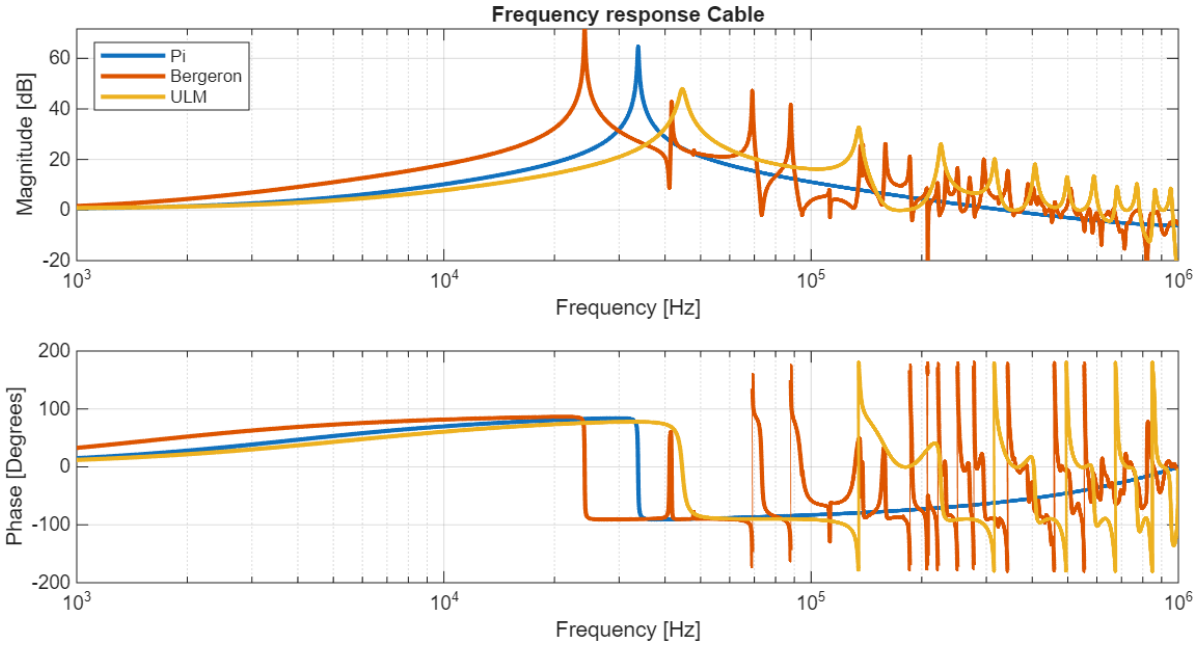

Figure 3.9: Frequency and phase spectrum of measured voltage at cable entrance with ULM model

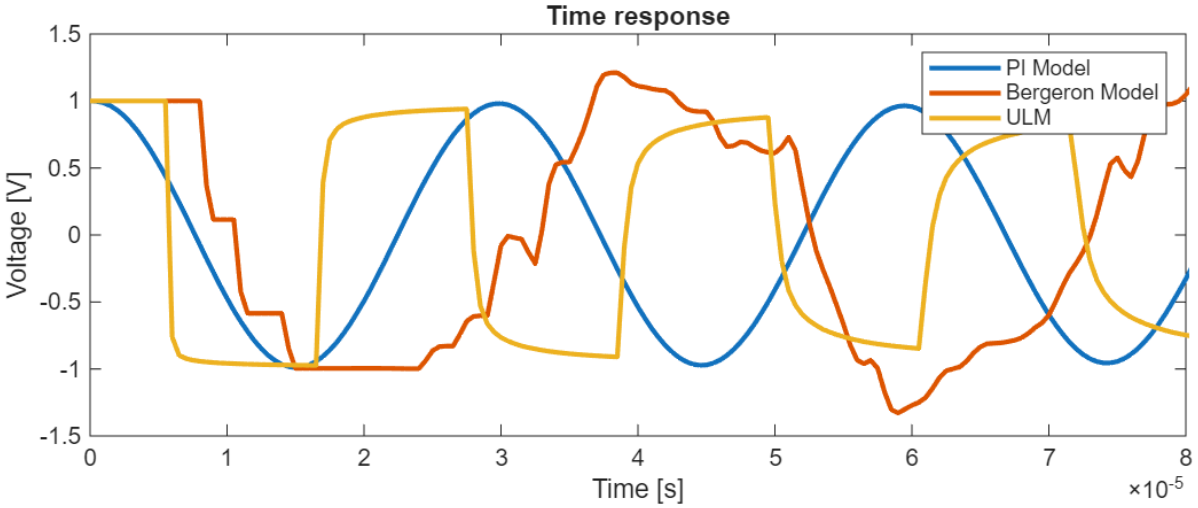

Figure 3.10: Time domain signal of measured voltage at cable entrance

In this case all frequencies in the bandwidth are considered when calculating the resonant frequency of the cable. One can observe that this leads to a ULM resonant frequency at 45kHz. This is more in line with the theoretical value and should include all higher frequency effects in its calculation. From the time domain plots it can also be seen that the voltages do not match. Additionally the Bergeron model shows erratic behavior when the operating frequency is set to a low frequency of 50Hz.

When it is assumed that the ULM model generates the most physically accurate resonant frequency, one can cross verify this by placing the set frequency of the Bergeron model at this new resonant frequency. This way the routine calculates the line parameters at the frequency that the ULM determines the line to resonate at. This gave the results shown in figure 3.11 and 3.12.

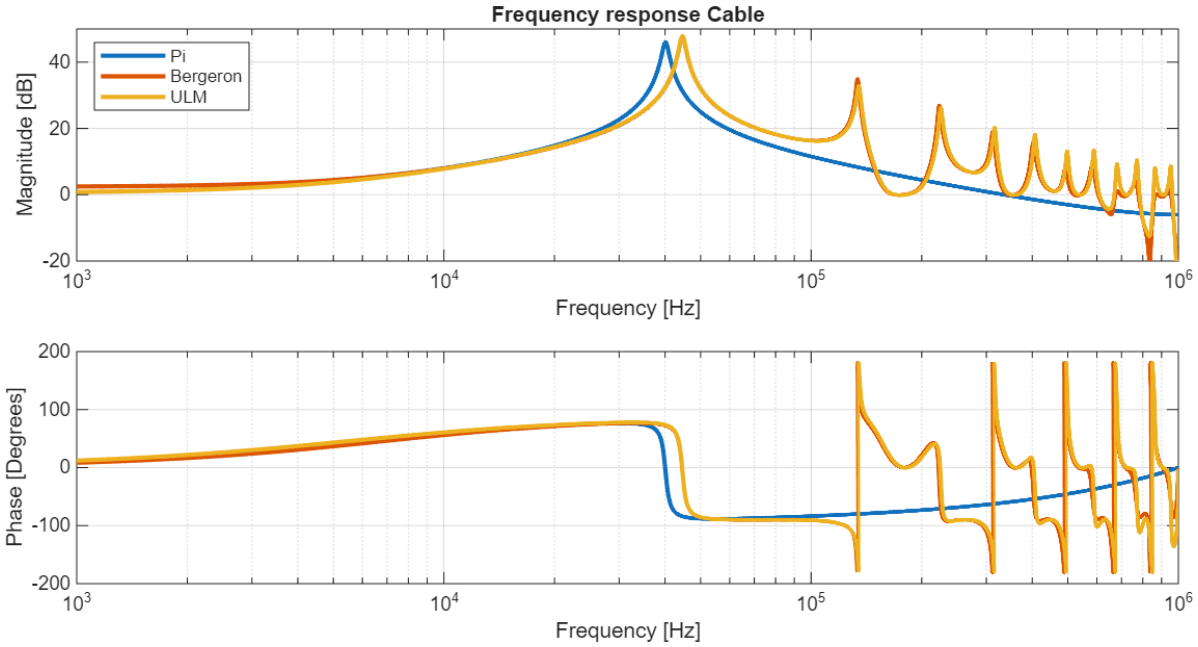

Figure 3.11: Frequency and phase spectrum of measured voltage at cable entrance with ULM model, operating frequency at 45 kHz

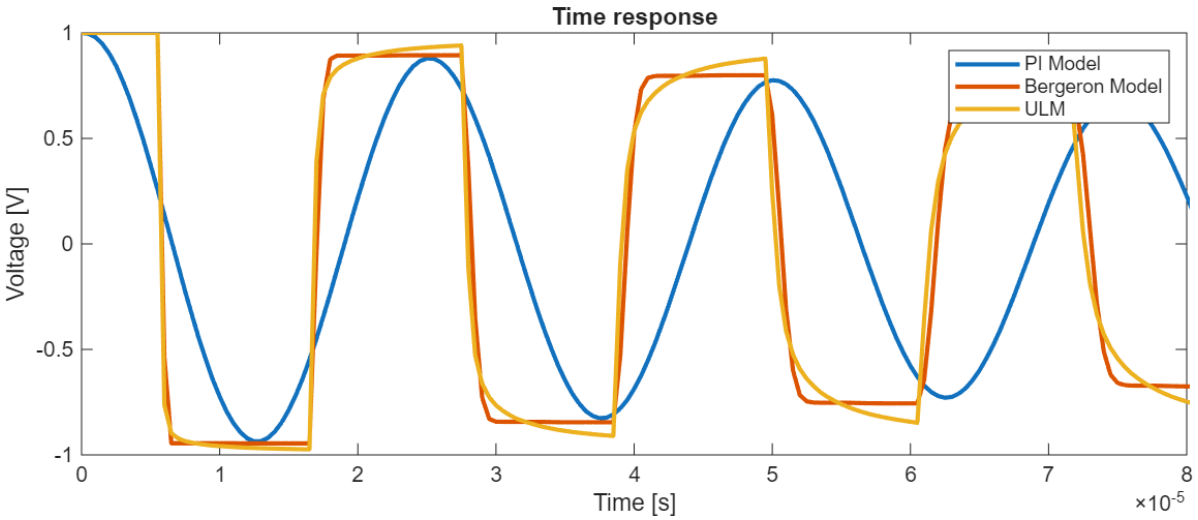

Figure 3.12: Time domain signal of measured voltage at cable entrance, operating frequency at 45 kHz

It is clear to see that the Bergeron and ULM model now match. This also confirms that the assumptions done for implementing the geometrical parameters are correct as the resonant frequencies match those of the theory. However, as the dominant frequencies in the signal when a disturbance occurs are not known, a more wideband model is preferred. Therefore the ULM model is the final choice of cable model.

3.6. Transformer Models

The transformer model is a crucial part for the simulation of the scenarios. Its frequency behavior is critical for transient studies as it is directly series connected to the feeding external 150kV grid. There are many ways to model a transformer but they can be categorized in 3 types: White box, Black Box and Grey box models [33][34][35]. The properties of these models are discussed further.

White box models are representations that allow for calculation of internal overvoltages due to lightning surges. These implementations can be done with either lumped parameter models or traveling wave models. However, for this model one needs detailed transformer design data from the manufacturer which usually is proprietary information. White box models are used when the component itself is the device to be tested. It can for example be used to simulate required insulation strength.

Black box models are focused on reproducing the transformer's terminal behavior. It therefore is used to do system studies (how the system reacts to the component) instead of studies on internal voltages. Its input data stems from terminal frequency sweep measurements.

Grey box models are the most general. Based on measurements done on factory and site acceptance tests, it tries to approximate internal and terminal transient behavior. What it sacrifices in comparative accuracy, it gains in ease of implementation.

The findings from these models out of their respective technical brochures can be summarized in Table 3.3.

Table 3.3: Comparison of White-Box, Black-Box, and Grey-Box Transformer Models

Feature	White-Box Model	Black-Box Model	Grey-Box Model
Data Required	Full transformer design details	Frequency response measurements	Test reports, simplified equivalent circuits
Accuracy	High (internal and external voltages)	High (only for terminal behavior)	Moderate (approximates internal + terminal behavior)
Computational Complexity	High	Moderate	Low to moderate
Includes Frequency Dependence?	Yes	Yes	Partially
Best For	Internal voltage calculations, insulation studies	EMT simulations, system-level transient response	Power system planning, simplified EMT studies
Weaknesses	Requires proprietary data	No insight into internal voltages	Less detailed than white-box models

Due to the availability of parameters and model simplicity, it was decided that the model type would be grey box.

3.6.1. Grey Box model

There are 5 types of grey box models (M1-M5)[35]. Each with different parameter requirements and approximations. These models only consider the terminal response only and are applied in situations where limited data is available.

The M1 model is a capacitance model where each phase is represented as a capacitance. This model can be used as a rough approximation for fast-front transient analysis, but lacks a lot of details. The transformer model does not include the voltage transfer, fault impedances and earthing configuration. As the studies chosen (fault current switching and transformer energization) do require the former information this model is not chosen.

The M2 model are artificial RLC models. This model represents the transformers linear low frequency behavior. It considers the first resonance and the high frequency capacitive behavior of the transformer. In essence this model represents the transformer as an RLC circuit based on nameplate data and open and short circuit measurements. This model is however single phase so does not account for the fact that Stedin uses 3 winding 3 phase transformers.

Models M3 and M4 are both similar single phase models. The main differences are added nonlinear magnetizing inductances and added shunt and series capacitances of the windings.

Model M5 is a topological 3-phase model. This model operates correctly in unbalanced situations and represents the physical fluxes starting from a magnetic circuit. For higher frequencies external capacitances are then added [11]. This model can represent an N winding transformer with a matrix of rank N[22]. In this matrix the resistances and mutual inductances are described. To this matrix representation external capacitances should be added. This matrix can be generated in most electromagnetic transient (EMT) programs using the BCTRAN routine using FAT and SAT measurement results.

3.6.2. BCTRAN Routine in ATPDraw

While no transformer is identical, common types feeding substations using the L-SEP GIS have the following characteristics:

- U = 150/50/10kV, YYd4
- S = 100/100/27MVA
- Manufacturer: Smit Trafo
- Core type: 3 legged core type

For these transformers site and/or factory acceptance test reports are available, containing the following information:

- Nameplate data
- Short circuit test
- Open circuit test
- Dielectric test

In ATPDraw there are multiple models that can represent transformer behavior. One can use coupled inductances, models based on geometrical parameters (XMFR) and models based on data from test reports; BCTRAN.

The BCTRAN model is a versatile model which uses test report data to represent the transfomer's terminal behaviour in terms of a resistance and inductance (R & L) matrix. The voltage is then represented as a vector containing phase voltages, the resistance as the losses between phases and the inductance matrix contains the mutual (between phases and windings) and self inductances of the transformer. This can be represented as follows $\mathbf{V} = (\mathbf{R} + j\omega\mathbf{L})\mathbf{I}$.

It can do this for multiple phases, winding configurations and earthing. Externally, nonlinearities and capacitances can be added [32][36]. The prompt window to enter data can be seen in Figure 3.13.

From this window one can see the input fields of the BCTRAN model. Among others, it is possible to change the amount of phases and windings, the winding configuration, core type and earthing. Under the open and short circuit tabs the test data can be filled in, with zero sequence data when applicable. Lastly it is possible to model the core magnetization based on up to 6 points of open circuit measurements. This will be a linear magnetization curve where more advanced curves can externally be modeled if desired.

Open Circuit Behavior

The open circuit test is done by connecting the lowest voltage terminal with its rated voltage. Then the current is measured flowing into this terminal when no loads are connected. Here the excitation current is measured which represents the required current to excite the magnetic field in the transformer core.

For the open circuit measurements usually the lowest voltage terminal is excited. However, sometimes connecting it to the delta winding can lead to instability. In those cases the lowest Y-connected can be used winding instead [36].

The measurement reports display open circuit currents per phase. This makes sense as each phase is wound around their core leg is at a different location within the transformer enclosure.

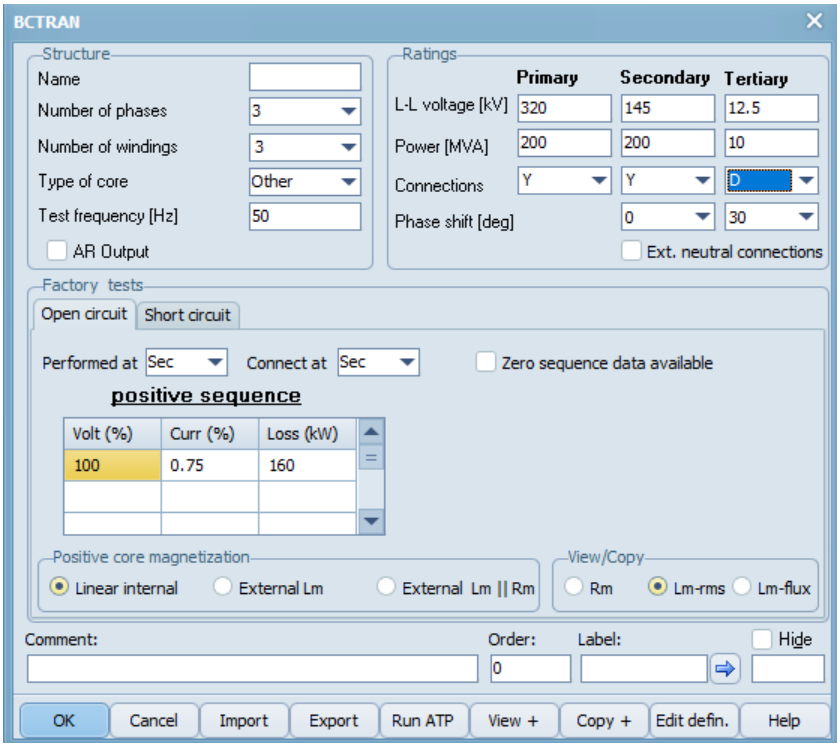

Figure 3.13: Example BCTRAN prompt window

This leads to differing fluxes and thus excitation currents. However, BCTRAN only allows input of a single excitation current. Therefore the average is taken of the three phases.

Short Circuit Behavior
The short circuit test is done in threefold for a three winding transformer. HV-MV, HV-LV and MV-LV. In these tests a voltage source is connected to the terminal while the output terminal is shorted. Then a voltage is applied such that the short circuit current is equal to the nominal current. This voltage is called the short circuit voltage, from which the short-circuit impedance can be calculated.

For the short circuit zero sequence impedances it was assumed that $Z_0 = Z_1$. This can be illustrated using the following approximation.

When one connects a zero sequence source to a YnD $N_1/N_2 = 1$ connected example transformer, two cases present themselves.

1. **Source connected to the delta winding**
   If the source is connected to the delta winding zero sequence currents circulate in the delta loop. This closed path prevents these currents from inducing zero sequence flow on the wye side.
2. **Source connected to the wye winding**
   If the source is connected on the wye side (with grounded neutral), zero sequence currents (I_0) will flow in the wye windings. While the total input current might be $3I_0$, the delta winding blocks the zero sequence currents from flowing to the delta network. In essence, any zero sequence current that attempts to cross the transformer to the delta side will circulate in the winding itself.

Therefore, for the short circuit test Z_0 as seen from Y to D can be regarded as approximately equal to Z_1.

When currents flow through the primary and secondary Y coils of the windings in regular operation, three magnetic fluxes get induced which are 120 degrees out of phase. Therefore these fluxes with their respective phases cancel out in the core. In the case of short circuit currents these fluxes sum to a nonzero value. This means the flux needs to find a return path outside of the core as shown in Figure 3.14.

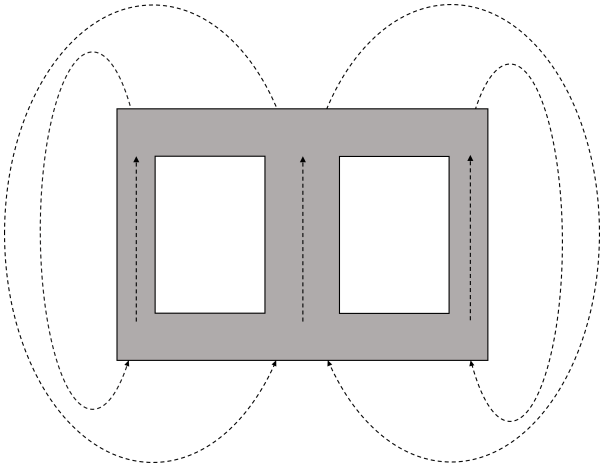

Figure 3.14: Zero sequence flux through a three legged transformer core

The zero sequence inductance is dependent on the magnetic reluctance (R_{m0}) which is defined as the sum of the magnetic reluctance of the core and airgap (R_{ag}, R_c respectively). It can be shown to be Equation 3.35 [37].

$$R_{m0} = R_{m,ag} + R_{m,core} = \frac{l_{ag}}{\mu_{ag} A_{ag}} + \frac{l_c}{\mu_C A_c} \tag{3.35}$$

Where l, A and μ are the flux path length, cross section and permeability. The formula to find the inductance can be seen in the following equation.

$$L_{m0} = \frac{N^2}{R_{m,ag} + R_{m,c}} \approx \frac{\mu_{ag} A_{ag} N^2}{l_{ag}} \tag{3.36}$$

As $\mu_c >> \mu_{ag}$. In other words, the zero sequence magnetizing inductance is mostly determined by the high airgap reluctance, leading to a low magnetizing reactance. To avoid heating of the core due to the high I_0 a tertiary delta winding can be added to control the currents.

All transformers that feed L-SEP GIS in the Stedin grid are YYD where either of the primary or secondary side is earthed. Literature describes a ratio 1-2.4 of X0/X1 [38]. In this study a ratio of 1 is chosen as lower short circuit impedance will lead to the largest single phase fault current. This leads to $Z_0 = Z_1$ for the primary to secondary of the transformer in the case of a short circuit.

Transient behavior
The model does not include capacitances, which are crucial for modeling transients in the case of switching transients [8][35]. The measurement reports include dielectric tests where the capacitance and loss tangent are measured between different terminals. The following measurements were included.

- LV to earth
- MV to earth
- HV to earth
- LV to MV
- HV to MV

These capacitances can externally be placed across the model terminals or shunted to earth. However, these cannot be used at the measured value. As these tests do not consider series capacitances as measurements are done from winding to enclosure. To circumvent this a 0.4-0.6 scaling factor should be implemented [35]. A scaling of 0.33-0.5 is recommended for star neutral grounding.

To more accurately represent the capacitances, the values are tuned such that the resonant peaks in their characteristic impulse response matches that of bode plots of comparative transformers. This will be done according to a measurement report[39] of a similar transformer which have equivalent rated voltages, power and manufacturer.

3.6.3. Transformer Model Verification

To check the validity of the models the BCTRAN transformer model is verified. This is done by reproducing the tests in ATPDraw and comparing the results to that of the measurement reports.

Open Circuit

This verification was done by connecting the tertiary winding of the transformer to a voltage source at its nominal voltage. Then the excitation current and copper losses are measured. The former by using current meters and the latter by using 3 watt meters and the identity $P_{tot} = V_a(t)I_a(t) + V_b(t)I_b(t) + V_c(t)I_c(t)$. The measurement setup can be seen in Figure 3.15

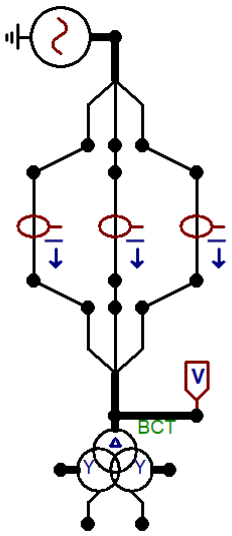

Figure 3.15: ATPDraw measurement setup for open circuit excitation current and losses

Table 3.4: Open circuit measurement results

	Measured Value	Test report value
Excitation line voltage [kV_{rms}]	10.5	10.5
Excitation Current [A_{rms}]	8.565	8.553
Excitation Loss [kW]	59.08	59.08

Short Circuit

The short circuit behavior was verified by exciting one winding while short circuiting the others. This is done in the order discussed before; HV-MV, HV-LV and MV-LV. The resistive losses are calculated using the same 3 watt meter setup as the open circuit method. The measurement setup can be seen in Figure 3.16. Note that the simulation uses a $1m\Omega$ resistance as a short circuit due to to ensure convergence.

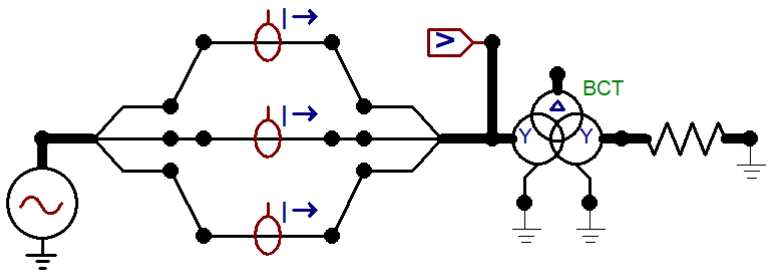

Figure 3.16: ATPDraw measurement setup for short circuit currents and losses

Table 3.5: Short circuit measurement results

	Measured Value	Test report value
HV-MV		
Short circuit voltage [%]	14.36	14.36
Short circuit current [A_{rms}]	384.89	384.9
Short circuit loss [kW]	230.8	230.79
HV-LV		
Short circuit voltage [%]	9.37	9.37
Short circuit current [A_{rms}]	1484.4	1485
Short circuit loss [kW]	64.3	64.3
MV-LV		
Short circuit voltage [%]	4.87	4.87
Short circuit current [A_{rms}]	1484.6	1485
Short circuit loss [kW]	59.7	59.7

From the results shown in table 3.4 and 3.5 one can conclude that the BCTRAN model has been implemented correctly for the measurements.

Transient

To correctly tune the transformer capacitances the values are tuned such that they match the bodeplot of a similar transformer. Suchh results were shared by KEMA laboratories [39]. As adding shunted capacitances are still an approximation, only the resonant frequencies will be matched. To obtain the measured frequency response, a standard lightning impulse (double exponent) will be fed through one of the phases. The output and input will be recorded and transformed to the frequency domain. Then the frequency response is taken by taking the fraction of output and input voltage. Note that all drawn capacitances are phase to earth, the phase to phase capacitances are neglected as the phases are on different windings.

The setup used to simulate these FRAs in ATPDraw can be seen in Figure 3.17.

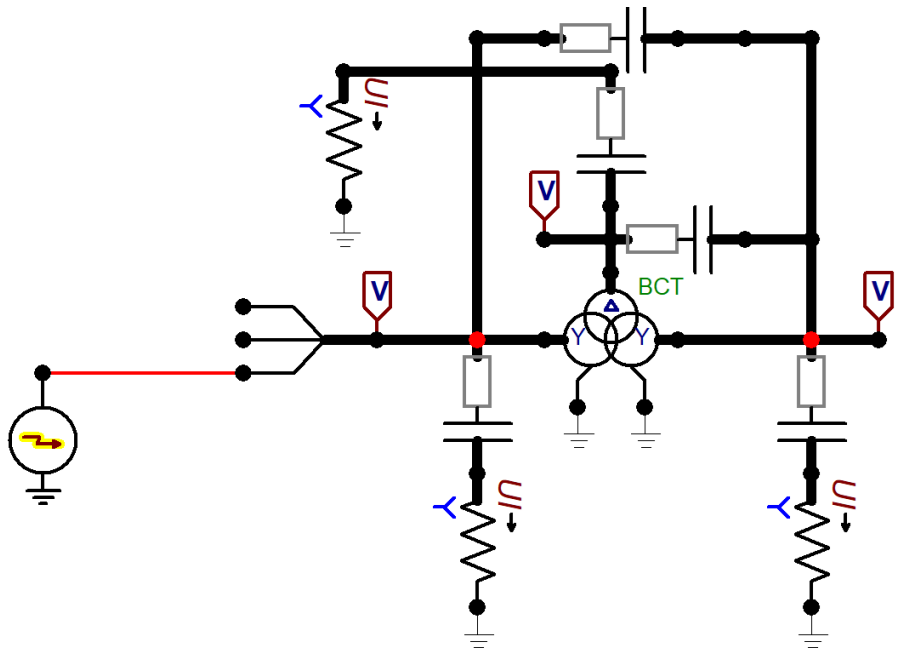

Figure 3.17: BCTRAN FRA Simulation

In this simulation one phase is connected to a double exponential lightning surge source. It matches the excitation signal used in the measurement report and the earthing configuration of the transformer. This source waveshape is a standard lightning impulse (with 3.6/18 μs) as stated in IEC60-2 (nowadays IEC60060-2). The capacitances represent the measured capacitances found in the measurement report. The series resistance is built-in and tuned to minimize numerical oscillations stemming from the trapezoid rule chosen such that it corresponds with a numerical damping of 0.1 [22]. In addition all shunted capacitances are shorted to avoid generation of floating sub-networks. After running the simulation the voltage transfer and admittance characteristics are calculated. This is done by dividing the FFT of the signals in frequency domain. Then the capacities are tweaked such that the first resonant frequencies from the simulation match those of the report.

After tuning, the final calculated FFT and the measured values from the report can be seen in Figure 3.18 , Figure 3.19 and 3.20.

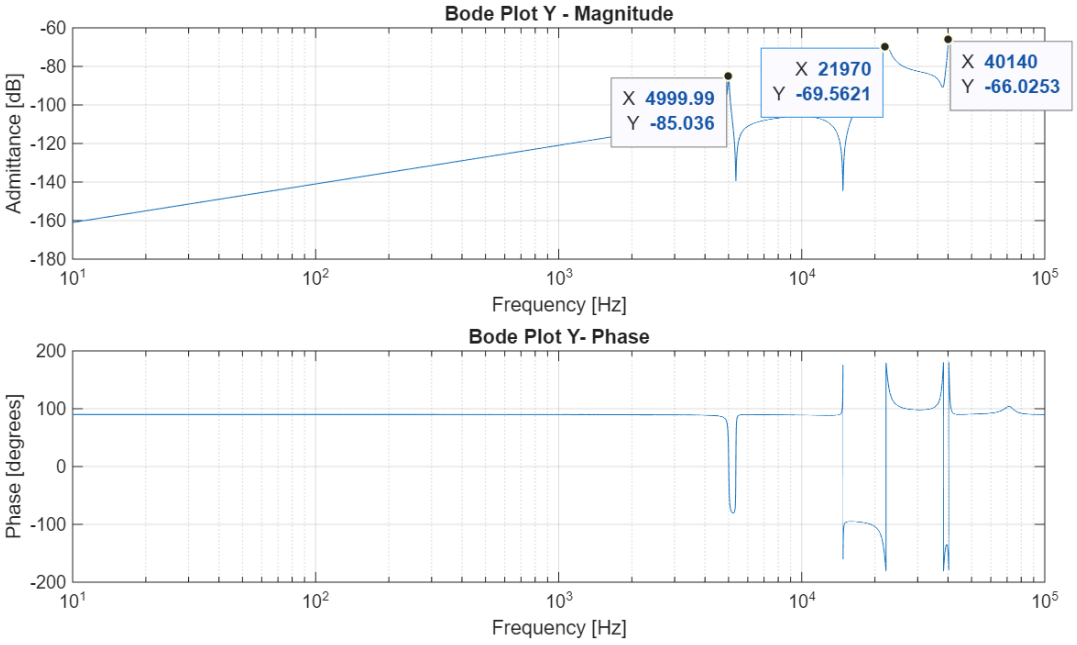

Figure 3.18: Calculated FRA with tuned capacitances

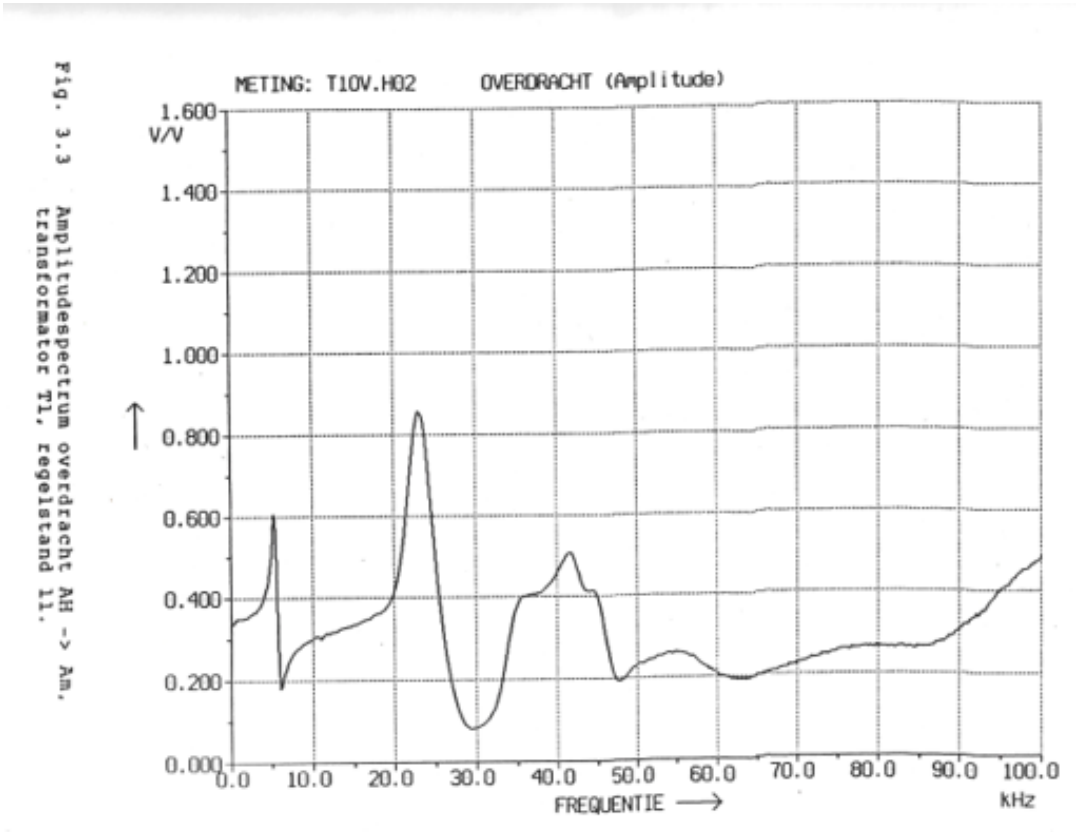

Figure 3.19: Measured FRA Amplitude transfer [39]

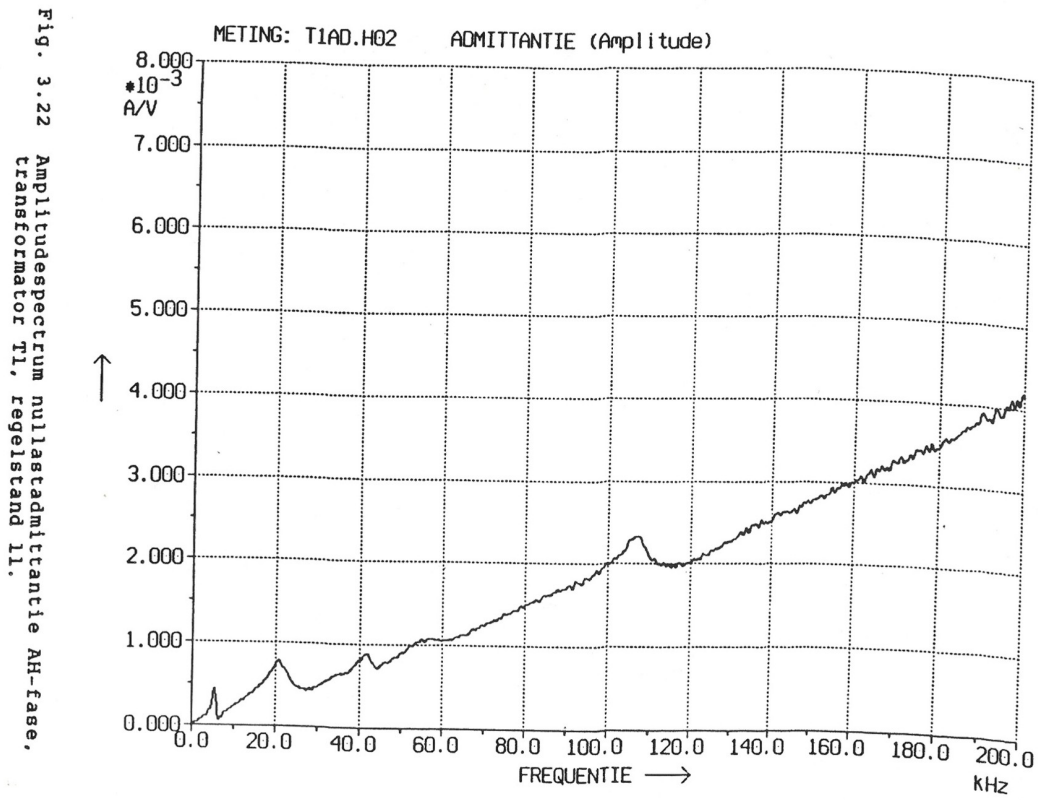

Figure 3.20: Measured FRA Admittance transfer [39]

Please note that the magnitudes are not matching in measurement and calculation. This was a conscious choice as it is determined by many more factors in the model. Matching the magnitude would require more detailed modeling as losses in the forms of core losses and winding resistances and other high frequency phenomena. In addition, series capacitances would need to be added. This would greatly increase the amount of parameters for fitting. Additionally, changing the transformer tap stance immediately changed the frequency transfer. Therefore, matching the resonant frequencies was assumed to be sufficient for the gray box model.

The final values of the capacitances can be seen in table Table 3.6, where CxN is the capacity to earth of primary, secondary or tertiary and Cxy the crossover capacity. While tuning the capacitances it was found that the crossover capacitances C_{12} and C_{23} and C_{2N} were most influential on the higher resonant frequencies. The 5kHz resonance was most sensitive to C_{1N} and C_{12}.

Table 3.6: Capacitance values of the transformer

Capacitance	**(nF)**
C1N	0.706666596
C2N	0.6673333128
C3N	7.952
C12	3.275
C23	0.534

Now that the cable and transformer models have been appropriately tested and tuned the simulation of the faults leading to the overvoltages can start.

4

Simulation Setup

This chapter will describe the implementation of the component models, integrated in a circuit simulating a generalized realistic grid section around a substation. First the type of scenario is discussed and how this can be modeled using the components in the previous chapter. Then the TSO thevenin equivalent (TenneT Thevenin circuit, voltage source, etc) is discussed.

4.1. Fault clearing

As mentioned before, the first transient origin to be evaluated will be fault clearing by the circuit breaker. There are many varieties in fault location and network topology which can lead to transient overvoltages. For example, the fault could be:

- In the substation
- Very close to the feeding transformer
- Behind the load transformer (50-20/10kV)
- Along a feeding cable
- Fed from multiple transformers
- In parallel to multiple cables or transformers

Which all lead to different fault currents and overvoltages.

As the goal of this study is to find the worst case, it is not required to take into account every permutation. The way this problem will be approached is to take the extremes in the case in addition to a "halfway point". For example, fault location is important for (mainly) the fault current. A location close to the feeding transformer can be taken (high fault current), plus a location far away and a fault in between.

This will still result in many combinations that are to be tested. A closer investigation will be done on combinations of components leading to the largest overvoltages. This is done to understand where they come from and how to mitigate them. The cases that will be considered are based on the observations made in subsection 3.1.1.

A schematic overview of the scenario can be seen in Figure A.1. This proposed circuit is based on the worst case and common case topologies that can be found in substations of Stedin that are equipped with the L-SEP GIS.

As the real substations are varied in size and components, completely modeling will be very complex (both in implementation and interpretation). It is easier to represent it in terms of its extremes using combinations of components and topologies.

This schematic is a collection of possible combinations. In other words, on each switchgear there is at least one of each branch drawn in the schematic. Some substations have more branches as the amount of bays is not equal everywhere, this in turn can also be parameterized. In the case that the busbar

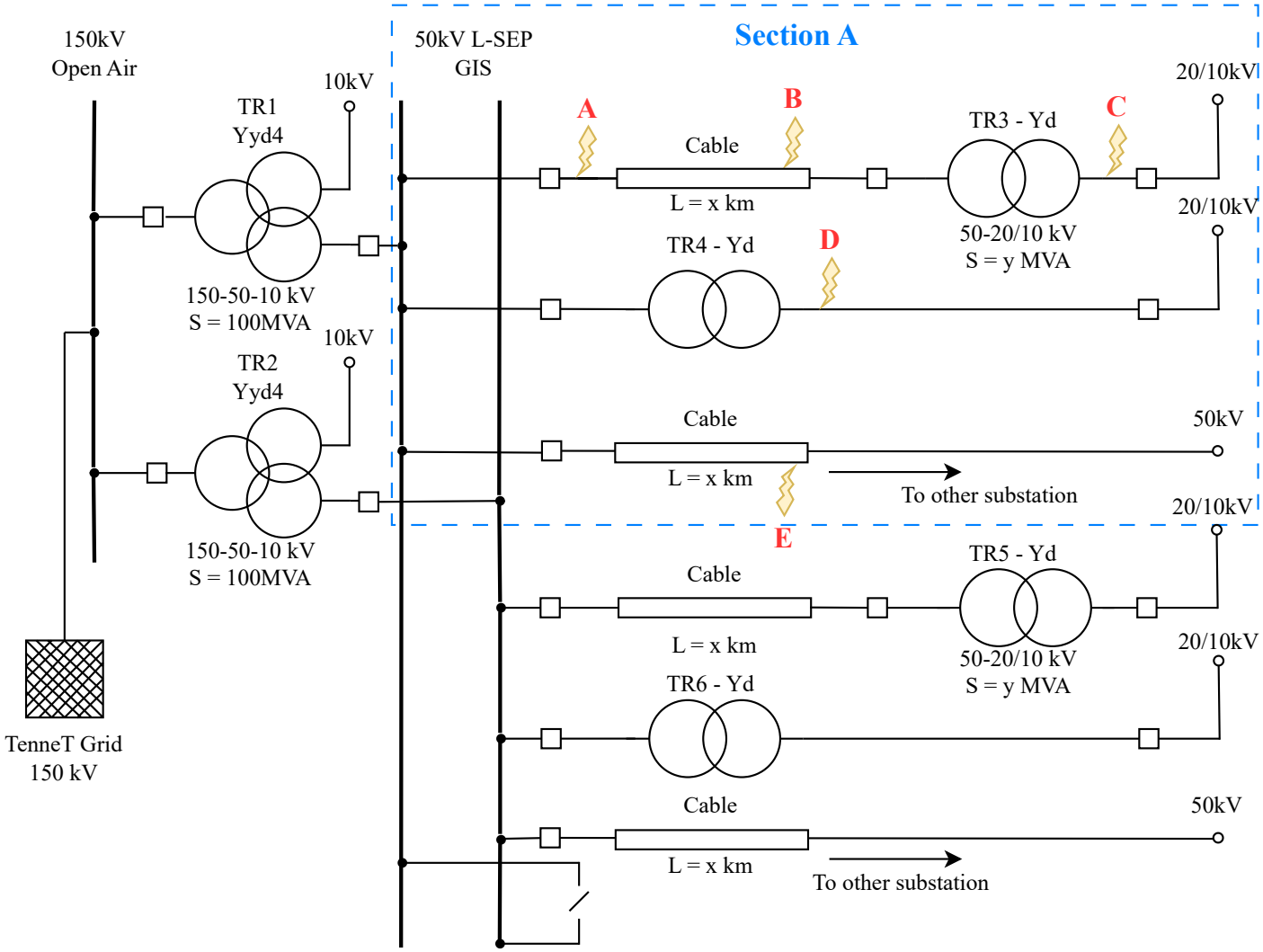

Figure 4.1: Schematic overview of the to be investigated scenario. Note that the busbar selection switch inside of the coupling bay is OPEN (N-1)

selection switch is open only one section (in this case section A) is studied starting with fault location A. An additional transformer can be added in parallel by closing this connection. Results from this study will in turn be used to see which combinations or topologies will not have to be investigated for other locations.

It is important to consider all capacitances (busbar, disconnector switch or GIS) of equal magnitude to the largest known one. In the case of no parallel branches capacitances in the order of the secondary winding of the feeding transformer to earth should be included. Take for example the case of Utrecht Merwedekanaal. In this case the transformer connects to the GIS via a bushing and Duresca busbar system with a shunted capacitance ($\sim 4nF$). The GIS capacitance ($300pF$ per bay) should then also be taken into account. In the worst case however, these are not included as they are negligible when components are added in parallel.

4.1.1. Fault location A

In the case of location A, a fault occurs between the breaker and the outgoing cable at the GIS terminal. Parallel to this there can be a transformer connected to the rail, a cable going to another 50kV substation

which can deliver or draw power from the substation or a cable connecting to another transformer.

For all components there are parameters which need to be varied as well. Namely: method transformer earthing, cable length and parallel components.

For the topologies it is important to consider what will be connected at what time. I.e. will the system be N-1 or N-0, which leads to more parallel connected components and higher short circuit power.

4.1.2. Fault location B

Location B is a fault which is along the cable, of length x, between the breaker and the outgoing 50-20/10 kV transformer. This fault is then located at length $L = \Delta x\%$. There are two extra variables in this case: Total cable length and fault distance. For Stedin the maximum length of such a cable is $\sim 10km$.

The results from location A can be used to exclude certain combinations for the study of location B.

4.1.3. Fault location C

Location C is a fault which occurs behind the 50-20/10kV transformer. Here it is important to use the correct transformer parameters. Just like with situation A & B, based on the results, combinations of certain parameters can be excluded from the study if they do not lead to high overvoltages..

4.1.4. Fault location D

Fault location D is similar to C, except for the transformer directly being connected to the breaker. It can be seen as a cable connection where the cable is too small to introduce wave like behavior or add significant capacitance.

4.1.5. Fault location E

This location is a fault located along a connecting cable between two substations. In addition to total cable length and fault distance there is an additional parameter: Whether this cable sends or receives power. This influences the fault current it needs to break and therefore the transient overvoltage. In essence this is similar to changing the short circuit power of the circuit.

4.1.6. Sensitivity analysis

To find the topology and parameter set leading to maximum overvoltages, a sensitivity analysis must be done. This starts of simple, and adds more parallel components with varying lengths to see what happens to the overvoltages. This way conclusions can be drawn on what parts greatly influence overvoltages.

The values which will be extracted from these simulations are:

- Peak overvoltage to earth $[kVp]$
- Peak fault current $[kAp]$
- Peak phase-to-phase overvoltage $[kVp]$
- Max $\frac{dV}{dt}$ $[kV/\mu s]$ (max RRRV) [1]

4.2. Simulation Setup

To simulate the scenarios, ATP-EMTP was used. The simulations were ran using ATPDraw, which easily allows for transient calculations on electrical power systems.

The setup for fault clearance takes into account multiple factors. Fault location and grid topology. The model for a fault at location A can be seen in Figure 4.2. The maximum three phase fault current supplied from the 150kV side to the 150/52kV transformers was requested from TenneT for the locations where the L-SEP has been installed. It was stated to be 32.8 kA with a grid constant (to settle the DC component) of 47.64 ms. The single phase fault current is 4.4kA. The source is connected by line which has a Thevenin impedance derived from the maximum three phase and single phase fault current and grid constant. For the single phase fault the relation for a single phase fault can be used.

[1] Note that this is faster than the official definition of RRRV as it is its maximum tangent

$$I = \frac{3V_{ph}}{Z_1 + Z_2 + Z_0} \text{ where } Z_1 = Z_2 \tag{4.1}$$

When this equation is rearranged to solve for Z_0 while keeping in mind that $\tau = \frac{L}{R}$, the following symmetrical impedance parameters can be obtained that represent the Thevenin equivalent circuit.

- $R_0 = 3.79\Omega$
- $L_0 = 0.1706mH$
- $R_1 = 186m\Omega$
- $L_1 = 8.4mH$

This then connects to the tuned BCTRAN model shown in Figure 3.17. The secondary terminal is then connected to the receiving end of the L-SEP GIS. The breaker is modeled as 3 parallel ideal switches which clear at the current zero time of the respective phases at a predetermined time. The closing time of the cable has been set at $t = -1$ ensuring steady state fault current (free of DC component) is flowing. Should this not be the case, a low valued series resistance is added to the fault. Behind the L-SEP is a shunted 3 phase breaker. This will simulate a short circuit between the terminal of the L-SEP and the outgoing cable. This cable is the same one as mentioned before and will vary in length for different fault locations and scenarios. Lastly a load is connected which is an equivalent impedance ensuring a nominal steady state current ($\sim 700A$) in the non faulted topology. An additional transformer can also be added and placed in parallel, to increase the short circuit power and simulate the closure of the coupling switch.

To account for parallel connections to the GIS, additional models can be placed in parallel. These models are: Single cable with star connected load (neutral earthed), single cable open end and cable connected outgoing transformer. Of these the lengths, amounts and in the case of outgoing transformer the earthing, can be varied for different values. The cables connect to an inductive load which draws nominal current. Purely inductive loads connected to a cable are rare in the Stedin grids, therefore the case of an open ended cable is also considered.

This model includes all components that can be connected in parallel. The transformer is a common MV-LV 50-20kV transformer. This model is a BCTRAN representation of the Tironi Yd transformer. This measurement report had the same open and short circuit parameters as that of the larger 150kV transformer but came with additional information on winding capacitances for transient behavior. This eliminated the need for another capacitor tuning routine.

To ensure the transient time domain plots can be observed the sample time of simulation is $\Delta t = 0.25\mu s$. The total runtime is $200ms$, where the breaker representing the short circuit has been open since time instance -1s. This is done to ensure steady state fault current at the instance of switching. The time when the breaker opens is at 60ms Nominal operating frequency is equal to $f = 50Hz$.

With a simulation plan and proper set up, investigation of transient overvoltages due to fault clearing can be started.

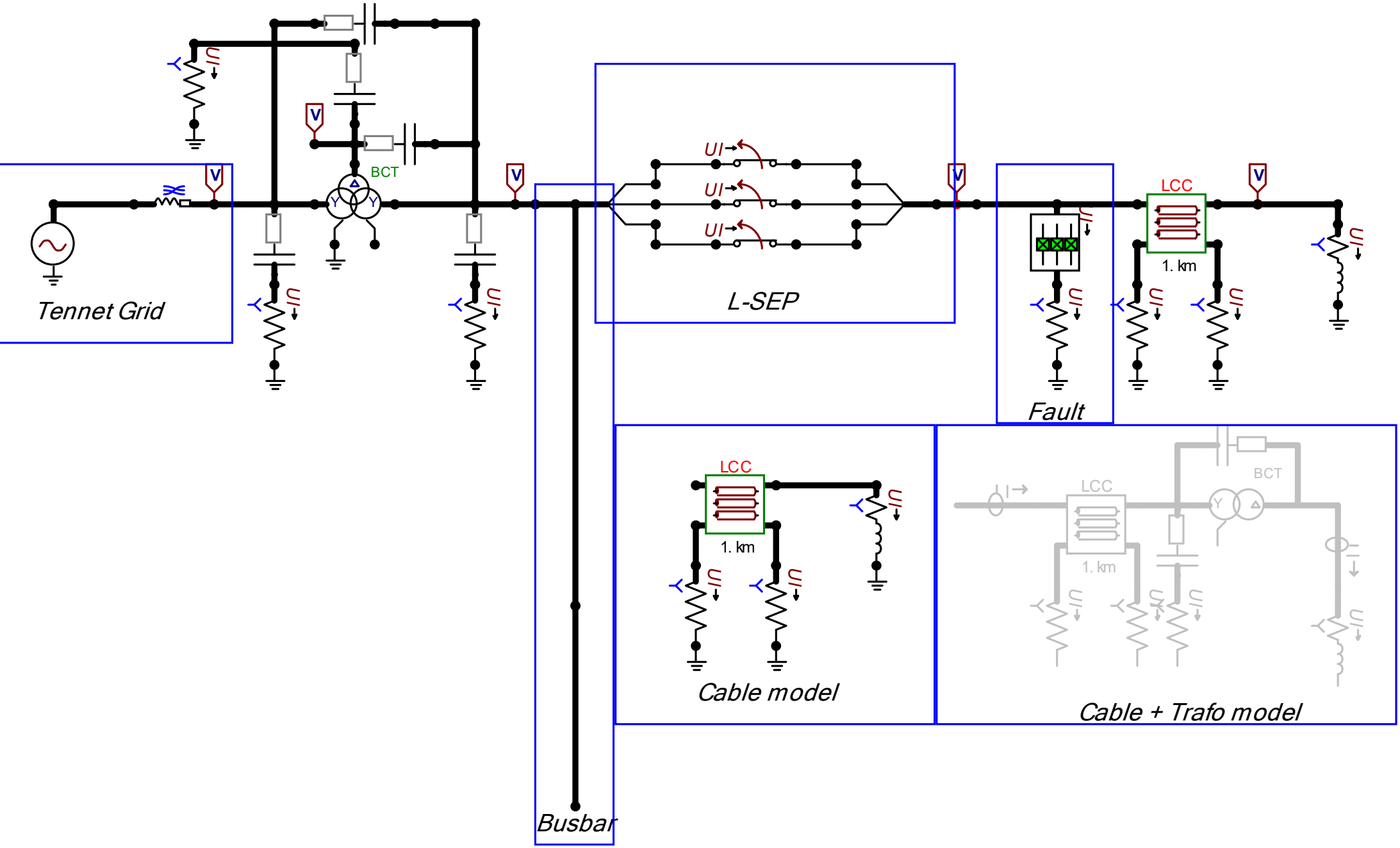

Figure 4.2: Simulation setup for calculation of fault currents due to switching fault currents

5

Results

To model transient overvoltages it is important to consider topology and location of the fault. In general, transient overvoltages are dependent on source reactance (determining short circuit power and the fault current), its capacitance, load impedance and damping. This fault current is dependent on net topology, location and other component parameters such as cable length and earthing. To gain intuition for finding the worst case overvoltage, a sensitivity analysis was done on the aforementioned dependencies.

As the study considers the worst case overvoltages, first three phase faults are considered. These generally lead to the highest overvoltages irrespective of other topologies. The conclusions drawn from those results will be used when considering other types of faults. There are however two types of three phase faults. Phase to earth and phase to phase. A phase to phase fault is rare to occur in the Stedin grid. Faults can occur inside the GIS, along cables or at terminations/joints. The faults that can occur are either that earthing switches are unintentionally closed, dielectric breakdown occurs, physical damage takes place or another failure mode activates. In all cases the a phase to phase fault will be earthed instead as well. For this reason the initial emphasis is on three phase to earth faults first.

The results are first seen from faults and changes in parameters at fault location A. These are tabulated and interpreted. From these results, conclusions are drawn and other locations and configurations are considered. From these results a selection of cases are made of which the results are explained. The upper ceiling on what is allowed in the current switchgear can be deduced from Figure 1.2 which is designed based on the IEC 62271-1 [40] standard. These values can be seen in Table 5.1, where common value means the voltage between phase and earth or phase to phase and acreoss isolating distance the voltage between opened breaker contacts.

Table 5.1: Rated Withstand Voltages (Ud and Up) in Peak kV for 52 kV and 72.5 kV GIS according to IEC 62271-1 (Series I). Note that the original common value was in RMS and adjusted to kVp

Rated Voltage (Ur)	Withstand Voltage Type	Common Value (kV peak)	Across Isolating Distance (kV peak)
52 kV	Ud (Power-Frequency)	≈ 134	≈ 156
	Up (Lightning Impulse)	250	290
72.5 kV	Ud (Power-Frequency)	≈ 198	≈ 226
	Up (Lightning Impulse)	325	375

5.1. Sensitivity analysis

To make sense of the results from the sensitivity analysis the simulations are assigned an ID based upon the parameters and topology shown in Appendix A Table A.1. Each study has its own unique case ID. In the case of fault location A, the studies start with ID A.x where x is the study number. The column next to it denotes the earthing configuration of the feeding transformer. YnY in this case, implies that the primary star neutral point is earthed while the secondary is unearthed. Note that it is Stedin policy to never earth both star neutral points at the same transformer.[1] This is to avoid the zero sequence component of the fault current propagating between higher and lower voltage levels. In the case that YnY - YnY is written down it implies that there are two feeding transformers with their respective star neutral point earthing configuration. Whenever an outgoing 50-10kV transformer is connected by cable, its earthing configuration is denoted in the third column. It is always of the type YD, where its primary star neutral point can be grounded. The last column denotes additional parallel components such as cables with their respective lengths.

The extraction of results and graphs has been automated by interfacing ATPDraw via a MATLAB livescript88 . The simulation flow went as follows:

1. ATPDraw simulation is altered to match case
2. ATPDraw is ran
3. Case number is iterated in MATLAB script
4. MATLAB script converts data files to .mat files
5. MATLAB script saves relevant figures and extracts values
    - Peak overvoltage to earth $[kVp]$
    - Peak fault current $[kAp]$
    - Peak phase-to-phase overvoltage $[kVp]$
    - Max $\frac{dV}{dt}$ $[kV/\mu s]$ (max RRRV)

It must be noted that the IEC standard defines the RRRV as a tangent line instead of the maximum derivative. This leads to lower values compared to the method used in this thesis.

Comprehensive tables of all results can be seen in Appendix B. This matches the case IDs described before, containing only contains a small description to further distinguish the simulations. Special individual cases will be denoted with ID X.x in later analysis. A table describing the abbreviations used can be seen in Table 5.2.

Table 5.2: Nomenclature for network configurations and components.

Abbreviation/Term	Description
YnY	earthing, Primary star neutral point earthed, secondary unearthed
1C	One parallel cable
Min	Minimal cable length(100m)
VS	Very short cable length(500m)
S	Short cable length(1km)
M	Medium cable length(5km)
L	Long cable length(10km)
2C	Two parallel cables
C2OT	Cable to outgoing transformer
YnY-YD	earthing of feeding and outgoing transformer
YnY/YnY-YnD	earthing of parallel feeding and outgoing transformer
1C OE	One cable open ended

[1] Note that the transformer is of the type Yyd, the delta winding is not noted in the naming convention but is part of every source transformer

5.2. Case A

From the initial simulations seen in Table B.1 a few conclusions can be drawn. To validate the results, a simplified model is created that can explain the observed simulation results. For this the following framework is used.

It is first assumed that the transient overvoltage consists out of two parts. One part that represents the steady state sinusoidal voltage, denoted as V_{ss}. The second part has to do with the transient from the oscillatory behavior of the connected components, denoted as V_t. In all cases peak value is considered unless stated otherwise.

In other words, the transient overvoltage can be denoted as

$$V_{overvoltage} = V_{ss} + V_t \text{ or } V_{overvoltage} = k_{pp} k_{af} V_{p,rated} \tag{5.1}$$

Where k_{pp} is the pole to clear factor and k_{af} is the amplitude factor. k_{pp} corresponds to the steady state part which is mainly determined by symmetrical components and earthing configuration. k_{af} determines the oscillatory transient part, which is determined by damping and the underlying differential equations of the network. This can be visualised in Figure 5.1

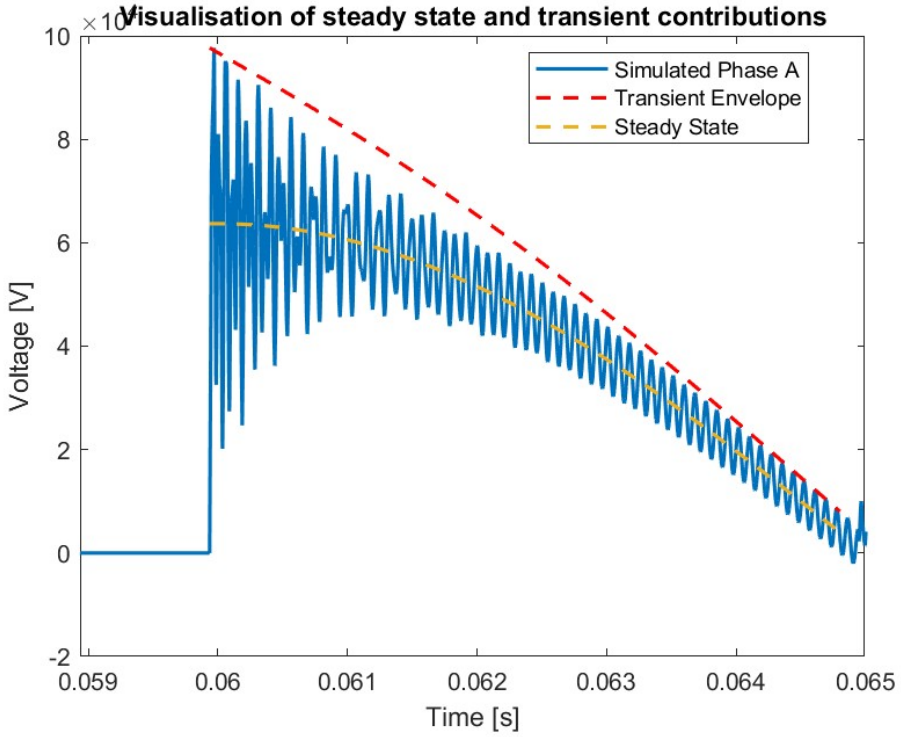

Figure 5.1: Example visualisation of the transient overvoltage components

More on this can be read in subsection 5.2.2.

The maximum values of these parameters are known. In the case of the steady state, the $k_{pp} \leq 1.5$ in the case of a unearthed network. In the case of the oscillatory part, $k_{af} \leq 2$ which corresponds to a pure LC resonance.

In the next subsections, first the k_{pp} factor, determined by symmetrical components, will be assessed. Then a simplified model will be introduced that can be used to understand the influence of capacitance and damping is to k_{af}.

5.2.1. Earthing configuration

From Table B.1, one can clearly observe the importance of earthing in reducing the peak overvoltage. When one takes the simplest case, a feeding transformer with its respective star neutral point earthing

and a terminal fault at location A, the difference in overvoltage is large. This is reflected in Table 5.3.

Table 5.3: Scenario A Selected Cases

Case ID	Description	Peak Fault Current (kAp)	Peak Overvoltage (kVp)	Peak Phase-Phase (kVp)	RRRV (kV/μs)
A.1	YnY Base	10.1	97.6	122.2	7.72
A.2	YYn Base	10.1	71.8	85.5	6.73

In this case no parallel components are added to the circuit. The only components are the BCTRAN transformer model, the breaker and a 3 phase short circuit to ground at its outgoing terminal. Please note that this case is highly unlikely, as the only direct capacitance to earth in the circuit is the transformer secondary winding capacitance. Nevertheless, this case can still describe a lot of information on transient behavior for other cases too.

One can observe that for a unearthed secondary winding the peak overvoltage is larger then when it is grounded. This can be seen in the time domain plots in Figure 5.2 and Figure 5.6

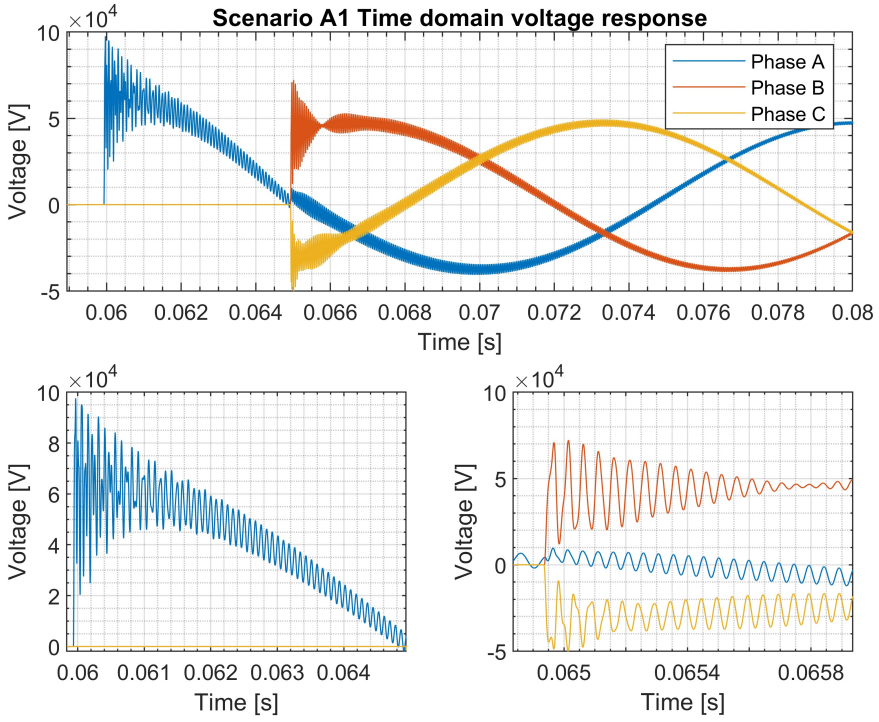

Figure 5.2: Case A1 Time domain plots, Top figure is the voltage decay, bottom left a zoom in of the first pole to clear, bottom right the second pole to clear.

The first thing one can observe is that the first pole to clear,phase A, of the unearthed network (feeding transformer YnY) has a significantly higher voltage compared to the other phases. The second and third phases then extinguish at the same time instance. When one observes the bottom left figure, one can observe that the transient is superimposed on top of a baseline 50 Hz voltage. At the instance of switching the first pole, the steady state part of the transient has an amplitude of $V_{a,1ph} = 64kVp$. If one takes a look at the voltage level when all phases are healthy and in steady state the value is $V_{a,ss} = 42kVp$ (average from positive and negative amplitude). From this the first pole to clear factor (FPTC) can be calculated. This is $k_{pp} = 1.5$.

For a brief refresher on symmetrical components, the reader can consult Appendix C section C.1. When

one considers case A.1 at the time that the first pole opens, it can be represented by the following approximated schematic.

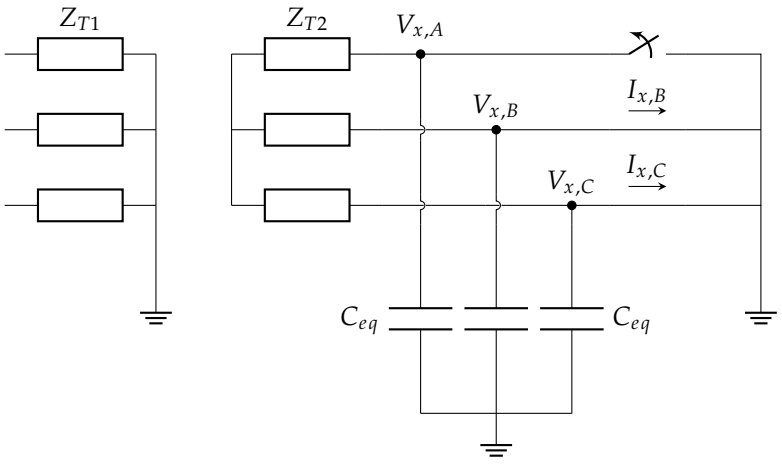

Figure 5.3: Equivalent circuit diagram

The sequence networks can be seen in Figure 5.4

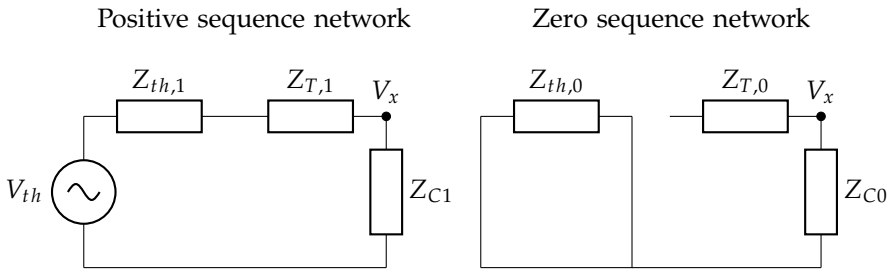

Figure 5.4: Sequence networks of positive and zero sequence

In the case of a double line to earth fault, the sequence networks should be connected in parallel at the location of the fault. This can be seen in Figure 5.5

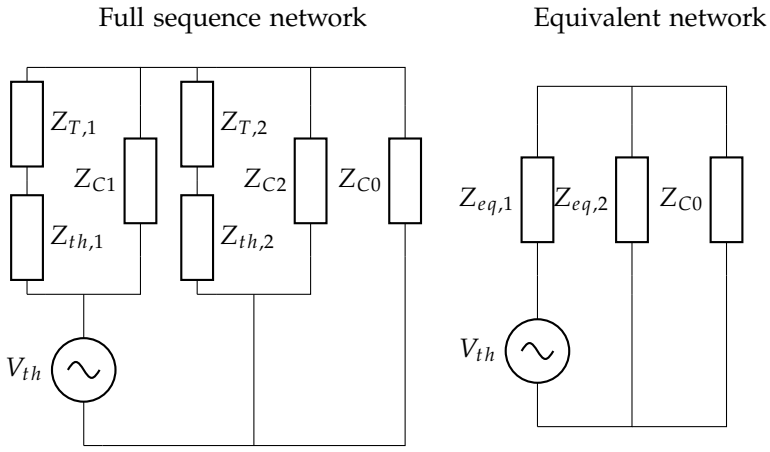

Figure 5.5: Sequence networks of positive and zero sequence

Where are $Z_{eq,1} = (Z_{T,1} + Z_{Th,1})//Z_{C1}$ and $Z_{eq,2} = (Z_{T,2} + Z_{Th,2})//Z_{C2}$ respectively. Connected

in parallel at at faulted location X. As the shunted capacitance is in the order of nano Farad and $Z_C = Z_{C0} = Z_{C1} = Z_{C2}$ the following holds:

$$Z_{eq,1} = Z_{T,1} + Z_{th,1} \;//\; Z_C \text{ where } Z_C >> Z_{T,1} + Z_{th,1} \tag{5.2}$$

$$Z_{eq,1} = Z_{T,1} + Z_{th,1} \tag{5.3}$$

Which also holds for $Z_{eq,2}$. At the instance of breaking the voltage at A can be found by using the relationship found in Equation C.40

$$V_a = 3V_{af}\left(\frac{Z_2 Z_0}{Z_1 Z_2 + Z_1 Z_0 + Z_2 Z_0}\right) \tag{5.4}$$

If one takes $k = \dfrac{Z_0}{Z_1}$ and assume $Z_1 = Z_2$ the following relation arises:

$$V_a = V_{af}\left(\frac{3k}{1+2k}\right) \tag{5.5}$$

Using this relation, one can determine the FPTC. In this case, the FPTC is calculated to be $k_{pp} = \frac{Va}{V_{af}} = 1.5$, which closely matches that of the observed ratio of $k_{pp} \approx 1.52$.

From Figure 5.2 it can also be observed that the remaining two phases clear at the same time instance. This can be attributed to the fact that the currents mirror each other in a double earth to ground fault which can be attributed to the relation Equation C.44. As discussed, $|Z_C| = |Z_0| >> Z_1 = Z_2$. This reduces the relations to:

$$I_0 = -\frac{V_{af} Z_2}{Z_0(Z_1 + Z_2)} \tag{5.6}$$

$$I_1 = \frac{V_{af}}{Z_1 + Z_2} \tag{5.7}$$

$$I_2 = -\frac{V_{af}}{Z_1 + Z_2} \tag{5.8}$$

Note that the positive and negative sequence currents are 180° out of phase. When one converts back to the phase domain, using Equation C.10, $\angle I_b = -\angle I_c$. As the breaker is ideal and switches at the current zero, this leads to a recovery voltage at the same time instance.

For the case of an earthed secondary star neutral point the overvoltage is significantly lower. Here one can observe that, again, the transient is composed of two parts: A 50Hz sinusoidal voltage and an additional transient. The sinusoidal voltage can be approximated at $V_{a,1ph} = 42kVp$ and the steady state as $V_{a,ss} = 42kV$. This leads to a measured FPTC factor of $k_{pp} \approx 1$. It can also be observed that the breaking of phases B and C can be seen on phase A. This has to do with the changing earthing configuration, and currents being able to flow through earth to the other phases when one closes [12].

Adding the star neutral to earth connection on the transformer secondary winding changes the zero sequence and faulted network. This can be seen in Figure 5.7

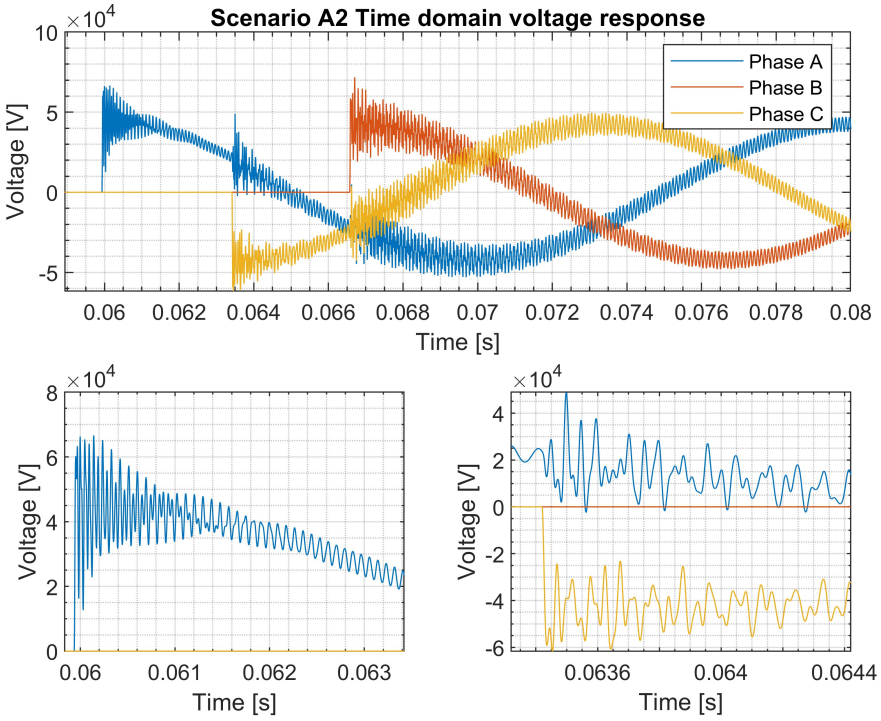

Figure 5.6: Case A2 Time domain plots, Top figure is the voltage decay, bottom left a zoom in of the first pole to clear, bottom right the second pole to clear.

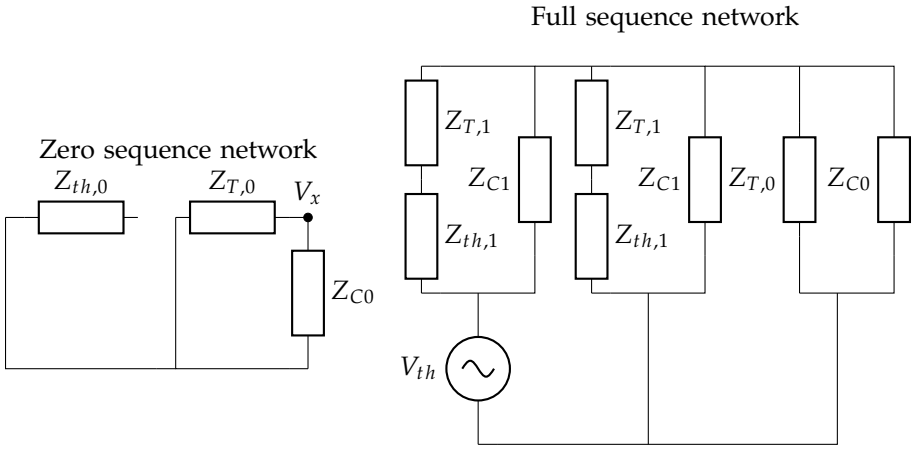

Figure 5.7: Zero and faulted sequence networks for inverted neutral winding earthing

In this case the $Z_{T,1}$ and $Z_{th,1}$ need to be obtained in order to find the ratio k.

From subsection 3.6.2, it can be stated that the short circuit voltage of the transformer is 14.36%. The transformer has a rated power of $S = 100\text{MVA}$ and a primary voltage of $150kV$. $Z_1 = Z_2$ can be calculated by first calculating the base impedance.

$$Z_b = \frac{(V_{r,kV})^2}{S_{MVA}} = \frac{150^2}{100} = 225\Omega \tag{5.9}$$

Then, $Z_{0,T2} = Z_{1,T2} = Z_{2,T2} = 14.36\% * Z_b = 32.3j\Omega$. As $Z_{eq,1} = Z_{T,1} + Z_{th,1}$, $Z_{th,1}$ is determined to be $2.64j\Omega$ from section 4.2. From this one can state that $Z_{T,1} >> Z_{th,1}$. This then leads to a $k = \frac{Z0}{Z1} = 1$.

Using the same relation found in Equation 5.5 an FPTC factor of $k_{pp} = 1$ is found. Compared to the YnY earthed case, the other phases do not close at the same time instance. When one takes Equation C.44 and the fact that $Z_{eq,0} = Z_{eq,1} = Z_{eq,2} = Z_{T,1}$, the following results can be observed:

$$I_0 = \frac{V_{af}}{3Z_{T2}} \tag{5.10}$$

$$I_1 = \frac{2V_{af}}{3Z_{T2}} \tag{5.11}$$

$$I_2 = -\frac{V_{af}}{3Z_{T2}} \tag{5.12}$$

Not that in this case $I_0 = -I_2$. When one converts back to the phase domain using Equation C.10 this leads to $\angle I_b = 120°$ and $\angle I_c = 240°$. This is also observed from the time domain voltage plots, as the phase difference of between the breaking times of phase C and B is approximately 60°. Which is indicative of the interruption of currents with relative phase difference of 120°.

5.2.2. The Amplitude Factor and Damping

As earlier stated, the overvoltage consists out of a steady state part and a transient part.

$$V_{overvoltage} = V_{ss} + V_t \tag{5.13}$$

In terms of peak overvoltage this can be simplified to

$$V_p = k_{af} k_{pp} V_{p,rated} \tag{5.14}$$

Where k_{pp} is the first pole to clear factor determined by the grid earthing, and k_{af} the amplitude factor of the transient part. Calculating the amplitude factor is non-trivial, which is why many standards exist to avoid calculation. The difficulty lies within the frequency characteristic of the grid. In the case of the YnY feeding transformer it has a tuned frequency response which reacts to a step voltage. Solving this analytically would require solving either very difficult differential equations or convolution integrals.

However, it is still possible to try and approximate the result using simplified parallel RLC networks, which is used to understand transient behavior in literature [41][12][9]. The idea is to create a model that describes the peak value (also referred to as overshoot or A, which relates to $k_{af} = 1 + A$) in terms of equivalent resistances, inductances and capacitances. The internal couplings via mutual inductances, winding losses and capacitive coupling modeled by the BCTRAN model will be simplified to an RLC. Whenever a parallel load then is added, such as a cable (which is again an approximation of the real cable which includes damping), only the shunt capacitance will change.

Once the simplified values for R,L and C are found more capacitance can be added to observe how k_{af} is influenced. This model can then be used when calculating phase to phase amplitude factors as the circuit network changes when more poles open. Note that when one changes the earthing configuration, the damping should be recalculated as coupled inductances change.

First the inductance L is obtained. As the shunted capacitances are all relatively small, the majority of the steady state current flows through the inductor. Its value is obtained from the steady state voltage $V_{p,ss} = V_{rated} k_{pp}$ and the peak fault current.

$$L = \frac{V_{p,ss}}{\omega_0 I_p} = 0.0202H \tag{5.15}$$

The capacitance is taken as an equivalent all capacitances connected to the transformer output node (see Figure 3.17) as seen in Figure 5.8a and is determined to be $C_{eq} = 1.7nF$. However, simply adding a capacitor in parallel to an inductor would lead to an amplitude factor of 2. This occurs due to the fact that there is no damping in this equivalent circuit compared to that of the BCTRAN model. To take into

account the damping a resistance is added in parallel too. The magnitude can be determined using the relations of overshoot an damping in a parallel RLC circuit.

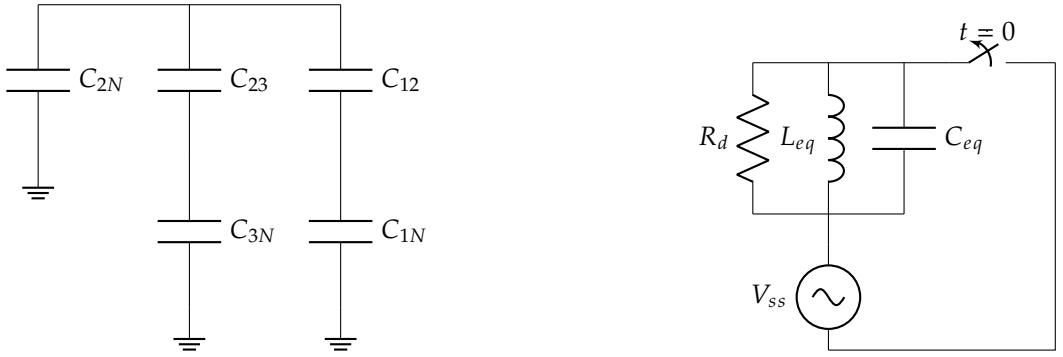

(a) Equivalent Shunt Capacitance **(b)** Parallel RLC model

Figure 5.8: Simplified Transient Model

The simulated k_{af} can be found by computing the ratio of $k_{af} = \dfrac{V_{p,sim}}{k_{pp} V_{p,rated}} = 1.53$. From this value, the overshoot and damping can be calculated. Consider the overshoot (A) of an underdampened parallel RLC circuit [42].

$$A = k_{af} - 1 = \exp\left(\frac{-\zeta\pi}{\sqrt{1-\zeta^2}}\right) \tag{5.16}$$

$$\zeta = \frac{-\ln A}{\sqrt{\pi^2 + \ln^2(A)}} \tag{5.17}$$

From this, the required damping is obtained for the measured k_{af} which can be implemented in the simplified model. This value is calculated to be $\zeta = 0.198$. Then, using the relationship for damping in a parallel RLC the resistance is found.

$$\zeta = \frac{1}{2R}\sqrt{\frac{L}{C}} \tag{5.18}$$

$$R = \frac{1}{2\zeta}\sqrt{\frac{L}{C}} = 8.7k\Omega \tag{5.19}$$

When one then creates the simplified equivalent model, the following time domain plots can be seen in Figure 5.9.

From the time domain plot one can observe that the BCTRAN phase A transient contains a lot of additional frequency components. Namely at the tuned frequencies of 20kHz & 40kHz and at another 12kHz resonance. During tuning it was observed that the crossover capacitances C_{12} and C_{23} and shunt capacitance C_{2N} determined the largest resonant frequencies. These are also the capacitances closest to the transient origin (i.e. breaker). The reason why the BCTRAN phase A transient has a differing lowest resonant frequency is suspected to be due to the following.

1. The first resonance has been tuned using a voltage and admittance transfer while in this case the transient origin is located on the secondary (unlike when tuning)
2. The transformer capacitances were tuned in accordance to the KEMA tests [39]. This means earthing (YnYn) and excitation signals (lightning vs step) are different.

As the equivalent model only has one LC pair, only one frequency can be represented. Nevertheless, the approximation displays the correct k_{af} which confirms the validity of the parallel RLC model.

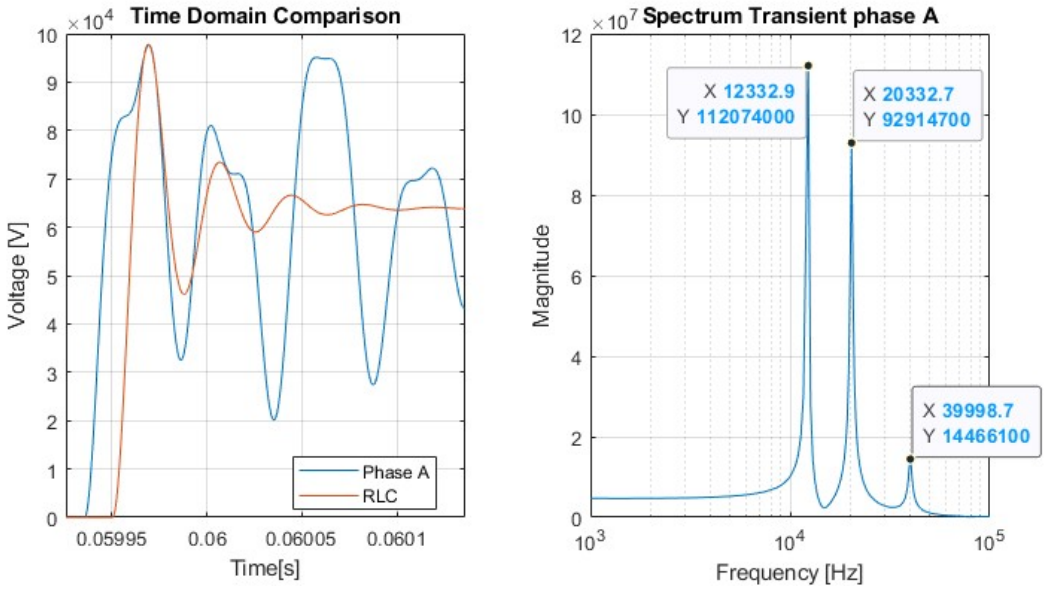

Figure 5.9: Left: Time domain comparison of equivalent circuit response and BCTRAN phase A. Right the spectral content of the phase A voltage

However, simply matching the observed phase to earth k_{af} to a damping with equivalent resistance is circular reasoning. The simplified RLC model, with fitted damping resistance representing the damping from the BCTRAN model only, can still be used to evaluate the overvoltages from the second and third poles that clear. Whenever the last two poles clear, the winding capacitances of the other phases are added in parallel to the source side of the breaker and the simplified RLC model. This is of importance for the other simulated quantity: the phase-to-phase voltage.

For unearthed networks (Non-effective earthing where only a capacitance to earth is added where $\frac{X0}{X1} \approx 1.2 * 10^6$), the phase-to-phase voltage is largest. This can be attributed to the simultaneous breaking of the second and third poles to clear. This breaking leads to a transient overvoltage which is essentially doubled in magnitude as the difference is taken of the peaks. The phase voltage and currents can be seen in Figure 5.10 and Figure 5.12

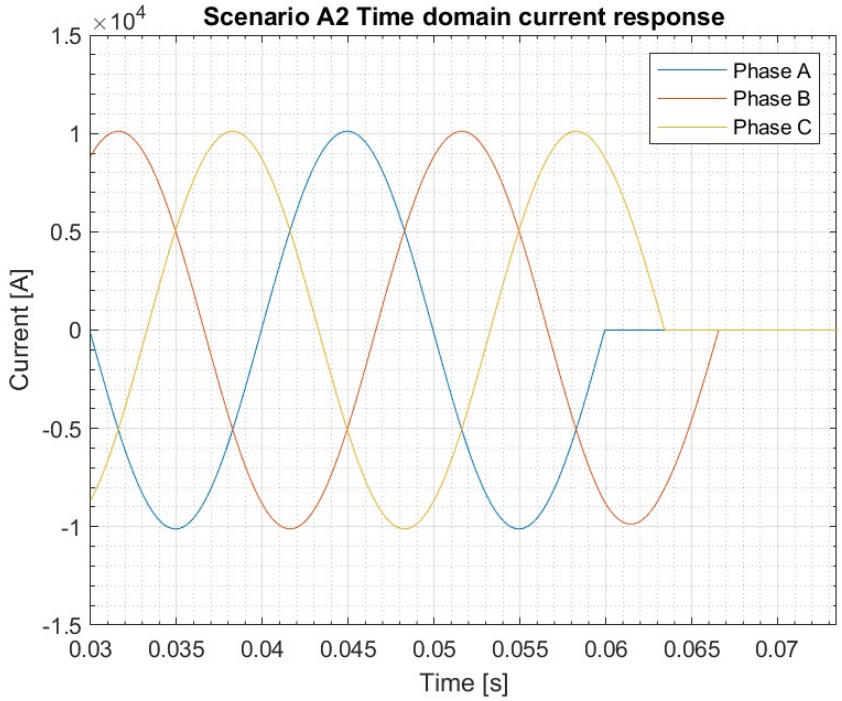

Figure 5.10: Phase currents for case A1

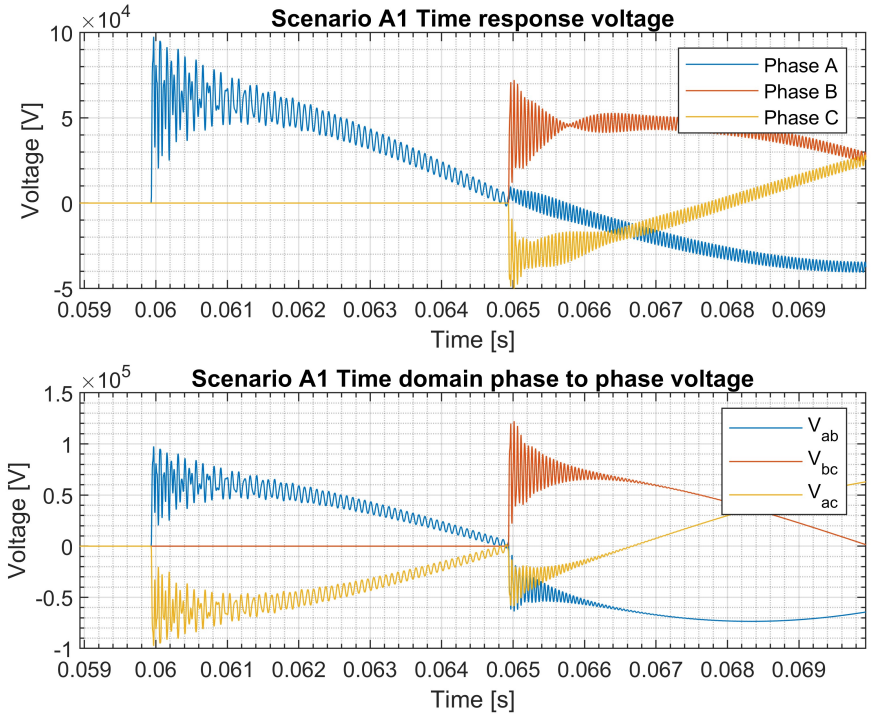

Figure 5.11: Phase to phase voltage for case A1

It is clear that the phase to phase voltage peak is an effect of the last two phases closing simultaneously. The peak value is $122.2kV$, which can be confirmed by usage of the amplitude and FPTC factor. From literature [41] k_{pp} of the second and third poles is $\frac{1}{2}\sqrt{2}$. Observing the steady state phase to phase voltage V_{ss} of V_{bc}, it can be approximated to $\approx 75kV$ which corresponds to $V_{ss,p2p} = 2 * V_{p,rated} * k_{pp} = 73.5kV$

from the respective k_{pp} Then using Equation 5.14 the theoretical phase to phase peak can be determined to be:

$$V_{p2p} = 2V_{p,rated} * k_{af} * k_{pp} = 112kV \tag{5.20}$$

This value is lower than the simulated value. As the second pole to clear factor seems to be calculated correctly, it implies that k_{af} is higher than expected. This in turn implies that the damping has decreased in the circuit when it changed from a 3 phase fault to a 2 phase fault. This new $k_{af,2p}$ for the circuit in a two phase to earth configuration is 1.673, which corresponds to a $\zeta_{2p} = 0.1249$. In other words, when the system changed to a new representation, damping decreased. It is suspected that the capacitance seen from the breaker terminal changed substantially. As the network ceases to be symmetrical, the simplified model from before does not sufficiently model the amplitude factor. Consider the equivalent model representing the grid just after breaking the first in Figure 5.12.

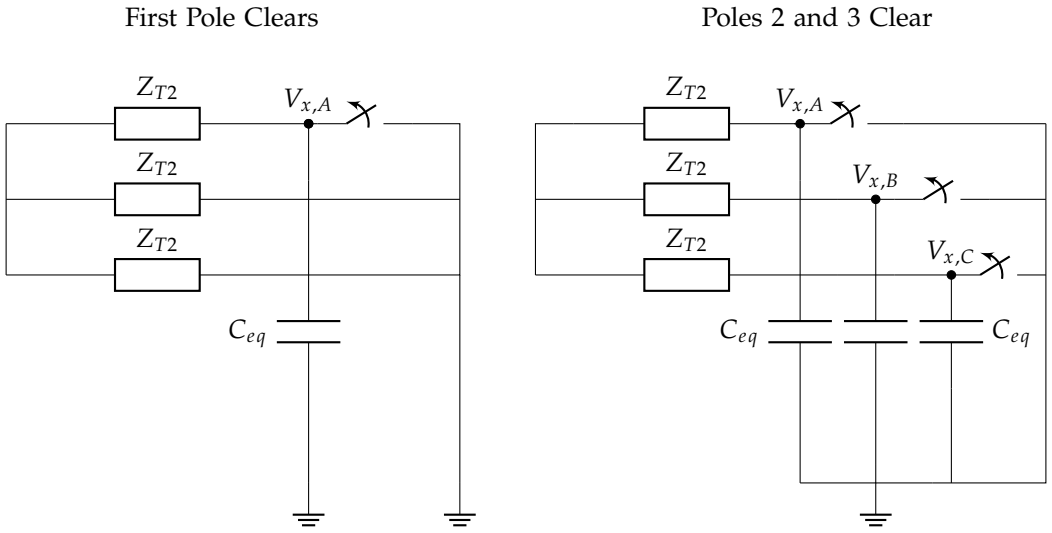

Figure 5.12: Left: Circuit at instance that one breaker opens. Right: Equivalent circuit at the instance that one breaker is opened and the second and third open at the same time.

As poles B and C clear at the same time and the phase to phase voltage is considered, the extra shunted capacitances C_{eq} in series with Z_{T2} can be seen as parallel branches to the same node. In this case, Z_{T2}, as seen from point A,B, and C does not change between clearings as the potential at $V_{x,B} = V_{x,C}$. Only more capacitance is added each clearance. Therefore, one can state that $C_{eq,2p} \approx 3C_{eq}$ and $Z_{T2,2p} = Z_{T2}$. This implies that, as Z_{T2} contains parameters on resistance and inductance, the R and L influencing the damping do not change when more poles clear . Using Equation 5.19 the new damping is calculated to be $\zeta_{2p} = 0.1132$, which corresponds to an amplitude factor of $k_{af} = 1.7$. This gives a theoretical peak phase to phase voltage of:

$$V_{p2p} = 2 * V_{p,rated} * k_{pp,23} * k_{af} = 124.9kV \tag{5.21}$$

Where the factor 2 comes from the fact that both phases close at the same time and are equal and opposite in phase, $k_{pp,23} = \frac{1}{2}\sqrt{3}$ from symmetrical components for a 2 phase to ground fault [41] and $k_{af} = 1.7$ from the added shunt capacitance. This then closely matches that of the simulated value of $V_{p,p2p} = 122.2kV$.

The RRRV is very high, this can be attributed to the exclusion of real-world parasitic capacitances or other sources of damping. In reality parasitic capacitances from busbars insulators or other substation equipment are in every substation, increasing capacitance and lowering transient steepness and RRRV. This capacitance increases even more in the case of added parallel components.

5.2.3. Theoretical maximum cases A.1 and A.2

From the model of the simplest cases, the theoretical maximum overvoltages occur for unearthed network with minimal damping. For a phase to earth overvoltage the value is:

$$V_{p,max} = k_{pp} k_{af} V_{p,rated} = 127.4kV \tag{5.22}$$

Where $k_{pp} = 1.5$ for the unearthed network, $k_{af} = 2$ in the case of 0 damping and $V_{p,rate} = 52kV$. When one takes a look at the results of the sensitivity analysis in Appendix B, no cases get a overvoltage higher than this theoretical maximum.

In case of the phase to phase voltage the theoretical maximum from this model is:

$$V_{p2p,max} = 2k_{pp} k_{af} V_{p,rated} = 147.1kV \tag{5.23}$$

Where $k_{pp,23} = \frac{1}{2}\sqrt{3}$ for the second and third poles to clear due to symmetrical components and $k_{af} = 2$ in the case of 0 damping. Note that some measurements taken in Appendix B exceed this value, implying that the simplified model does not account for all worst cases. This is investigated in the next subsection.

5.2.4. Parallel Components

The previous case was the most basic case. This still gave insight into what constituted the transient overvoltage, but is a simplification of reality. No parallel components were connected and parasitics were not modeled. This limits the amount of capacitance in the circuit and leads to very high RRRV. In reality there is the substation capacitance and parasitic capacitance from the L-SEP to the enclosure or busbar rails. These capacitances are however in the nano/pico range and vanish when parallel components are added. To every Stedin substation where the L-SEP is installed cables are connected. Some of these cables connect to other substations while others are connected to outgoing 50-20k/10kV Yd transformers. These transformers can be seen as large inductances or high impedances for transients. The highest possible impedance can be regarded as an open circuit or in the case of a cable an open end.

First, parallel open ended cables are considered, A case which can occur in the Stedin grid. The simulation results from this study can be seen in Table 5.4

Table 5.4: Scenario A Parallel Cable overvoltages

Case ID	Description	Peak Fault Current (kAp)	Peak Overvoltage (kVp)	Peak Phase-Phase (kVp)	RRRV (kV/μs)
A.10	YnY 1C OE M	10.1	125.6	140	0.39
A.13	YYn 1C OE M	10.1	95.2	137.3	0.33
A.16	YnY 2C OE S/M	10.1	125.8	155.7	0.36
A.22	YYn 2C OE S/L	10.1	86.6	103.3	0.22

From these simulations, the first observations state that system earthing is once again important. Strong earthing configurations lead to lower maximum overvoltages due to lower k_{pp} when the secondary neutral point is grounded. The overall peak overvoltages however, are generally higher. This can be attributed to the added shunt capacitance which lowers the damping and increases the k_{af}. In addition more parallel capacitance (in the form of multiple parallel or longer connected cables) does not lead to more increases to the voltage due to the limit of the k_{af} of 2. However, the phase to phase voltage is higher than the calculated maximum value of 147kV.

This can be seen from Figure 5.13.

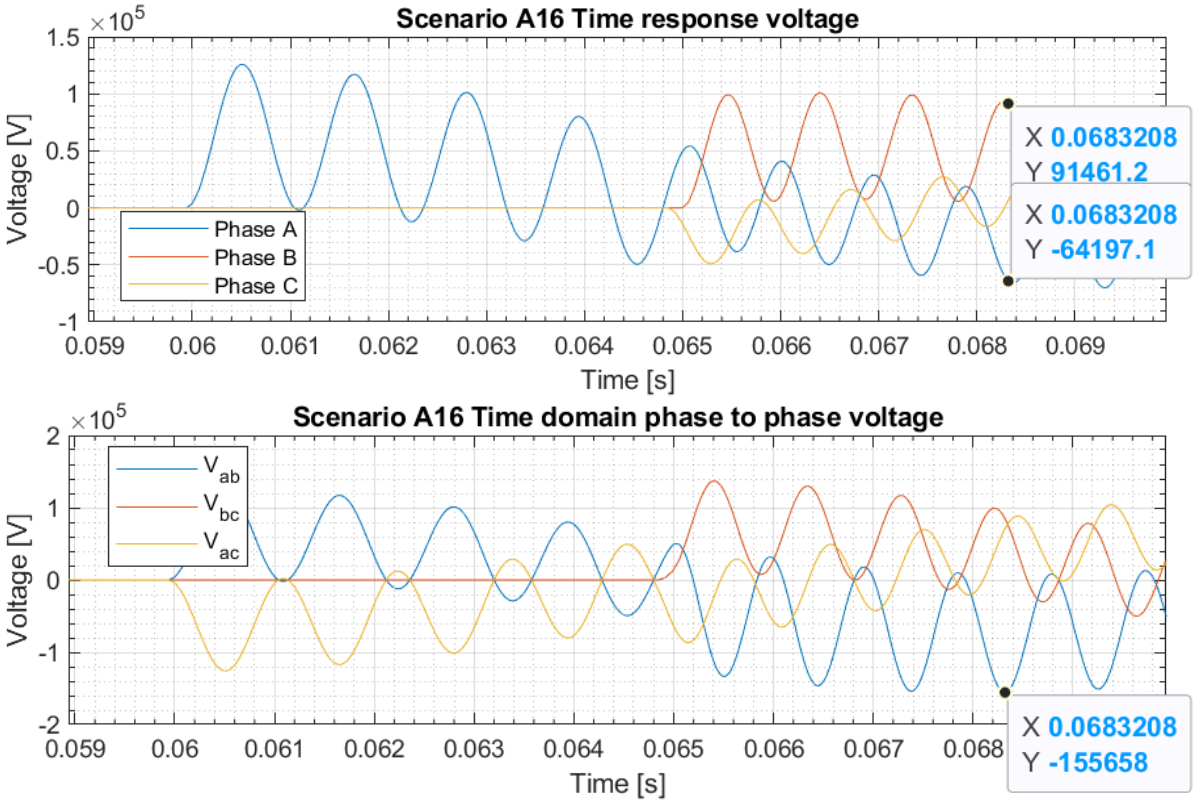

Figure 5.13: Time domain phase to earth and phase to phase plots of case A.16

Due to a large amount of added parallel capacitance, the damping is so low that the transient of phase A has not disappeared when the other phases are cleared. Moreover, the largest phase to phase overvoltage does not occur at the breaking instance of phase b and c. It occurs later, when the very underdamped phases A and B are in phase opposition. There is no factor $k_{pp} = \frac{1}{2}\sqrt{3}$ from unbalance in the circuit, as the faults have been cleared and the overvoltage occurs in the steady state. This means that the methodology to determine the maximum phase to phase overvoltage of the previous subsection cannot be used for large parallel capacitances.

In the case that the theoretical maximum phase to phase overvoltage is determined by phase opposition another bound can be used, shown below:

$$V_{p2p,max} = 2k_{af} * V_{rated} = 170kV \tag{5.24}$$

Where the factor 2 corresponds to a perfect opposition between the two phases, $k_{af} = 2$ in the case of minimal damping and V_{rated} the regular 52kV operating voltage. Note that Appendix B contains no phase to phase voltages higher than 170kV. It must however be noted that the cables do include resistive damping, which increased as length increases. This increases the damping for longer cables, which lowers the peak phase to phase overvoltage. The assumption that $k_{af} = 2$ is therefore a rough one, as damping will increase again at a certain length due to the cable resistance and losses.

In the case that Yd transformers are connected, an additional parameter can be varied: The earthing of the primary starpoint.

Table 5.5: Scenario A Parallel Cable overvoltages

Case ID	Description	Peak Fault Current (kAp)	Peak Overvoltage (kVp)	Peak Phase-Phase (kVp)	RRRV (kV/μs)
A.24	YnY-Yd C2OT Min	10.1	121.13	143	2.22
A.25	YnY-Ynd C2OT Min	10.1	104.8	104.8	2.08
A.26	YnY-Yd C2OT VS	10.1	125	145.3	1.16
A.27	YnY-Ynd C2OT VS	10.1	107.9	130.8	1.08
A.28	YYn-Yd C2OT Min	10.1	84.6	95.5	1.88
A.29	YYn-Ynd C2OT Min	10.1	79.7	124.6	1.78
A.30	YYn-Yd C2OT VS	10.1	87.4	127.1	0.98
A.31	YYn-Ynd C2OT VS	10.1	80.3	126	0.97
A.32	YnY-Yd C2OT S	10.1	126	145.7	0.91
A.33	YnY-Ynd C2OT L	10.1	107.3	131.9	0.26

As established above, better earthing of the 50kV network leads to lower overvoltages. This can be observed in the results from Table 5.5. Whenever a secondary star neutral point of the source transformer is earthed, the overvoltages are lower than when it is unearthed. In addition, when a by cable connected load side transformer has a grounded star neutral point, the overvoltages are lower in magnitude too. This has to do with the pole factors, which become lower for better earthing (i.e. X_0/X_1).

This is also observed for when the railconnector (as seen in Figure 3.1) is closed. This allows for more flexible earthing, but higher fault currents. This was modelled in ATPDraw by copying the source network and transformer in parallel. In reality this is not the case as the Thevenin equivalent impedance should stay the same compared to the new source impedance being halved. This does however lead to a higher fault current (due to lower short circit impedance) compared to when only the transformer models are doubled. As established earlier, and observed from the results seen in Table 5.6, the overvoltages get lowered.

Table 5.6: Scenario A Parallel Source Transformer

Case ID	Description	Peak Fault Current (kAp)	Peak Overvoltage (kVp)	Peak Phase-Phase (kVp)	RRRV (kV/μs)
A.36	(YnY/YnY)-Yd C2OT Min	20.2	119.4	143.5	2.93
A.37	(YnY/YnY)-Ynd C2OT Min	20.2	110.7	110.7	2.81
A.38	(YnY/YnY)-Yd C2OT S	20.2	125.5	136.5	1.21
A.39	(YnY/YnY)-Ynd C2OT S	20.2	116.8	127.6	1.17
A.40	(YnY/YYn)-Yd C2OT Min	20.2	98.5	98.5	2.64
A.41	(YnY/YYn)-Ynd C2OT Min	20.2	92.6	92.6	2.57
A.42	(YnY/YYn)-Yd C2OT S	20.2	103.3	122.6	1.1
A.43	(YnY/YYn)-Ynd C2OT S	20.2	102.3	113.4	1.1

One would expect higher overvoltages as the magnitude of the short circuit current increases. This, because it leads to a higher $\frac{di}{dt}$ at $t = 0$ and more magnetic energy being stored on the source side $E_m = 0.5LI^2$ (which is transferred to the shunt capacitance in the form of $E_m = 0.5CV^2$, raising the voltage [9]) before breaking the current. Still, the value cannot exceed the theoretical bounds stated before. This is due to the physical limitations of the differential equations which model the phenomena and earthing configurations, which manifest themselves in a maximum $k_{pp} = 1.5$ and $k_{af} = 2$ in case of unearthed networks and pure LC resonances without damping.

5.2.5. Scenario B

Scenario B considers a fault along the cable. This scenario is evaluated in the same way as the previous, where the simplest case is observed first and gradual expansions are added. As can be concluded from the previous scenario, non-effective earthing leads to the highest transients. To limit the amount of studies the emphasis will be on the parameters leading to the worst case overvoltages. In this case

non-effective earthing. The results of the simulation can be seen in Table B.2 of which a selection is shown in Table 5.7.

The main observation is that the overvoltages do not exceed values observed in Scenario A. For faults further along the cable, the peak fault current decreases. This makes sense as the impedance between source and fault increases. In addition, the cable impedance leads to a higher voltage at the terminals of the L-SEP. When breaking this leads to a smaller jump in voltage to the new steady state compared to when a fault is directly at the terminal.

Table 5.7: Scenario B Selected Results

Case ID	Description	Peak Fault Current (kAp)	Peak Overvoltage (kVp)	Peak Phase-Phase (kVp)	RRRV (kV/μs)
B.1	YnY Direct Fault Min	9.8	94.6	118.4	7.19
B.3x	YnY Direct Fault L	7.1	83.4	107	5.64
B.10	YnY 1C OE (Min) Fault at S	9	119	138	2.35
B.16	YnY-YD C2OT (M) Fault at Min	9.25	123.1	136.3	0.38

Longer cables also lead to the voltage and current becoming more in phase. This can be seen from case B.3x which has the following time response seen in Figure 5.14.

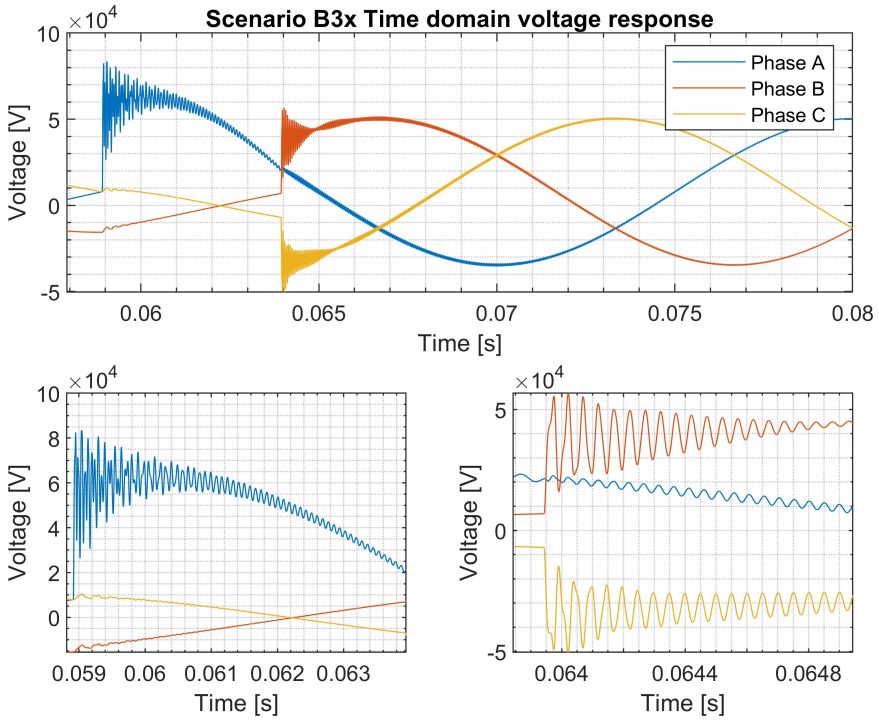

Figure 5.14: Case B.3x Time domain plots, Top figure is the voltage decay, bottom left a zoom in of the first pole to clear, bottom right the second pole to clear.

From this one can observe that the voltage from which the transient starts is not at 0. This follows from the impedance of the cable which is in series with the fault. Which leads to lower fault current and lower overvoltages by the same reason explained in subsection 5.2.1.

It can again be observed that increased capacitance in parallel leads to higher overvoltages due to damping, as observed in subsection 5.2.1 and Appendix B. In turn, ensuring more effective earthing also decreases peak overvoltages due to the pole factor getting improved.

5.2.6. Scenario C,D and E

Scenarios C and D are similar in that the fault occurs on the load side of the HV-MV transformer. This leads to drastically lower fault currents due to a large impedance being connected in series with to the fault. This is reflected in the results of Table B.3 and Table B.4.

This is confirmed when one considers the short circuit impedances of the source and load transformers. The short circuit impedance of the source transformer is $Z_{T,S} = 0.1436pu$. The load transformer has a short circuit impedance of $Z_{T,L,old} = 0.1144pu$. The secondary transformer has a rating of S = 30MVA. Converting this to a 100MVA base is done by the following relation

$$Z_{T,L} = Z_{T,L,old}\frac{S_{b,new}}{S_{b,old}} = 0.3813pu \tag{5.25}$$

In the case of Scenario D the total new short circuit impedance seen by the 150kV source is $Z_{T,D} = Z_{Thevenin} + Z_{T,L} + Z_{T,S} = 0.5368$. When comparing the short circuit impedances and fault currents the ratios approximately match.

$$\frac{Z_{T,A}}{Z_{T,D}} = \frac{I_{sc,A}}{I_{sc,D}} = 3.45 \tag{5.26}$$

Due to this lowered fault current, the overvoltages are lower than those of earlier scenarios.

Scenario E considers a fault in a cable which leads to another substation. This is modeled by placing an additional source transformer connected to the fault by cable. However, due to the shorting of this source when the fault occurs, this has comparable results to those obtained in scenario B, where cables are connected in series to the fault.

5.3. Special Cases

Some cases have been considered that are different from the original scenario. In the case of switching fault currents, single phase to earth faults generally lead to lower fault currents and thus overvoltages. In addition a three phase to phase fault can also lead to raised fault currents. The effects of these faults in terms of worst case overvoltages led to lower overvoltages, as can be seen in Table B.6.

Seeing that the values from these cases are lower than or comparable to the previously mentioned cases, further exploration will not be done in this thesis.

6

Discussion

This chapter discusses the results obtained in the previous section. It touches upon how the cases relate to the real Stedin substation locations and the observed effects of changing grid configurations. Then the limitations and approximations of the study are concisely shared.

6.1. Discussion of Key Findings

The sensitivity analysis and examination of fault scenarios have provided many insights into the transient behavior in terms of overvoltages. Many scenarios and cases have been investigated which generalize the circumstances at the 50kV Stedin Grid locations where the L-SEP GIS is installed. The simulation rests upon verification of the Stedin grid components most influential to the transient overvoltages, namely the source transformer and cable connections. From these results were extracted for several scenarios which were specified in their respective cases. The results highlight that there are three dominant factors that govern the maximum worst case transient overvoltages.

- Grid earthing configuration
- Shunt capacitance at source side of transformer
- Short circuit current magnitude

The conclusions drawn from the simulation results are as follows:

6.1.1. Grid Earthing

The earthing method of the feeding transformer's neutral star point determines the overvoltage through its effects on the pole clearing factor. Configurations with non-effectively earthed secondary neutral (YnY), or in this case an unearthed network, consistently result in higher phase to earth and phase to phase overvoltages.

This behavior is attributable to the pole clearing factor k_{pp}, which in turn is determined by the ratio of zero sequence and positive sequence impedance of the network. unearthed neutral earthing configurations lead to a high impedance path for zero sequence currents through the secondary winding capacitances of the source transformer. This leads to an unbalance in the voltages, resulting in an increase of the new steady state voltage of $k_{pp} = 1.5$. Ensuring proper effective earthing (i.e. connecting the star neutral point via a low impedance path to ground, in the extreme case 0Ω) consistently leads to lower overvoltages for all scenarios.

This effect extends to the broader network topology. When components that improve the grid's earthing are added, such as load transformers with grounded neutral (YnD) or closing a rail connection to parallel source transformers with at least one effectively earthed, the overvoltages are observed to be lower. Even when the fault current increases.

6.1.2. Parallel Capacitance

The addition of parallel capacitance to the source side of the breaker leads to high overvoltages. Specifically, cases with long open ended cables lead to high overvoltages for both phase to earth or phase to phase.

This phenomenon is explained by the influence of the capacitance on the amplitude factor k_{af}. Adding shunt capacitance lowers the circuit's damping ζ which leads to a higher overshoot as the circuit approaches an ideal LC resonance with maximum overshoot of $k_{af} = 2$. For a single phase to earth fault the maximum theoretical overvoltage was calculated to be 127kV, which matches the simulation results for all scenarios and cases.

The initial simplified model suggested a maximum phase to phase voltage of 147.1kV. But simulations with large parallel capacitances exceeded this value, reaching values up to 157.8kV. This discrepancy occurs because the initial model does not account for low-damping cases where the transient oscillations fail to decay in time and align in perfect opposition. To circumvent this case from occurring the new maximum theoretical overvoltage was determined to be $2k_{af}V_{p,rated} = 170kV$, assuming an ideal LC resonance ($k_{af} = 2$).This is consistent with all simulation results in B. It must be noted that this is very rare to occur, as it assumes no damping has occurred between first clearance and two phases are in perfect opposition.

6.1.3. Fault Location

In general, terminal faults (Scenario A) represent the worst case conditions for overvoltages. These respectively correspond to the highest fault currents. When the fault location moves further away from the breaker to after a cable (Scenario B) or behind a load transformer (Scenario C and D) the series impedance to the fault increases. This leads to lower fault current magnitudes and lower overvoltages compared to that of terminal faults.

A fault in a cable connecting two substations (Scenario E) produces results which are comparable to a fault along a single cable (Scenario B). This is due to the second substation's source effectively being short circuited.

6.1.4. Implications for the Stedin Grid

Substations with a high amount of parallel capacitance, such as Utrecht Merwedekanaal, are prone to sustain higher overvoltages due to lower damping and increased amplitude factor. It should however be noted that in reality, damping does occur, which lowers this overvoltage. The simulated worst case results should be manageable by the current switchgear, as all overvoltages (theoretical and simulated) are well below the rated specifications of the L-SEP seen inFigure 1.2.

Substations that are directly fed by transformers or have the option of improving the earthing will experience lowered overvoltages. In the case of substations which are fed by a cable of other substations (Goes Evertsenstraat, S'Gravendeel and Waaiersluis) all improvements in earthing (from both source and load transformers) help reduce the k_{pp} and thus the transient overvoltages.

6.2. Limitations

As with most studies, there are approximations and omissions were made to speed up calculation and research. These limit the accuracy and validity of the study and are important to list for reproduction in the case of further studies. This section consists our of four subsections. The first two focus on approximations and assumptions on cable and transformer modeling, the next one touches on the modeling and simulation assumptions and the last one on the analysis and calculation.

6.2.1. Cable Modeling

As the Stedin grid where L-SEP are connected are mainly cable based, some assumptions and approximations were made to simplify the problem. The main one was that complex cable routes, consisting of multiple cable sections (with different insulation, cross-section and conductor materials) and joints, were modeled as a single average cable. This was done to reduce the amount of inter cable reflections and computational load. By modeling the cable as a single piece, additional damping because of increased travel length due to reflections is ignored. This leads to higher calculated peak overvoltages.

As not all parameters were given in the cable datasheet, some were derived analytically using equations for a co-axial type cable. This includes the equivalent permittivity of the insulation and semiconducting layers, the geometric coaxial inductance, equivalent resistance of the stranded conductor and the meshed screen thickness.

Of this semiconducting layer the resistive nature is omitted in this approximation. This was assumed to be no problem as this generally only happens at much higher frequencies.

Finally, the phase to phase capacitances are neglected as each phase is enclosed by a sheath.

6.2.2. Transformer Modeling

Transformers are difficult components to model. They are very dependent on measurement data and the bandwidth of the signal it is exposed to. Furthermore, truly accurate models usually require proprietary geometrical design parameters or detailed frequency analysis models, both of which are not available for the transformers in this study.

Therefore a simplified model was used in this study: the Grey-Box model. This approximates the transformer's terminal behavior and is less detailed than white box (Used for internal voltage simulation) and black box (requires detailed digitized FRA data) models. The transformer was fitted and tuned using the SAT and FAT reports given by Stedin.

However, not all parameters were supplied by these measurement reports. Namely the zero sequence impedances and excitation currents. The zero sequence impedance was assumed to be equal to the positive sequence impedance, which came from a given range supplied by literature [38]. It is taken as the lower end to ensure the worst case single phase fault current. The excitation currents were measured per phase and differed from each other. The model could only take one value, so the open circuit currents were averaged.

The transient behavior of the transformer could not simply be measured using the measured capacitances from the SAT. These values were capacitances measured from the winding to the enclosure and disregarded the geometrical orientations. Therefore shunt and crossover capacitances were tuned using a FRA [39] measured in 1988 of a comparable transformer. However, only the resonant frequencies were tuned to a given bodeplot. The magnitudes, which are affected by complex damping phenomena like core and winding losses, were not fitted using the capacitances.

As the windings are on separate core legs, the phase to phase capacitances are neglected.

6.2.3. Modeling and Simulation Assumptions

For simulation ATPDraw was used, which meant some assumptions had to be made to correctly model the grid behavior. One of these was the representation of the TenneT grid as a Thevenin equivalent circuit, derived from the maximum three phase fault current, single phase fault current and grid time constant.

The circuit breakers are modeled as ideal switches that always open at the current zero crossing (no chopping occurs). They do not model the voltage drop of the arc that is to be extinguished and are restrike free. Parasitic capacitances from the busbars, insulators and current/voltage transformers are not considered in the simulation. Including an arc model would introduce additional sources of energy dissipation and damping. This in turn leads to lower peak overvoltages and reduced RRRV.

In the case of grid earthing, either very effective earthing ($X0/X1 = 1$) or non effective was considered $X0/X1 = \infty$. But in reality the earthing is between these values. This leads to two things: Lower k_{pp} and different clearing current zero times for the second and third phases. Both aspects will lead to lower transient overvoltages, phase to earth or phase to phase.

Lastly numerical oscillations from inductances and capacitances stemming from the trapezoidal rule are damped using a numerical damping coefficient.

6.2.4. Analysis and Calculation

In explaining and obtaining results a few assumptions were done. For the obtained value of the RRRV a non standard method was used. Instead of drawing tangent lines from specified values along the curve,

this study calculated the RRRV as a maximum derivative of the signal. This was implemented to speed up calculation from simulated values as it is easier to automate. It generally leads to higher values, as no averaging is done by the tangent line.

The largest approximation was done in using a simplified RLC model to understand the amplitude factor k_{af}. This approximation is done in most literature as it simplifies the complex damping that is in the model. In this case the transformer damping is simplified by usage of a resistance representing the damping. Using this model led to the conclusion that capacitance in parallel leads to reduced damping.

7

Remedial Actions

The simulation results from chapter 5 have identified the network topologies and parameters that produce the highest transient overvoltages in the Stedin 52kV grid. Non-effectively earthed systems combined with systems with large source side parallel capacitances lead to large overvoltages. These approach the theoretical maxima determined by the pole to clear k_{pp} and amplitude k_{af} factors. While the analysis showed that the worst case simulated overvoltages (e.g. case A.16 with a 158 kV peak to peak overvoltage) stay well below the L-SEP rated withstand voltages, this still might be too high in the case of retrofilling the machine with a weaker insulation gas. This chapter explores practical remedial actions that can be taken to reduce the transient overvoltages. The goal is to provide strategies that increase the safety margins.

7.1. Cases and Stedin Grid Implications

The extensive sensitivity analysis was a method to reduce the large amount of simulations required for analysis of specific substations. It was used to gain an understanding on what drives the transient overvoltages in the network while reducing computational complexity. Instead of modeling every permutation a general model was created in chapter 4 representing the topological (in terms of components and their respective parameters) extremes found in the Stedin switchgear with installed L-SEPs.

Now that the extremes have been found in chapter 5, it is important to link these high risk cases to the individual Stedin substations. By mapping the characteristics of the cases describing the worst case simulations, the reader can assess which substations are at risk and might benefit from remedial actions should the retrofill be done.

Based on the substation characteristics as seen in Table 3.1 and the simulation results the cases with largest overvoltages can be linked to the real world locations.

7.1.1. Utrecht Merwedekanaal and Soest 02

Utrecht Merwedekanaal is the largest substation where the L-SEP is installed. There is a large amount of connected capacitance (match 2) it is directly fed from a source transformer (match 3) and has connections to other substations (match 4). Soest 02 is a substation which is also directly connected to a source transformer. It is the second largest substation in terms of bays and therefore cases matching those of Utrecht Merwedekanaal can also occur in Soest 02.

The cases generating the largest overvoltages contain configurations of multiple parallel connections of cables which are left open ended or connected to a load transformer. This leads to the highest overvoltages seen in cases A.16 and A.19 of 159 kVp phase to phase.

The large number of bays (21) means that the substation is most likely to have a high number of parallel cable connections, leading to the lowest amount of damping and the highest overvoltages (or k_{af}). It is therefore at risk of transient oscillations that are severely underdampened and opposite in phase. While

the direct feeding by multiple transformers allows for effective earthing, lowering the overvoltages as seen in Case A.21, the inherently large capacitance still leads to raised overvoltages.

7.1.2. Goes Evertsenstraat, S'Gravendeel, and Waaiersluis

The common points from these substations are that they have a relatively low amount of parallel connections and are fed via cable from another 52 kV substation. Even though the amount of parallel connected cables is relatively low, large cables might still lead to problems with overvoltages due to the added capacitance. But cases that lead to large overvoltages that match these topologies are found in Case B and E, where the fault is located along a cable. Take for example case E.7, where a phase to earth and phase to phase overvoltage of 124.3kVp and 137.5kVp can occur. For these substations not only local earthing is important but also the configuration of the remote source transformers. This could potentially reduce the overvoltage contribution of the pole to clear factor k_{pp}.

7.2. Mitigation by Altering Earthing Configuration

As established in Chapter 5, more effective earthing consistently reduces the peak overvoltages. The earthing method directly controls the first, second and third pole to clear factors which determine the steady state component of the transient overvoltage. This steady state component sets the base for the peak transient stress. The simulations display the following trends.

7.2.1. Primary Transformer Neutral Earthing

The most impactful decision is to ground the secondary (52kV) star neutral point of the main source transformer. The simulations show that non effective earthing leads to large peak overvoltages compared to those which are effectively earthed. The reduction is in the order of 50%, as is observed from the calculated and simulated values of k_{pp}. It must be noted that it is against Stedin policy to earth both primary and secondary neutral points on the same transformer. This is to avoid fault currents being sensed from primary to secondary networks or vice versa.

7.2.2. Load-Side Transformer Earthing

The lower overvoltages from effective earthing are not limited to exclusively source transformers. earthing the neutral of outgoing 50/20 or 50/10kV Ynd transformers also reduces the measured transient overvoltages. This is reflected in the results seen in Appendix B, where adding better earthing in parallel to the source generally lowers the peak overvoltage.

7.2.3. Parallel Source Transformer Earthing

For substations with multiple incoming source transformers the operational configuration (in the case of a redundant busbar system with open rail connector) can provide better earthing. This leads to higher fault currents due to the increase short circuit power but leads to lower overvoltages when earthing is made more effective. As seen from the results, the peak overvoltages become lower whenever more secondary neutral points are connected to earth. In short: in the case of more effective the earthing the transient overvoltages due to switching fault currents become lower.

7.2.4. Tradeoff

Improving earthing does however come at a price. More effective earthing leads to higher fault currents which greatly impacts the power system. Larger fault currents lead to higher power dissipation and mechanical stresses for the equipment. Some equipment might not be rated for this and would need to be replaced or revised. Next to physical equipment damage a large time investment would be needed to redo protection configuration in the form of fault studies. As the fault current changes, relay settings need to be reconfigured to ensure selectivity and general protection of the system.

7.3. Mitigation via Surge Arresters

Another way to mitigate the overvoltages is by using of Surge Arresters (SA). When we consider an operating range of $52 \pm 5\% = 55kV$, surge arresters can be installed to reduce the maximum voltage seen on the L-SEP terminals. For this case A.16 is considered, as it leads to the largest overvoltage.

To mitigate this SAs will be chosen based upon the method described in the IEC standard [19].

First the continuous operating voltage U_c (also regarded as Maximum Continuous Operating Voltage) is determined.

$$U_c = 1.05\frac{52}{\sqrt{3}} = 31.52kV \tag{7.1}$$

However, the SA must be able to withstand temporary overvoltages for up to 10 seconds. This factor is related to the earthing of the network. From chapter 5 the worst case steady state overvoltage is in the case of a floating network, which raises the base voltage by a factor of $k_{pp} = 1.5$. The rated voltage U_r of the SA should be 45kV. Furthermore the type is selected is the substation type arrester which can handle the energy dissipation and is commonly used in substations.

How SAs can be used to lower overvoltages will be shown in the example study below. Here Case A.16, with phase to earth overvoltage of 125.8 kV and a phase to phase overvoltage of 157.6kV, is evaluated when SAs are implemented.

To generate a general V-I characteristic with the specifications mentioned before, an excel tool made for implementation to ATPDraw was used [43].[1] From this an arrester V-I characteristic was generated for the required U_r that can be seen in Figure 7.2.

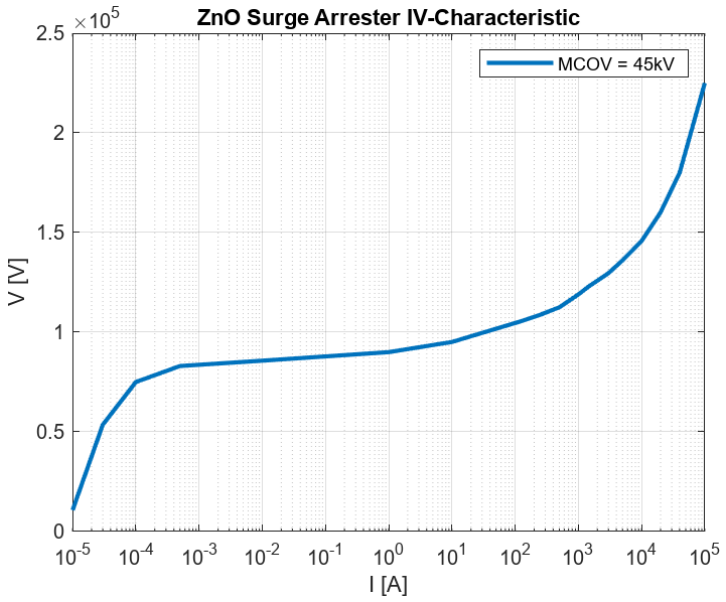

Figure 7.1: V-I characteristic of general gapless ZnO surge arrester with $U_r = 45kV$

The SA is then implemented in ATPDraw using simplified model of a SA. It consist out of a nonlinear resistance (NLRES92) element, where the I-V characteristic can be entered, and a series inductance of $1\mu H$ which is an approximated value for a 1 meter SA [43]. As the phase to phase overvoltages are generally larger than the phase to earth, the SAs can be oriented between the phases in a star formation with a fourth one connecting the neutral point to earth. This can be seen in the diagram shown in Figure 7.2

[1] The author of this file is a surge arrester consultant and Distinguished PES IEEE Lecturer

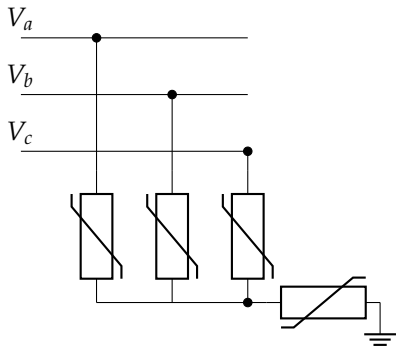

Figure 7.2: SA orientation to circumvent overvoltages at the terminals

To verify this implementation method, case A.16 is taken with implementation of the SA configuration connected to the GIS rail. This led to the results seen in Figure 7.3 and Figure 7.4.

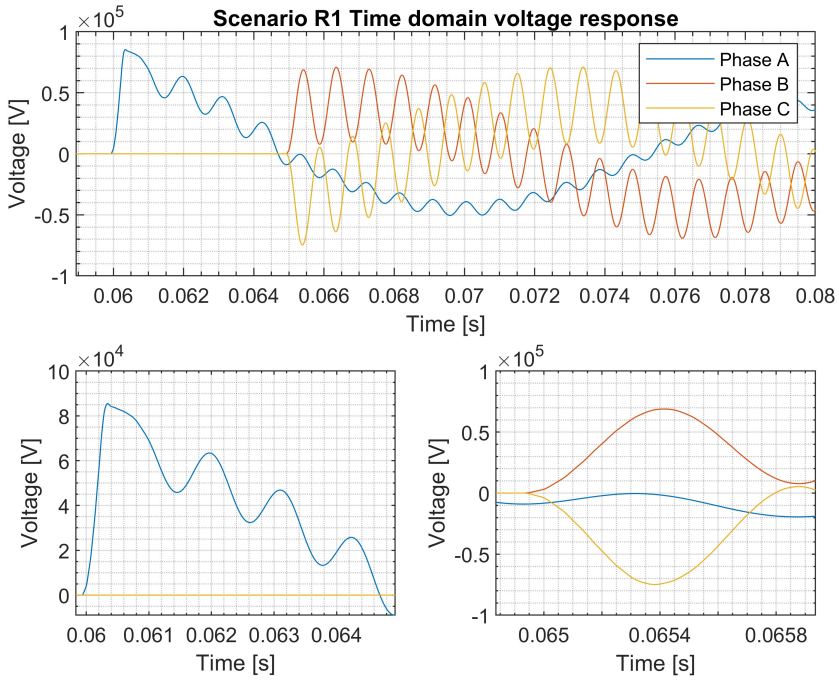

Figure 7.3: Case R.1 time domain phase to earth overvoltages with implemented SA configuration

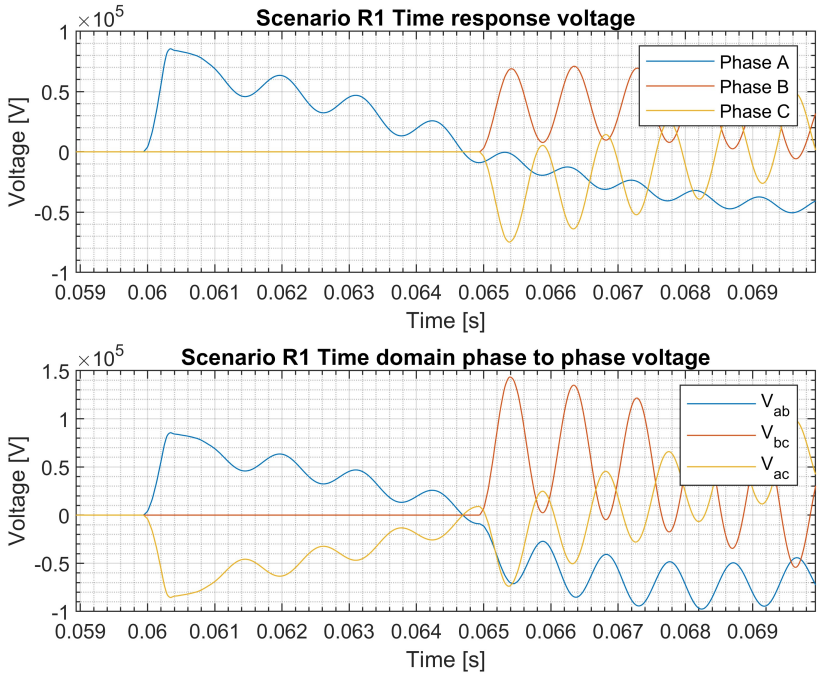

Figure 7.4: Case R.1 time domain phase to phase overvoltages with implemented SA configuration

From these results the new simulated overvoltages are reduced. The phase to earth voltage is now $85.5kV$ and the phase to phase voltage $143kV$ reinforcing implementation of SAs as a remedial action.

8

Conclusion & Recommendations

This thesis was written to investigate feasibility (from a power system perspective) of retrofilling the L-SEP GIS installed in the Stedin 52kV grid. The study is motivated in view of European SF_6 regulations and the need to assess feasibility of changing the insulation gas (not the quenching gas) to an alternative gas such as pressurized clean air. This was determined by quantifying the transient overvoltages it is exposed to under worst case conditions at their respective substations. This work provides a foundation for Stedin to gain insight into the transient behavior of their grid and allows for informed decisions regarding asset management and grid development. This chapter summarizes the key findings to answer the research questions and lists recommendations for mitigation and further study.

8.1. The Research Problem

The main research problem, as stated in Chapter 1, was formulated as: What is the **worst case** transient overvoltage, contact to enclosure or phase-to-phase, that the GIS is exposed to at their respective locations in the Stedin grid? This research question was subdivided into 4 sub questions.

1. What events will cause transient overvoltages given the current Stedin grid?
2. What does the Stedin grid topology and configuration look like?
3. What are the main contributors in terms of grid topology or configuration to the terminal overvoltage?
4. How can the contributors be altered to lower the maximum transient overvoltage?

The main goal of Stedin is to identify the grid conditions to determine if derating the insulation by retrofilling the GIS would be possible and if so, what the margin is between what it can do and what it has to withstand. This required identifying the most severe transient events and respective grid topologies. Mitigation strategies are then discussed to lower the resulting transient overvoltages.

8.2. Summary of the Research Approach and Modeling

To address the research question a methodology was employed using the ATP-EMTP software. The first contribution of this work was a systematic review and prioritization of transient origins that can occur in the Stedin substations. This identified clearing fault currents as the most critical scenario to investigate.

The focus then shifted to developing (partially) frequency dependent component models to represent the system's response to the applied disturbance. As utility data was incomplete, this posed a practical challenge. Still, using FATs, SATs, datasheets and old measurement reports it was possible to overcome this problem. The components were implemented by converting the aforementioned information to a frequency dependent Universal Line Model for cables and a Grey Box BCTRAN model for transformers. The key contribution was the tuning of this transformer model against historical Frequency Response Analysis data to represent its transient behavior. These validated models formed the basis for a

comprehensive sensitivity analysis across various fault locations and grid topologies to identify the main contributors of the overvoltages.

8.3. Conclusions

This study was guided by a main research question and four subquestions. The conclusions of this thesis are presented below as direct answers to these questions.

What events will cause transient overvoltages given the current Stedin grid?
Through a literature review and systematic analysis of potential transient origins (rating them on assumed overvoltage severity and validity), fault clearing was identified as the most critical event for producing transient overvoltages in the L-SEP substations of Stedin. Many transient origins were discussed in chapter 2. Among other phenomena, lightning or switching with restrikes were determined to have a low probability of occurrance (validity). This was due to the cable dominated nature of the grid and the tested performance of the breaker puffer mechanism.

What are the main contributors in terms of grid topology or configuration to the terminal overvoltage?
The sensitivity analysis revealed two dominant factors in the topology that determine the transient overvoltage magnitude:

- The earthing configuration is a very important driver of the transient overvoltage magnitude. Non-effectively earthed systems consistently lead to higher overvoltages due to an increased pole clearing factor k_{pp}. Earthing the neutral point of the source transformer secondary winding produced the largest reduction in terms of the transients.
- The amount of damping from parallel capacitance (in the form of parallel open ended cables) or transformer frequency behavior significantly impacts the oscillatory part of the transient. A low amount of damping leads to a large amplitude factor (k_{af}) resulting in more severe overvoltages.

These key characteristics were captured in the most crucial components and their respective models. In particular the ULM model for cables and the Grey Box BCTRAN model for transformers.

What is the worst-case transient overvoltage that the GIS is exposed to?
In direct response to the research questions, the theoretical worst case transient overvoltages were calculated to be 127 and 170 kVp for phase to earth and phase to phase respectively, as can be seen in chapter 5. The largest simulated overvoltage was observed to be a phase to phase overvoltage of 158kVp (Case A.19).

While this value is significant, it remains well below the L-SEP's rated lightning impulse withstand voltage of 325kVp and power frequency temporary (1 min) overvoltage value of 198kVp. This significant margin suggests that there is room for retrofilling the compartment SF_6 to a dielectrically weaker alternative gas. It must be noted however, that the withstand voltages of the air filled L-SEP are not yet known.

How can the contributors be altered to lower the maximum transient overvoltage?
The analysis identified two mitigation strategies to lower the transient overvoltages. They include improving earthing and installation of surge arresters. More on this can be found in chapter 7 and subsection 8.4.2

8.4. Recommendations

Based on the conclusions of this research, recommendations are proposed for Stedin. These aim to ease further studies and manage the transient overvoltages in the case of required reduction.

8.4.1. Further Research

Before the retrofilling can commence, additional research needs to be done on what the new withstand voltage (for steady state and transient) will be for the L-SEP filled with alternative gases. This requires physical modifications and to, for example, manage the electrical fields at sharp edges or deal with potential increases in insulation gas pressure. This is crucial and allows for an educated decision on whether mitigation strategies are needed.

As the values obtained are considering the worst case, future simulations should focus on improving component model detail. Especially when high risk substations or edge cases are considered. This includes modeling more complex cable routes with multiple sections and joints and developing more advanced Black Box transformer models based on detailed Frequency Response Analysis (FRA) measurements. Current cable models consider only one average cable in the Stedin grid and transformer models are not tuned to the magnitude of the frequency response. Adding these effects lead to a more realistic amount of damping in the circuit which will bring down the maximum simulated transient overvoltage to more realistic values.

In addition, the respective stations' X_0/X_1 values can be obtained as completely unearthed networks lead to the highest overvoltages $k_{pp} = 1.5$. If in reality the ratio X_0/X_1 is better (i.e. the network is effectively earthed) the pole factor is reduced and current zero times of the second and third phases to clear will be different (this is important for phase to phase overvoltages). The resulting lowered maximum transient overvoltage will then be more representative of reality.

8.4.2. Mitigation strategies

To limit the transient overvoltage magnitudes on the 52kV network Stedin can alter grid earthing configurations. Whenever the star winding neutral point of a connected transformer to the 52kV grid is earthed on the L-SEP side, the k_{pp} decreases leading to lower transient overvoltages. From the results it was observed that every additional neutral to earth connection helps lower the overvoltage. Be it load or (parallel) source transformers connected to the GIS. This does come at the cost of higher fault currents, which requires a review of equipment ratings and protection schemes.

If this is not sufficient, surge arresters (SA) can be installed in the substation L-SEPs with large amounts of parallel connected capacitance (Utrecht Merwedekanaal & Soest 02) or that are cable fed and have limited local earthing options (Goes Evertsenstraat, S'Gravendeel & Waaiersluis). This study demonstrated that correctly specified SAs installed in a phase to phase and neutral to earth configuration can reduce the worst case maximum overvoltages. In the case of A.16 this led to a reduction of the phase to earth overvoltage from 127kV to 86kV and phase to phase from 158kV to 143kV.

References

[1] S. Merkportal, *Stedin beheersgebied*, Stedin Merkportal, 2025.

[2] S. Group, *Annual report 2023*, Accessed: 2024-11-19, 2023. [Online]. Available: https://annualreport.stedingroup.com/2023.

[3] P. Rudenko, C. Wallner, and M. Behne, "State of the art gis technology and trends," in *2012 IEEE Power and Energy Society General Meeting*, IEEE, IEEE, 2012, pp. 1–5. DOI: 10.1109/PESGM.2012.6344760.

[4] E. Husain and R. S. Nema, "Analysis of paschen curves for air, n2 and sf6 using the townsend breakdown equation," *IEEE Transactions on Electrical Insulation*, vol. EI-17, no. 4, pp. 350–353, 1982. DOI: 10.1109/TEI.1982.298506.

[5] D. van der Born, M. G. Niasar, C. Engelbrecht, and A. Lathouwers, *High voltage testing and diagnostics: Lecture slides*, Lecture Slides, Personal Collection, TU Delft, available at the course, 2024. [Online]. Available: https://studiegids.tudelft.nl/a101_displayCourse.do?course_id=67688.

[6] E. Commission, *Regulation (eu) 2024/573 of the european parliament and of the council of 7 february 2024 on fluorinated greenhouse gases*, https://eur-lex.europa.eu/legal-content/EN/ALL/?uri=CELEX:32024R0573, Articles 13.7 and 13.9, 2024.

[7] P. G. Simmonds, M. Rigby, A. J. Manning, *et al.*, "The increasing atmospheric burden of the greenhouse gas sulfur hexafluoride (sf6)," *Atmospheric Chemistry and Physics*, vol. 20, pp. 7271–7290, 2020. DOI: 10.5194/acp-20-7271-2020.

[8] WG 33.02 C4, *Guidelines for representation of network elements when calculating transients*, Working Group 02 (Internal overvoltages) of Study Committee 33 (Overvoltages and Insulation Coordination), 1990.

[9] L. van der Sluis, Ed., *Transients in Power Systems*. Wiley, New York, 2001, ISBN: 9781601195890. DOI: 10.1002/0470846186.

[10] P. C. Sen, *Principles of Electric Machines and Power Electronics*, 3rd. New York: John Wiley and Sons, 2013, ISBN: 978-1-118-80434-6.

[11] G. C. Paap, A. A. Alkema, and L. van der Sluis, "Overvoltages in power transformers caused by no-load switching," *IEEE Transactions on Power Delivery*, vol. 10, no. 1, pp. 301–307, 1995. DOI: 10.1109/61.368385.

[12] R. Smeets, L. van der Sluis, M. Kapetanovic, D. F. Peelo, and A. Janssen, *Switching in electrical transmission and distribution systems*. Wiley-IEEE Press, 2013, ISBN: 9781118381351.

[13] KEMA, "Report of performance - 498-90 - trisep 170kv - small reactive interruption 160a," KEMA, Tech. Rep.

[14] KEMA, "Report of performance - 497-90 - trisep 170kv - small reactive interruption 10a," KEMA, Tech. Rep.

[15] KEMA, "Kema test report - 2122-20 - trisep 170kv," KEMA, Tech. Rep., 10-06-2020.

[16] G.-J. van Raamsdonk, "Inspectie bisep vermogensschakelaar na de capacitieve stroom onderbreking beproeving," Siemens Energy, Tech. Rep., 17-07-2020.

[17] International Electrotechnical Commission, *Iec 62305-1: Protection against lightning – part 1: General principles*, https://webstore.iec.ch/publication/2227, IEC Standard, Edition 2.0, 2010.

[18] Working Group C4.407, "Lightning parameters for engineering applications," CIGRE (International Council on Large Electric Systems), Paris, France, Technical Brochure 549, 2013, Convenor: V.A. Rakov; Secretary: A. Borghetti; Multiple contributors from international institutions.

[19] International Electrotechnical Commission, *Iec 60071-2:2023 – insulation coordination – part 2: Application guidelines*, https://webstore.iec.ch/publication/67944, IEC Standard, Edition 4.0, 2023.

[20] KEMA, "70240001.001 tdt 02-27626a - l-sep 170 kv," KEMA, Tech. Rep.

[21] J. A. Martinez Velasco, *Transient Analysis of Power Systems: A Practical Approach*. Wiley-IEEE Press, 2020, ISBN: 9781119593347.

[22] V. Brandwajn, H. Donnel, and I. Dommel, "Matrix representation of three-phase n-winding transformers for steady-state and transient studies," *IEEE Transactions on Power Apparatus and Systems*, vol. PAS-101, no. 6, pp. 1369–1378, 1982. DOI: 10.1109/TPAS.1982.317184.

[23] A. Morched, B. Gustavsen, and M. Tartibi, "A universal model for accurate calculation of electromagnetic transients on overhead lines and underground cables," *IEEE Transactions on Power Delivery*, vol. 14, no. 3, pp. 1032–1040, 1999. DOI: 10.1109/61.772331.

[24] L. M. Wedepohl and S. E. T. Mohamed, "Multiconductor transmission lines: Theory of natural modes and fourier integral applied to transient analysis," *Proc. IEE*, vol. 116, pp. 1553–1563, 9 1969.

[25] J. Marti, "Accurate modelling of frequency-dependent transmission lines in electromagnetic transient simulations," *IEEE Transactions on Power Apparatus and Systems*, vol. PAS-101, pp. 147–155, 1 1982.

[26] P. Magnusson, "Travelling waves on multi-conductor open-wire lines-a numerical survey of the effects of frequency dependence of modal composition," *IEEE Trans. Power Apparatus and Systems*, vol. PAS-92, pp. 999–1008, May 1973.

[27] T. Noda, N. Nagaoka, and A. Ametani, "Phase domain modeling of frequency-dependent transmission lines by means of an arma model," *IEEE Transactions on Power Delivery*, vol. 11, pp. 401–411, 1 1996.

[28] H. K. Høidalen and A. H. Soloot, "Cable modelling in atp - from noda to type94," in *Conference Paper*, Aug. 2010.

[29] A. Morched, B. Gustavsen, and M. Tartibi, "A universal model for accurate calculation of electromagnetic transients on overhead lines and underground cables," *IEEE Transactions on Power Delivery*, vol. 14, pp. 1032–1038, 3 1999.

[30] D. M. G. Niasar and P. P. Vaessen, *High voltage technology*, Course code: ET4103, 4 ECTS, part of the Master Electrical Engineering program, 2024. [Online]. Available: https://studiegids.tudelft.nl/a101_displayCourse.do?course_id=67679.

[31] J. A. Martinez Velasco, *Power System Transients Parameter Estimation*. Wiley-IEEE Press, 2021, ISBN: 9781119713368.

[32] W. S. Meyer and H. W. Dommel, *Rulebook of ATP: Alternative Transients Program (ATP)*. Portland, Oregon, USA: Canadian / American EMTP User Group, Jun. 1996, Copyright © 1987-92 by Canadian / American EMTP User Group. ATP is an extension of EMTP, originally developed by H.W. Dommel.

[33] CIGRE Joint Working Group A2/C4.52, *High-Frequency Transformer and Reactor Models for Network Studies: Part A: White-Box Models* (Technical Brochures 900). CIGRE, Apr. 2023, ISBN: 978-2-85873-605-8.

[34] CIGRE Joint Working Group A2/C4.52, *High-Frequency Transformer and Reactor Models for Network Studies: Part B: Black-Box Models* (Technical Brochures 901). CIGRE, Apr. 2023, ISBN: 978-2-85873-606-5.

[35] CIGRE Joint Working Group A2/C4.52, *High-Frequency Transformer and Reactor Models for Network Studies: Part C: Grey-Box Models* (Technical Brochures 902). CIGRE, Apr. 2023, ISBN: 978-2-85873-607-2.

[36] H. K. Høidalen, L. Prikler, and F. Peñaloza, *Atpdraw version 7.5 for windows: Users' manual*, 1.0, Available via ATP secure FTP servers and regional EMTP-ATP Users Groups., Trondheim, Norway, Nov. 2023.

[37] J. S. Song, J. S. Kim, G. J. Cho, C. H. Kim, and N. H. Cho, "Determination method for zero-sequence impedance of 3-limb core transformer," in *Proceedings of the International Conference on Power Systems Transients (IPST2019)*, Paper No. 19IPST061, IPST, Perpignan, France, Jun. 2019.

[38] P. to Phase, *Netten voor distributie van elektriciteit*. Phase to Phase, 2011.

[39] P. Vaessen, "Frequentie responsie metingen aan twee transformatoren van 100mva, in opdracht van geb amsterdam," KEMA, Tech. Rep., 26-04-1988.

[40] International Electrotechnical Commission, *High-voltage switchgear and controlgear - Part 1: Common specifications for alternating current switchgear and controlgear*. Geneva, Switzerland: IEC, 2017.

[41] D. F. Peelo, *Current Interruption Transients Calculation*, Second Edition. Wiley, 2020.

[42] B. C. Kuo and M. F. Golnaraghi, *Automatic Control Systems*, 8th. John Wiley & Sons, 2003.

[43] J. Woodworth, *Arrester Facts 003: A Simple Arrester Model for EMTP and ATP*, `http://www.arresterworks.com/arresterfacts/Arresterfacts_Arrester_Modeling.php`, Accessed: 2025-06-06, ArresterWorks.

[44] M. Popov, *Power system analysis ii*, Course, Faculty of Electrical Engineering, Mathematics and Computer Science, Delft University of Technology, Delft, Netherlands, 2023.

[45] Alstom Grid, *Network Protection & Automation Guide*, May 2011. Alstom Grid, 2011, ISBN: 978-0-9568678-0-3. [Online]. Available: `https://www.alstom.com/grid/sas`.

[46] J. J. Grainger and W. D. Stevenson, *Power System Analysis*. New York, USA: McGraw-Hill, Inc., 1994, ISBN: 0-07-061293-5.

A

Sensitivity analysis Table

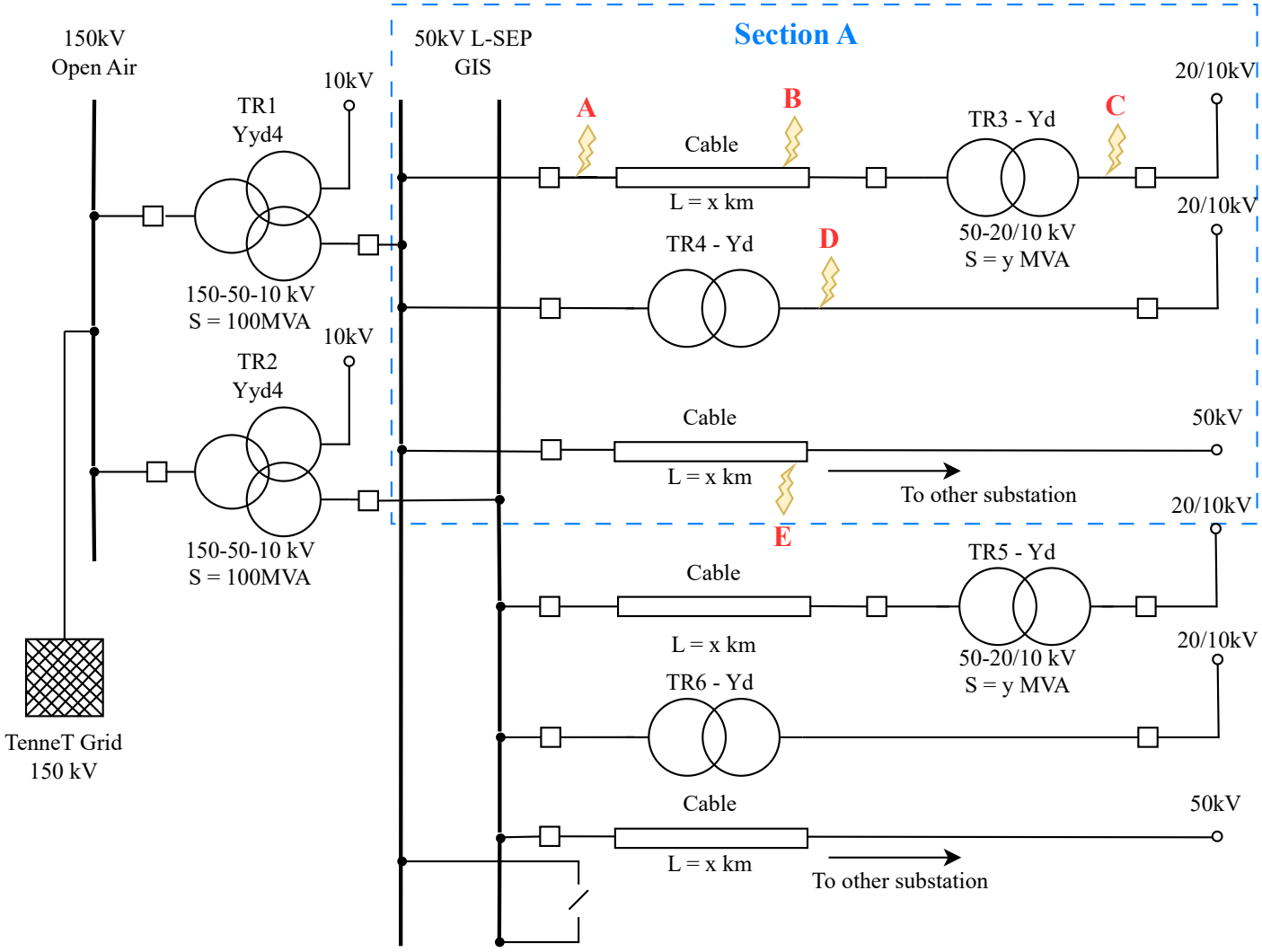

Figure A.1: Schematical overview of the to be investigated scenario. Note that the rail disconnector inside of the coupling bay is OPEN (N-1)

Table A.1: Grid Parameter and Topology Scenario A Part 1

Scenario ID	Main Transformer Grounding	Outgoing Transformer Grounding	Parallel Cables and Lengths
A.1	YnY	N/A	None
A.2	YYn	N/A	None
A.3	YnY	N/A	One Cable: Short (1km) with Yn load
A.4	YnY	N/A	One Cable: Medium (5 km) with Yn load
A.5	YnY	N/A	One Cable: Long (10 km) with Yn load
A.6	YYn	N/A	One Cable: Short (1 km) with Yn load
A.7	YYn	N/A	One Cable: Medium (5 km) with Yn load
A.8	YYn	N/A	One Cable: Long (10 km) with Yn load
A.9	YnY	N/A	One Cable Open End: Short (1km)
A.10	YnY	N/A	One Cable Open End: Medium (5 km)
A.11	YnY	N/A	One Cable Open End: Long (10 km)
A.12	YYn	N/A	One Cable Open End: Short (1 km)
A.13	YYn	N/A	One Cable Open End: Medium (5 km)
A.14	YYn	N/A	One Cable Open End: Long (10 km)
A.15	YnY	N/A	Two Cables: Short (Cable 1, 1km), Short (Cable 2, 1km) with open end
A.16	YnY	N/A	Two Cables: Short (Cable 1, 1km), Medium (Cable 2, 5km) with open end
A.17	YnY	N/A	Two Cables: Short (Cable 1, 1km), Long (Cable 2, 10km) with open end
A.18	YnY	N/A	Two Cables: Medium (Cable 2, 5km), Long (Cable 2, 10km) with open end
A.19	YnY	N/A	Two Cables: Long (Cable 2, 10km), Long (Cable 2, 10km) with open end
A.20	YYn	N/A	Two Cables: Short (Cable 1, 1km), Short (Cable 2, 1km) with open end
A.21	YYn	N/A	Two Cables: Short (Cable 1, 1km), Medium (Cable 2, 5km) with open end
A.22	YYn	N/A	Two Cables: Short (Cable 1, 1km), Long (Cable 2, 10km) with open end
A.23	YYn	N/A	Two Cables: Medium (Cable 2, 5km), Long (Cable 2, 10km) with open end

Table A.2: Grid Parameter and Topology Scenario A Part 2

Scenario ID	Main Transformer Grounding	Outgoing Transformer Grounding	Parallel Cables and Lengths
A.24	YnY	YD	Cable to Outgoing Transformer: Minimal 100m
A.25	YnY	YnD	Cable to Outgoing Transformer: Minimal 100m
A.26	YnY	YD	Cable to Outgoing Transformer: Very Short 500m
A.27	YnY	YnD	Cable to Outgoing Transformer: Very Short 500m
A.28	YYn	YD	Cable to Outgoing Transformer: Minimal 100m
A.29	YYn	YnD	Cable to Outgoing Transformer: Minimal 100m
A.30	YYn	YD	Cable to Outgoing Transformer: Very Short 500m
A.31	YYn	YnD	Cable to Outgoing Transformer: Very Short 500m
A.32	YnY	YD	Cable to Outgoing Transformer: Short (Cable 1, 1km)
A.33	YnY	YnD	Cable to Outgoing Transformer: Long (Cable 1, 10km)
A.34	YnY	YD	Cable to Outgoing Transformer: Long (Cable 1, 10km)
A.35	YYn	YnD	Cable to Outgoing Transformer: Long (Cable 1, 10km)
A.36	YnY - YnY	YD	Cable to Outgoing Transformer: Minimal 100m
A.37	YnY - YnY	YnD	Cable to Outgoing Transformer: Minimal 100m
A.38	YnY - YnY	YD	Cable to Outgoing Transformer: Short (Cable 1, 1km)
A.39	YnY - YnY	YnD	Cable to Outgoing Transformer: Short (Cable 1, 1km)
A.40	YnY - YYn	YD	Cable to Outgoing Transformer: Minimal 100m
A.41	YnY - YYn	YnD	Cable to Outgoing Transformer: Minimal 100m
A.42	YnY - YYn	YD	Cable to Outgoing Transformer: Short (Cable 1, 1km)
A.43	YnY - YYn	YnD	Cable to Outgoing Transformer: Short (Cable 1, 1km)

Table A.3: Grid Parameter and Topology Scenario B

Scenario ID	Main Transformer Grounding	Outgoing Transformer Grounding	Configuration and Fault Location
B.1	YnY	N/A	Direct Fault: Min 100m
B.2	YnY	N/A	Direct Fault: Short 1000m
B.3	YnY	N/A	Direct Fault: Medium (5 km)
B.3x	YnY	N/A	Direct Fault: Long (10 km)
B.4	YYn	N/A	Direct Fault: Min 100m
B.5	YYn	N/A	Direct Fault: Short 1000m
B.6	YYn	N/A	Direct Fault: Medium (5 km)
B.7	YYn	N/A	Direct Fault: Long (10 km)
B.8	YnY	N/A	One Cable OE: Short 1000m; Fault at Min 100m
B.9	YnY	N/A	One Cable OE: Min 100m; Fault at Min 100m
B.10	YnY	N/A	One Cable OE: Min 100m; Fault at Short 1000m
B.11	YnY	N/A	One Cable OE: Long (10 km); Fault at Short 1000m
B.12	YnY	N/A	Two Cables: S,M; Fault at Min 100m
B.13	YnY	N/A	Two Cables: S,L; Fault at Min 100m
B.14	YnY	YD	Cable to Outgoing Transformer: Minimal 100m; Fault at Minimal 100m
B.15	YnY	YnD	Cable to Outgoing Transformer: Minimal 100m; Fault at Minimal 100m
B.16	YnY	YD	Cable to Outgoing Transformer: Medium (5 km); Fault at Minimal 100m
B.17	YnY	YnD	Cable to Outgoing Transformer: Medium (5 km); Fault at Minimal 100m

Table A.4: Grid Parameter and Topology for Scenario C

Scenario ID	Main Transformer Grounding	Parallel Components on GIS Bus	Faulted Branch Description
C.1	YnY	N/A	Fault behind Yd transformer, connected via Min (100m) cable.
C.2	YnY	N/A	Fault behind YnD transformer, connected via Min (100m) cable.
C.3	YnY	N/A	Fault behind Yd transformer, connected via Short (1km) cable.
C.4	YnY	N/A	Fault behind YnD transformer, connected via Short (1km) cable.
C.5	YYn	N/A	Fault behind Yd transformer, connected via Min (100m) cable.
C.6	YYn	N/A	Fault behind YnD transformer, connected via Min (100m) cable.
C.7	YYn	N/A	Fault behind Yd transformer, connected via Short (1km) cable.
C.8	YnY	One Cable OE: Min (100m)	Fault behind Yd transformer, connected via Min (100m) cable.
C.9	YnY	One Cable OE: Min (100m)	Fault behind YnD transformer, connected via Min (100m) cable.
C.10	YnY	One Cable OE: Short (1km)	Fault behind Yd transformer, connected via Min (100m) cable.
C.11	YnY	One Cable OE: Short (1km)	Fault behind YnD transformer, connected via Min (100m) cable.
C.12	YnY	Two Cables OE: S (1km), M (5km)	Fault behind YnD transformer, connected via Min (100m) cable.
C.13	YnY	Two Cables OE: S (1km), L (10km)	Fault behind YnD transformer, connected via Min (100m) cable.
C.14	YnY	Two Cables OE: S (1km), L (10km)	Fault behind Yd transformer, connected via Min (100m) cable.
C.15	YnY	C2OT (Min, YD)	Fault behind YnD transformer, connected via Min (100m) cable.
C.16	YnY	C2OT (Min, YD)	Fault behind Yd transformer, connected via Min (100m) cable.
C.17	YnY	C2OT (Min, YnD)	Fault behind YnD transformer, connected via Min (100m) cable.
C.18	YnY	C2OT (M, YD)	Fault behind YnD transformer, connected via Min (100m) cable.
C.19	YnY	C2OT (M, YnD)	Fault behind YnD transformer, connected via Min (100m) cable.

Table A.5: Grid Parameter and Topology for Scenario D

Scenario ID	Main Transformer Grounding	Parallel Components on GIS Bus	Faulted Branch Description
D.1	YnY	N/A	Fault behind directly connected Yd transformer.
D.2	YnY	N/A	Fault behind directly connected YnD transformer.
D.3	YYn	N/A	Fault behind directly connected Yd transformer.
D.4	YYn	N/A	Fault behind directly connected YnD transformer.
D.5	YnY	One Cable OE: Min (100m)	Fault behind directly connected Yd transformer.
D.6	YnY	One Cable OE: Min (100m)	Fault behind directly connected YnD transformer.
D.7	YnY	One Cable OE: Short (1km)	Fault behind directly connected Yd transformer.
D.8	YnY	One Cable OE: Short (1km)	Fault behind directly connected YnD transformer.
D.9	YnY	Two Cables OE: S (1km), M (5km)	Fault behind directly connected YnD transformer.
D.10	YnY	Two Cables OE: S (1km), M (5km)	Fault behind directly connected Yd transformer.
D.11	YnY	C2OT (Min, YD)	Fault behind directly connected YnD transformer.
D.12	YnY	C2OT (Min, YD)	Fault behind directly connected Yd transformer.
D.13	YnY	C2OT (Min, YnD)	Fault behind directly connected YnD transformer.
D.14	YnY	C2OT (M, YD)	Fault behind directly connected YnD transformer.
D.15	YnY	C2OT (M, YnD)	Fault behind directly connected YnD transformer.

Table A.6: Grid Parameter and Topology for Scenario E

Scenario ID	Main Transformer Grounding	Parallel Components on GIS Bus	Fault Location on Inter-Substation Cable
E.1	YnY	N/A	Min (100m)
E.2	YnY	N/A	Short (1km)
E.3	YnY	N/A	Medium (5km)
E.4	YnY	N/A	Long (10km)
E.5	YnY	One Cable OE: Min (100m)	Short (1km)
E.6	YnY	One Cable OE: Short (1km)	Short (1km)
E.7	YnY	Two Cables OE: S (1km), M (5km)	Short (1km)
E.8	YnY	C2OT (Min, YnD)	Short (1km)
E.9	YnY	C2OT (Min, YD)	Short (1km)

Table A.7: Grid Parameter and Topology for Scenario S

Scenario ID	Main Transformer Grounding	Parallel Component Details	Fault Type
S.1	YnY	None	3 Phase to Phase
S.2	YnY	Cable Open Ended, Len 1km	3 Phase to Phase
S.3	YnY	Cable to transformer Yd, Len 100m	3 Phase to Phase
S.4	YnY	None	Single Phase
S.5	YnY	Cable Open Ended, Len 1km	Single Phase
S.6	YnY	Cable to transformer Yd, Len 100m	Single Phase

B

Sensitivity Analysis Results

Table B.1: Sensitivity Analysis results scenario A, Note that A3-A5 does not occur in Stedin grid and have been removed

Case ID	Description	Peak Fault Current (kAp)	Peak Overvolt. (kVp)	Peak Ph-Ph (kVp)	RRRV (kV/μs)
A.1	YnY Base	10.1	97.6	122.2	7.72
A.2	YYn Base	10.1	71.8	85.5	6.73
A.6	YYn 1C S	10.1	81.6	135	0.7
A.7	YYn 1C M	10.1	91	124.9	0.32
A.8	YYn 1C L	10.1	79.7	122.1	0.22
A.9	YnY 1C OE S	10.1	126.6	142	0.86
A.10	YnY 1C OE M	10.1	125.6	140	0.39
A.11	YnY 1C OE L	10.1	124.1	146.8	0.28
A.12	YYn 1C OE S	10.1	90.5	137.8	0.73
A.13	YYn 1C OE M	10.1	95.2	137.3	0.33
A.14	YYn 1C OE L	10.1	86.5	119.3	0.23
A.15	YnY 2C OE S/S	10.1	126.7	157.6	0.65
A.16	YnY 2C OE S/M	10.1	125.8	155.7	0.36
A.17	YnY 2C OE S/L	10.1	121.4	136.9	0.27
A.18	YnY 2C OE M/L	10.1	124.5	144.9	0.22
A.19	YnY 2C OE L/L	10.1	123.9	157.8	0.2
A.20	YYn 2C OE S/S	10.1	88.6	112.7	0.51
A.21	YYn 2C OE S/M	10.1	94.5	130.7	0.3
A.22	YYn 2C OE S/L	10.1	86.6	103.3	0.22
A.23	YYn 2C OE M/L	10.1	87.1	149.2	0.19
A.24	YnY-Yd C2OT Min	10.1	121.13	143	2.22
A.25	YnY-Ynd C2OT Min	10.1	104.8	104.8	2.08
A.26	YnY-Yd C2OT VS	10.1	125	145.3	1.16
A.27	YnY-Ynd C2OT VS	10.1	107.9	130.8	1.08
A.28	YYn-Yd C2OT Min	10.1	84.6	95.5	1.88
A.29	YYn-Ynd C2OT Min	10.1	79.7	124.6	1.78
A.30	YYn-Yd C2OT VS	10.1	87.4	127.1	0.98
A.31	YYn-Ynd C2OT VS	10.1	80.3	126	0.97
A.32	YnY-Yd C2OT S	10.1	126	145.7	0.91
A.33	YnY-Ynd C2OT L	10.1	107.3	131.9	0.26
A.34	YnY-Yd C2OT L	10.1	123.6	146.1	0.28
A.35	YYn-Ynd C2OT L	10.1	83.9	151.1	0.23
A.36	(YnY/YnY)-Yd C2OT Min	20.2	119.4	143.5	2.93
A.37	(YnY/YnY)-Ynd C2OT Min	20.2	110.7	110.7	2.81
A.38	(YnY/YnY)-Yd C2OT S	20.2	125.5	136.5	1.21
A.39	(YnY/YnY)-Ynd C2OT S	20.2	116.8	127.6	1.17
A.40	(YnY/YYn)-Yd C2OT Min	20.2	98.5	98.5	2.64
A.41	(YnY/YYn)-Ynd C2OT Min	20.2	92.6	92.6	2.57
A.42	(YnY/YYn)-Yd C2OT S	20.2	103.3	122.6	1.1
A.43	(YnY/YYn)-Ynd C2OT S	20.2	102.3	113.4	1.1

Table B.2: Sensitivity Analysis results scenario B

Case ID	Description	Peak Fault Current (kAp)	Peak Overvolt. (kVp)	Peak Ph-Ph (kVp)	RRRV (kV/μs)
B.1	YnY Direct Fault Min	9.8	94.6	118.4	7.19
B.2	YnY Direct Fault S	9.6	93.2	117.3	7.03
B.3	YnY Direct Fault M	8.5	88.5	112.3	6.35
B.3x	YnY Direct Fault L	7.1	83.4	107	5.64
B.4	YYn Direct Fault Min	9.4	76	97.7	6.74
B.5	YYn Direct Fault S	9.24	69.9	97.6	6.37
B.6	YYn Direct Fault M	8.34	63	94.3	5.76
B.7	YYn Direct Fault L	7.5	62	92.5	5.1
B.8	YnY 1C OE (S) Fault at Min	9.25	123.4	138.3	0.84
B.9	YnY 1C OE (Min) Fault at Min	9.25	120.7	139.8	2.4
B.10	YnY 1C OE (Min) Fault at S	9	119	138	2.35
B.11	YnY 1C OE (L) Fault at S	9	121.4	134.9	0.27
B.12	YnY 2C OE (S/M) Fault at Min	9	122.5	143.6	0.34
B.13	YnY 2C OE (S/L) Fault at Min	9	121.7	132.6	0.25
B.14	YnY-YD C2OT (Min) Fault at Min	9.25	117.7	138.6	2.15
B.15	YnY-YnD C2OT (Min) Fault at Min	9.25	101.6	111.1	2.01
B.16	YnY-YD C2OT (M) Fault at Min	9.25	123.1	136.3	0.38
B.17	YnY-YnD C2OT (M) Fault at Min	9.25	111.7	152.9	0.36

Table B.3: Sensitivity Analysis Results Scenario C

Case ID	Description	Peak Fault Current (kAp)	Peak Overvolt. (kVp)	Peak Ph-Ph (kVp)	RRRV (kV/μs)
C.1	YnY, connection: Min to Yd	2.5	78.7	82	2.02
C.2	YnY, connection: Min to YnD	2.5	82.6	82.6	2.02
C.3	YnY, connection: Short to Yd	2.49	79.8	92.9	2.07
C.4	YnY, connection: Short to Ynd	2.49	80.2	93	2.07
C.5	YYn, connection: Min to Yd	2.5	51.1	85.9	1.83
C.6	YYn, connection: Min to YnD	2.6	54.8	79	1.83
C.7	YYn, connection: Short to Yd	2.48	59.6	89.3	1.88
C.8	YnY, 1C OE (Min), conn: Min to Yd	2.5	72.2	86.8	0.71
C.9	YnY, 1C OE (Min), conn: Min to YnD	2.5	86.1	88.3	0.69
C.10	YnY, 1C OE (S), conn: Min to Yd	2.5	60	94.2	0.25
C.11	YnY, 1C OE (S), conn: Min to YnD	2.5	92.5	91	0.25
C.12	YnY, 2C OE (S/M), conn: Min to YnD	2.51	89.3	95.4	0.09
C.13	YnY, 2C OE (S/L), conn: Min to YnD	2.54	88.5	94.5	0.08
C.14	YnY, 2C OE (S/L), conn: Min to YD	2.52	58.2	94.5	0.07
C.15	YnY-YD C2OT (Min), conn: Min to YnD	2.5	88.1	84.9	0.66
C.16	YnY-YD C2OT (Min), conn: Min to YD	2.5	69.7	88	0.62
C.17	YnY-YnD C2OT (Min), conn: Min to YnD	2.53	59.6	80.7	0.57
C.18	YnY-YD C2OT (M), conn: Min to YnD	2.51	89	94.6	0.12
C.19	YnY-YnD C2OT (M), conn: Min to YnD	2.56	61.3	94.6	0.11

Table B.4: Sensitivity Analysis Results Scenario D

Case ID	Description	Peak Fault Current (kAp)	Peak Overvolt. (kVp)	Peak Ph-Ph (kVp)	RRRV (kV/μs)
D.1	YnY connected to Yd	2.91	75.2	84	2.16
D.2	YnY connected to YnD	2.91	87.2	87.5	2.17
D.3	YYn connected to Yd	2.92	52.5	84.4	2.3
D.4	YYn connected to YnD	2.92	51.8	73.8	1.96
D.5	YnY, 1C OE (Min) connected to Yd	2.92	70.2	94.8	1.04
D.6	YnY, 1C OE (Min) connected to YnD	2.92	96.7	94	0.94
D.7	YnY, 1C OE (S) connected to Yd	2.91	59.9	94.5	0.23
D.8	YnY, 1C OE (S) connected to YnD	2.91	92.6	91.6	0.26
D.9	YnY, 2C OE (S/M) connected to YnD	2.92	91.6	93.9	0.08
D.10	YnY, 2C OE (S/M) connected to YD	2.92	59.1	95.7	0.08
D.11	YnY-YD C2OT (Min), conn: Min to YnD	2.91	91.7	92.9	0.72
D.12	YnY-YD C2OT (Min), conn: Min to YD	2.91	67.6	94.7	0.93
D.13	YnY-YnD C2OT (Min), conn: Min to YnD	2.91	61.6	81	0.61
D.14	YnY-YD C2OT (M), conn: Min to YnD	2.92	91	92.9	0.13
D.15	YnY-YnD C2OT (M), conn: Min to YnD	2.92	64.3	93.5	0.12

Table B.5: Sensitivity Analysis Results Scenario E

Case ID	Description	Peak Fault Current (kAp)	Peak Overvolt. (kVp)	Peak Ph-Ph (kVp)	RRRV (kV/μs)
E.1	YnY Direct Fault Min	4.5	79.4	114.7	6.37
E.2	YnY Direct Fault S	9.6	96.3	101.1	7.28
E.3	YnY Direct Fault M	8.8	92	116.8	6.62
E.4	YnY Direct Fault L	7.6	87.2	110.8	5.92
E.5	YnY 1C OE (Min) Fault at S	5.2	122.9	123.3	2.43
E.6	YnY 1C OE (S) Fault at S	5.2	125	128	0.84
E.7	YnY 2C OE (S/M) Fault at S	5.2	124.3	137.5	0.35
E.8	YnY-Ynd C2OT (Min) Fault at S	5.2	103.4	124.4	2.03
E.9	YnY-Yd C2OT (Min) Fault at S	5.2	119.8	120.3	2.17

Table B.6: Simulation Results for S Series Scenarios

Case ID	Description	Peak Fault Current (kAp)	Peak Overvoltage (kVp)	Peak Ph-Ph (kVp)	RRRV (kV/μs)
S.1	YnY, 3Ph-Ph Fault, None	10.1	101.6	121.3	7.06
S.2	YnY, 3Ph-Ph Fault, 1C OE, Len 1km	10.1	114.2	142.5	0.72
S.3	YnY, 3Ph-Ph Fault, C2OT, Len 100m, Par.Yd	10.1	90	114.7	1.9
S.4	YnY, Single Ph. Fault, None	1.8	71.9	80.6	2.39
S.5	YnY, Single Ph. Fault, 1C OE, Len 1km	1.88	4.9	100.4	0.33
S.6	YnY, Single Ph. Fault, C2OT, Len 100m, Par.Yd	1.87	5.6	98	1.4

For the description the following logic holds:

Table B.7: Nomenclature for network configurations and components.

Abbreviation/Term	Description
YnY	Grounding, Primary star neutral point earthed, secondary floating
1C	One parallel cable
Min	Minimal (100m)
VS	Very short (500m)
S	Short (1km)
M	Medium (5km)
L	Long (10km)
2C	Two parallel cables
C2OT	Cable to outgoing transformer
YnY-YD	Grounding of feeding and outgoing transformer
YnY/YnY-YD	Grounding of parallel feeding and outgoing transformer
1C OE	One cable open ended
Direct Fault Min	Fault on line at distance Min (100m)

C

Appendix C

C.1. Symmetrical components

In the case of an imbalanced circuit the phases are not symmetric. Phases will not be equal magnitude and equally spaced. An easier way to describe voltages and currents in unbalanced systems is by usage of symmetric components. An example is given in Figure C.1 [44]

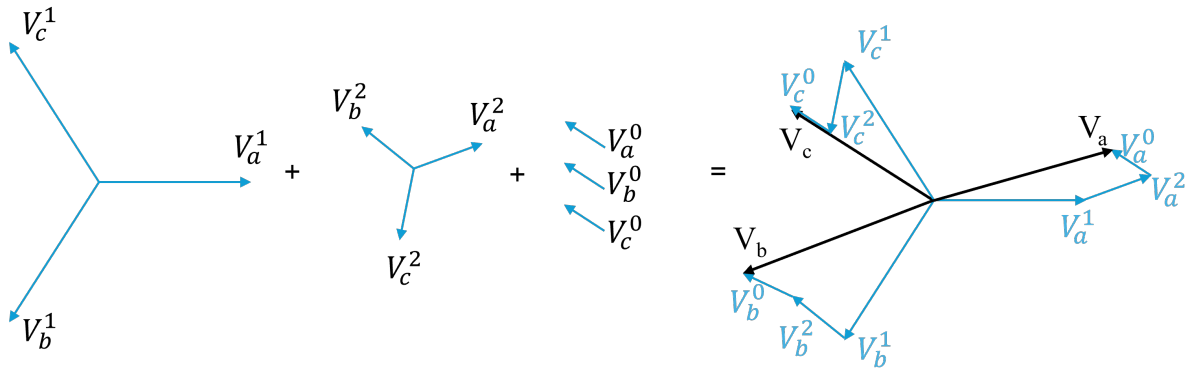

Figure C.1: Symmetrical components in an unbalanced system

Here one can observe that the voltages in an unbalanced system are unequal in magnitude, phase shifted and not equally seperated by phase. additionally, they can be split up in three parts, the positive sequence V^1 which represents the part of the phasor rotating counter clockwise, the negative sequence V^2 which represents the part of the phasor rotating clockwise and the zero sequence V^0 which is equal in magnitude but also direction in all phases.

Using the A matrix, a transformation can be used to convert phase voltages to their respective positive, negative and zero sequence components. This transformation will now be derived.

$$\mathbf{V}_{abc} = \begin{bmatrix} V_a \\ V_b \\ V_c \end{bmatrix} = \begin{bmatrix} V_a^0 \\ V_b^0 \\ V_c^0 \end{bmatrix} + \begin{bmatrix} V_a^1 \\ V_b^1 \\ V_c^1 \end{bmatrix} + \begin{bmatrix} V_a^2 \\ V_b^2 \\ V_c^2 \end{bmatrix} = \begin{bmatrix} V_a^0 \\ V_a^0 \\ V_a^0 \end{bmatrix} + \begin{bmatrix} V_a^1 \\ a^2 V_a^1 \\ a V_a^1 \end{bmatrix} + \begin{bmatrix} V_a^2 \\ a V_a^2 \\ a^2 V_a^2 \end{bmatrix} \tag{C.1}$$

One can observe from Equation C.1 that transforming from phase voltages to symmetrical components the following holds:

$$\mathbf{V}_{abc} = \begin{bmatrix} 1 & 1 & 1 \\ 1 & a & a^2 \\ 1 & a^2 & a \end{bmatrix} \begin{bmatrix} V_0 \\ V_1 \\ V_2 \end{bmatrix} = \mathbf{A}\mathbf{V}_{012} \tag{C.2}$$

From Equation C.2 one can see that $\mathbf{V}_{012} = \mathbf{A}^{-1}\mathbf{V}_{abc}$. Where

$$\mathbf{A}^{-1} = \frac{1}{3}\begin{bmatrix} 1 & 1 & 1 \\ 1 & a & a^2 \\ 1 & a^2 & a \end{bmatrix} \quad \text{and} \quad \mathbf{A} = \begin{bmatrix} 1 & 1 & 1 \\ 1 & a^2 & a \\ 1 & a & a^2 \end{bmatrix} \tag{C.3}$$

Combining Equation C.1 until C.3, the following symmetrical component transform can be deduced.

$$\begin{bmatrix} V_0 \\ V_1 \\ V_2 \end{bmatrix} = \frac{1}{3}\begin{bmatrix} 1 & 1 & 1 \\ 1 & a & a^2 \\ 1 & a^2 & a \end{bmatrix} \begin{bmatrix} V_a \\ V_b \\ V_c \end{bmatrix} \quad \text{and} \quad \begin{bmatrix} V_a \\ V_b \\ V_c \end{bmatrix} = \begin{bmatrix} 1 & 1 & 1 \\ 1 & a^2 & a \\ 1 & a & a^2 \end{bmatrix} \begin{bmatrix} V_0 \\ V_1 \\ V_2 \end{bmatrix} \tag{C.4}$$

Similarly, the symmetrical component transformation for the currents is given by:

$$\begin{bmatrix} I_0 \\ I_1 \\ I_2 \end{bmatrix} = \frac{1}{3}\begin{bmatrix} 1 & 1 & 1 \\ 1 & a & a^2 \\ 1 & a^2 & a \end{bmatrix} \begin{bmatrix} I_a \\ I_b \\ I_c \end{bmatrix} \quad \text{and} \quad \begin{bmatrix} I_a \\ I_b \\ I_c \end{bmatrix} = \begin{bmatrix} 1 & 1 & 1 \\ 1 & a^2 & a \\ 1 & a & a^2 \end{bmatrix} \begin{bmatrix} I_0 \\ I_1 \\ I_2 \end{bmatrix} \tag{C.5}$$

Using the symmetrical components, Y and delta impedances can be converted to their respective sequence networks.

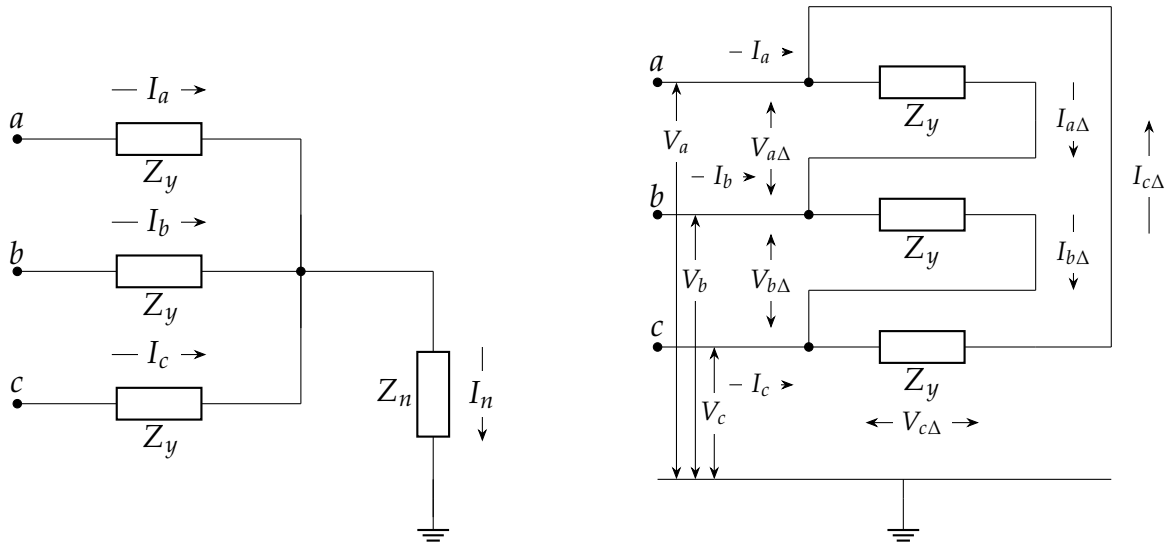

(a) Y-connected load circuit diagram.

(b) Delta-connected load circuit diagram.

Figure C.2: Comparison of Y-connected and Delta-connected load circuit diagrams.

For Figure C.2a one can state the following:

$$I_n = I_a + I_b + I_c \tag{C.6}$$

$$\mathbf{V}_{abc} = \mathbf{V}_{abc\mathbf{n}} + \mathbf{V}_n \tag{C.7}$$

$$\mathbf{V}_{abc} = Z_y\mathbf{I}_{abc} + Z_n\mathbf{I}_n \tag{C.8}$$

$$I_0 = \frac{1}{3}(I_a + I_b + I_c) = \frac{1}{3}I_n \tag{C.9}$$

The neutral current is the sum of all phase currents. The phase to ground voltages are the sum of the phase to neutral voltage and the neutral voltage. Equation C.9 follows from Equation C.5 and C.6.

To determine the sequence impedances the **A** matrices C.3 are used in combination with the relations

$$\mathbf{V}_{abc} = \mathbf{A}\mathbf{V}_{012} \quad \text{and} \quad \mathbf{I}_{abc} = \mathbf{A}\mathbf{I}_{012} \tag{C.10}$$

to obtain an expression of sequence voltage, currents and impedances as shown in

$$\mathbf{A}\begin{bmatrix} V_0 \\ V_1 \\ V_2 \end{bmatrix} = Z_y\mathbf{A}\begin{bmatrix} I_0 \\ I_1 \\ I_2 \end{bmatrix} + 3Z_n\begin{bmatrix} I_0 \\ I_0 \\ I_0 \end{bmatrix} \quad \Rightarrow \quad \begin{bmatrix} V_0 \\ V_1 \\ V_2 \end{bmatrix} = Z_y\begin{bmatrix} I_0 \\ I_1 \\ I_2 \end{bmatrix} + 3Z_nI_0\mathbf{A}^{-1}\begin{bmatrix} 1 \\ 1 \\ 1 \end{bmatrix} \tag{C.11}$$

When one multiplies $\mathbf{A}^{-1}$ with the unity vector the following arises:

$$\begin{bmatrix} V_0 \\ V_1 \\ V_2 \end{bmatrix} = Z_y\begin{bmatrix} I_0 \\ I_1 \\ I_2 \end{bmatrix} + 3Z_n\begin{bmatrix} I_0 \\ 0 \\ 0 \end{bmatrix} \tag{C.12}$$

One can now conclude that the sequence impedances are

$$Z_0 = Z_y + 3Z_n \tag{C.13}$$
$$Z_1 = Z_y \tag{C.14}$$
$$Z_2 = Z_y \tag{C.15}$$

Which implies that for delta loads all sequence impedances are equal except the zero sequence, which in addition to the common Z_y also takes in to account $3Z_n$.

For Figure C.2b, one can derive the following relation of the phase to phase voltages:

$$V_{a\Delta} + V_{b\Delta} + V_{c\Delta} = 0 \tag{C.16}$$

$$\begin{bmatrix} V^0_{a\Delta} \\ V^1_{a\Delta} \\ V^2_{c\Delta} \end{bmatrix} = \frac{1}{3}\mathbf{A}^{-1}\begin{bmatrix} V_{a\Delta} \\ V_{b\Delta} \\ V_{c\Delta} \end{bmatrix} \tag{C.17}$$

From this one can state that:

$$V_{a\Delta} + V_{b\Delta} + V_{c\Delta} = 3V^0_{a\Delta} = 3Z_\Delta I^0_{a\Delta} \tag{C.18}$$

But when one considers Equation C.16:

$$V^0_{a\Delta} = I^0_{a\Delta} = 0 \tag{C.19}$$

Thus, in delta connected circuit, there can not be any 0 sequence currents and voltages.

C.1.1. Sequence Impedances

To calculate the zero sequence impedance one can use the following relation.

$$V_{abc} = Z_{abc} I_{abc} \text{ and } V_{012} = Z_{012} I_{012} \tag{C.20}$$

From Equation C.4 and Equation C.5 the following can be stated:

$$AV_{012} = Z_{abc}(AI_{012}) \tag{C.21}$$
$$A^{-1}(AV_{012}) = A^{-1}(Z_{abc} A I_{012}) \tag{C.22}$$
$$IV_{012} = (A^{-1} Z_{abc} A) I_{012} \tag{C.23}$$
$$Z_{012} = A^{-1} Z_{abc} A \tag{C.24}$$

Where,

$$Z_{abc} = \begin{pmatrix} Z_{aa} & Z_{ab} & Z_{ac} \\ Z_{ba} & Z_{bb} & Z_{bc} \\ Z_{ca} & Z_{cb} & Z_{cc} \end{pmatrix} \text{ and } Z_{012} = \begin{pmatrix} Z_{00} & Z_{01} & Z_{02} \\ Z_{10} & Z_{11} & Z_{12} \\ Z_{20} & Z_{21} & Z_{22} \end{pmatrix} \tag{C.25}$$

Assuming equal self impedances (balanced) $Z_{aa} = Z_{bb} = Z_{cc} = Zs$ mutual impedances (i.e. non diagonal impedances) $Z_{ac} = Z_{ba} = Z_{bc} = ... = Z_m$, the sequence impedances can be simplified to:

$$Z_{00} = Z_s + 2Z_m \tag{C.26}$$
$$Z_{11} = Z_s - Z_m \tag{C.27}$$
$$Z_{22} = Z_s - Z_m \tag{C.28}$$

C.2. Fault currents

One source of transient overvoltages are the switching of fault currents. [9] This will be discussed in the next section. Fault currents appear when an unintended connection is made by one or more phases. Normally this leads to an unbalanced system [45]. The usage of symmetrical components allows us to simplify the calculation by making use of sequence networks. There are 9 faults that can occur in a three phase power system:

- 3x Single phase to ground
- 3x Double line to ground
- 3x Line to line faults
- 1x 3 Phase to ground fault
- 1x 3 Phase to Phase fault

A fault current consists of two parts: the DC component which decays to zero with its respective time constant and a steady state current which exists due to the new fault topology. This in itself is a transient but will not be discussed. In this brief review only the single phase to ground, three phase to ground fault and two phase to ground fault steady state is discussed, as it is the switching phenomena that will be discussed. This theory has been taken from [44][41].

C.2.1. Three phase fault current

Three phase faults are balanced faults. This means the positive sequence is the only contributing component. The fault current can therefore be extracted from the single phase circuit diagram with its respective positive sequence impedances [46][45].

C.2.2. Single phase fault current

When a single conductor is connected to ground, the circuit diagram can be drawn as seen in Figure C.3a.

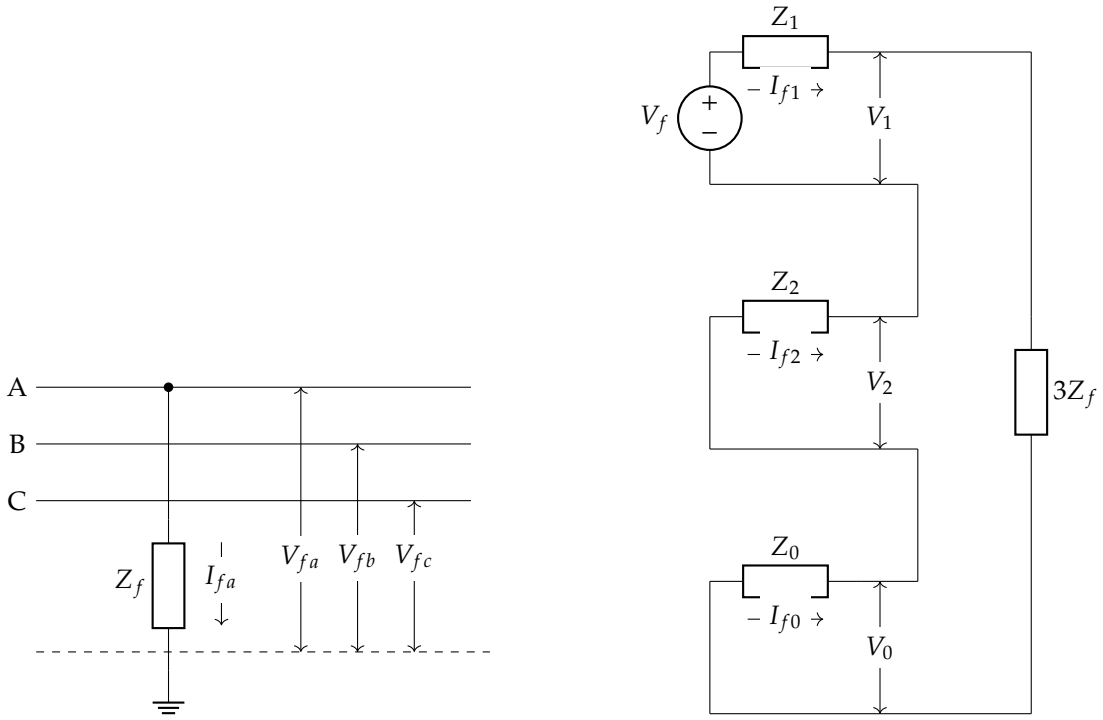

(a) Single-phase fault circuit diagram

(b) Sequence network diagram

Figure C.3: Comparison of single-phase fault circuit and sequence network diagrams

Where Z_1, Z_2 and Z_0 are thevenin equivalent network impedances for a certain faulted node.

From this one can see the following fault conditions

$$V_{fa} = Z_f I_{af} \tag{C.29}$$

$$I_{fb} = I_{fc} = 0 \tag{C.30}$$

Then, using Equation C.10, the following arises:

$$I_{f0} = I_{f1} = I_{f2} = I_{fa} \tag{C.31}$$

$$V_{f0} + V_{f1} + V_{f2} = Z_f(I_{f0} + I_{f1} + I_{f2}) = 3Z_f I_{f0} \tag{C.32}$$

$$\tag{C.33}$$

If the circuit phases A,B and C are connected to have thevenin equivalent impedances (say, from a ZBUS matrix) one can connected the sequence circuits in series at the fault location, as seen in Figure C.3b.

This results in

$$V_f = (Z_0 + Z_1 + Z_2 + 3Z_f)I_{f0} \tag{C.34}$$

C.2.3. Double line to ground fault current

In the case that the first out of three circuit breakers opens, the circuit becomes a double line to ground fault. This can be seen in Figure C.4a. In this case the following relation holds holds: Applying the sequence transformation A:

$$\begin{bmatrix} V_0 \\ V_1 \\ V_2 \end{bmatrix} = A \begin{bmatrix} V_a \\ 0 \\ 0 \end{bmatrix}$$

giving

$$V_0 = V_1 = V_2 = \frac{1}{3} V_a$$

and

$$\begin{bmatrix} I_0 \\ I_1 \\ I_2 \end{bmatrix} = A \begin{bmatrix} 0 \\ I_b \\ I_c \end{bmatrix}$$

$$I_0 = \frac{1}{3}(I_b + I_c) \tag{C.35}$$

$$I_1 = \frac{1}{3}(aI_b + a^2 I_c) \tag{C.36}$$

$$I_2 = \frac{1}{3}(a^2 I_b + aI_c) \tag{C.37}$$

Where,

$$I_0 + I_1 + I_2 = 0 \tag{C.38}$$

From this the circuit seen in Figure C.4b can be created as the sequence currents are in parallel.

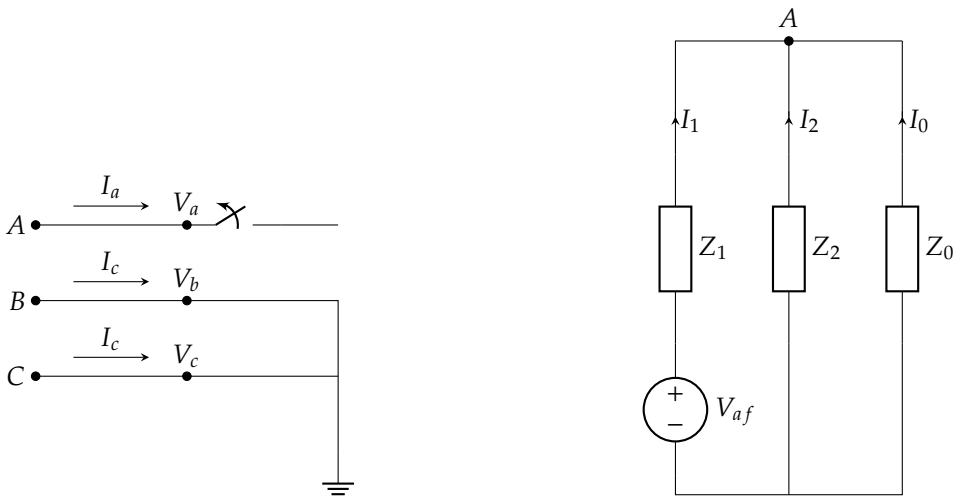

(a) Double-phase to earth diagram

(b) Sequence network diagram

Figure C.4: Comparison of single-phase fault circuit and sequence network diagrams

From Figure C.4b, one can see that:

$$V_a = V_{af} - Z_1 I_1 \text{ and } I_1 = \frac{V_{af}}{Z_1 + \frac{Z_2 Z_0}{Z_2 + Z_0}} \tag{C.39}$$

Therefore,

$$V_a = 3V_{af}\left(\frac{Z_2Z_0}{Z_1Z_2 + Z_1Z_0 + Z_2Z_0}\right) \tag{C.40}$$

and as $V_0 = V_1 = V_2$,

$$I_2Z_2 = I_0Z_0 \rightarrow I_2 = I_0\frac{Z_0}{Z_2} \tag{C.41}$$

$$V_{af} - I_1Z_1 = -I_0Z_0 \rightarrow I_1 = \frac{V_{af} + I_0Z_0}{Z_1} \tag{C.42}$$

This can then be substituted into Equation C.38 to get,

$$I_0 + \frac{V_{af} + I_0Z_0}{Z_1} + I_0\frac{Z_0}{Z_2} = 0 \tag{C.43}$$

Solving for I_0 leads to:

$$I_0 = -\frac{V_{af}Z_2}{Z_1Z_2 + Z_0Z_2 + Z_0Z_1} \tag{C.44}$$

$$I_1 = \frac{V_{af}(Z_0 + Z_2)}{Z_1Z_2 + Z_0Z_2 + Z_0Z_1} \tag{C.45}$$

$$I_2 = -\frac{V_{af}Z_0}{Z_1Z_2 + Z_0Z_2 + Z_0Z_1} \tag{C.46}$$

$$\tag{C.47}$$

Where, after conversion.

$$I_a = 0 \tag{C.48}$$

$$I_b = \frac{1}{3}(I_0 + a^{-1}I_1 + aI_2) \tag{C.49}$$

$$I_c = \frac{1}{3}(I_0 + aI_1 + a^{-1}I_2) \tag{C.50}$$